REVERSING RESISTANCE IN MELANOMA AND MALARIA: TARGETING
AUTOPHAGY WITH LYSOSOMOTROPIC AGENTS

By

Megan Lynne Goodall

A DISSERTATION

Submitted to
Michigan State University
in partial fulfillment of the requirements
for the degree of

Genetics- Doctor of Philosophy

2013

ABSTRACT

REVERSING RESISTANCE IN MELANOMA AND MALARIA: TARGETING AUTOPHAGY WITH LYSOSOMOTROPIC AGENTS

By

Megan Lynne Goodall

The autophagic pathway is a conserved cellular process whereby portions of the cytosol are targeted for lysosomal degradation. Under times of stress, autophagy is upregulated in order to promote cell survival. Accordingly, this process has been shown to be exploited by cancers and contribute to their progression and therapeutic resistance. Autophagy can be inhibited by lysosomotropic agents, such as chloroquine (CQ). CQ has long been used for malaria and more recently investigated in cancer therapy. Unfortunately, CQ is a relatively ineffective autophagy inhibitor requiring high concentrations. To address this, we screened related anti-malarial molecules and discovered quinacrine (QN) has sixty-fold greater potency at autophagy inhibition than CQ; however, it is also fairly cytotoxic. A quinacrine scaffold was used to synthesize a novel series of analogues and their autophagy inhibition screened. Several potent analogues were created including VATG032, which showed little cytotoxicity (see Chapter 2). We were also able to demonstrate that VATG032, along with a cytotoxic VATG014, prevented lysosomal turnover by increased pH. We next tested these inhibitors in patient-derived melanoma cell lines with oncogenic BRAF, shown to have high basal autophagy. We discovered that both VATG014 and VATG032 sensitized melanoma cells to the BRAF-V600E-selective inhibitor, vemurafenib (PLX-4032), in a more than additive fashion (Chapter 4).

Other mechanisms besides autophagy are known to contribute to therapeutic resistance, such as mutations that directly impair the activity of molecularly targeted drugs. Although resistance mutations in BRAF have yet to be identified, therapeutic resistance to vemurafenib

represents a major clinical problem. Vemurafenib functions by preferentially binding to the active form of the BRAF kinase domain, BRAF V600E is constitutively active, making vemurafenib a BRAF V600E selective inhibitor. We investigated a BRAF-V600E melanoma case study that did not respond to vemurafenib, and was later found to harbor a second kinase domain mutation, L567V (see Chapter 5). We determined that the dual V600E/L567V mutation diminished kinase activity as compared to the V600E mutation alone. Moreover, the BRAF double mutant was less sensitive to vemurafenib *in vitro* than BRAF V600E. We hypothesize that the L567V mutation, which restores V600E kinase activity to wild-type levels, disrupts preferential binding of vemurafenib and may represent a classical revertant mutation.

Resistance in malaria is also extremely problematic. With the development of novel autophagy inhibitors derived from quinacrine, we questioned whether these agents may also have potential antimalarial activity. We tested blood cultures containing the malaria parasite, *P.falciparum*, with VATG014 and VATG032 and found that both were effective in reducing parasite viability. Both compounds maintained well-tolerated cytotoxicity profiles in mammalian cells that did not kill at concentrations that were sufficient for parasite toxicity. Taken together, these molecules may offer a therapeutic window in the treatment of malaria (see Chapter 3).

Lastly, given the highly dynamic nature of autophagy, monitoring autophagic flux is a challenging issue. Many assays are currently used to measure autophagy; however, not all are suitable. We created a novel autophagy reporter assay utilizing the photoconvertible protein, mEOS2, fused to the autophagosome marker, LC3 (see Chapter 6). We demonstrate that this assay can be used to accurately monitor whole autophagosome populations, single or multiple autophagosomes, as well as translocation of cytosolic LC3 to autophagosomes. In sum, this multifaceted assay represents a flexible and tractable tool for investigating autophagy.

ACKNOWLEDGEMENTS

TABLE OF CONTENTS

LIST OF TABLES

LIST OF FIGURES

KEY TO ABBREVIATIONS

ACTs- Artemisinin-based Combination Therapies

ATG- autophagy related gene

BafA1- Bafiloymycin A1

BECN1- Beclin 1

cLogP- partition coefficient or the logarithm of the ratio of the concentrations of the un-ionized solute in the solvents or a measure of lipophilicity

CQ- Chloroquine

EC- Effective Concentration

EC_{CQ}- Effective Concentration of Chloroquine

EGFR- Epidermal Growth Factor Receptor

ESCRT- Endosomal Sorting Complexes Required for Transport

FBS- Fetal Bovine Serum

FLAC- Fluorescent Localization After Conversion

GFP- Green Fluorescent Protein

HDAC- Histone Deacetylase

LAMP1- Lysosome Associated Membrane Protein 1

LC3- see MAP1LC3

LD_{50}- Lethal Dose of 50%

LUT- LookUp Table

MCC-Mander's Colocalization Coefficient

MAP1LC3B- microtubule-associated protein1 light chain 3 Beta

MCC- Mander's Colocalization coefficient

MMV- Medicines for Malaria Venture

MQ- Mefloquine

mTOR1- mammalian Target Of Rapamycin 1

mTORC1- mammalian Target Of Rapamycin Complex 1

NSCLC- non-small-cell lung cancer

NT- Non-Targeting

PDGFR- Platelet-Derived Growth Factor 1 Receptor

QN- Quinacrine

Rap- Rapamycin

RBC- Red Blood Cell

RFP- Red Fluorescent Protein

RTK- Receptor Tyrosine Kinase

SNARE- Soluble *N*-ethylmaleimide-sensitive Attachment factor Receptor

TEM- Transmission Electron Microscopy

tfLC3- tandem fluorescent LC3

TGEN- Translational Genomics Research Institute

TKI- Tyrosine Kinase Inhibitors

ULK1- Unc-51 Like Autophagy Activating Kinase 1

U2OS- Human Osteosarcoma Cell Line

WHO- World Health Organization

CHAPTER 1

INTRODUCTION

The development of chloroquine (CQ): A history

Chloroquine and its predecessors, the quinolones, are some of the oldest drugs that are still in use today. The first use of the quinolones was unknowingly through the treatment of the Countess Chinchon, the wife of the Peruvian Viceroy, suffering from malaria in 1630 (Foley and Tilley 1998; Lee, Silverman et al. 2011). Her treatment came from a powder made from the bark of the cinchona tree, eventually named after her. Before this time, the tree was known as the "fever tree" known to cure 'tertian fever' (malaria) which was distributed by the Jesuits in Europe during the 17th century. This led to multiple names for the powdered bark: "china powder", "Jesuit's powder", "fever bark", and "Countess's powder". Due to variations of bark preparations, the quality of treatment varied and necessitated the need to determine the active ingredient. This was achieved in 1820 when the first quinine was isolated by the chemists Pelletier and Caventou.

Throughout the 19th century, determining a method for quinine synthesis was sought after by chemists as additional establishments of cinchona plantations outside of Peru and the high demand for quinine during World War I was unable to be met (Greenwood 1995). The demand for quinine was only exacerbated in World War II, when the Allies were cut off from quinine supplies after cinchona plantations in Java, Indonesia were captured by the Japanese (Guerra 1977; Greenwood 1995). In attempts to remedy the need for quinine, the American and British were able to derive a way to synthesize quinacrine, an antimalarial still selectively used today, from German patent literature. Quinacrine became essential to the earlier war effort in the Pacific by Allied forces. Meanwhile in Germany, Bayer laboratories synthesized the antimalarial, Resochin, now known today as chloroquine. Due to a pre-war disclosure between Bayer and the American company, Winthrop, chloroquine was taken into clinical trials in 1943

and has been used for malaria treatment ever since (Foley and Tilley 1998; Jensen and Mehlhorn 2009).

Despite the fact that chloroquine was originally developed as an antimalarial agent chloroquine has since been repurposed for several additional diseases. The first repositioning of chloroquine was for its anti-inflammatory effects in the treatment of autoimmune diseases, such as rheumatoid arthritis and lupus erythematosus. In more recent years, chloroquine has also been shown to be valuable as an adjuvant anticancer agent. The mechanism thought to mediate its anticancer activity is the ability of chloroquine to inhibit autophagy, a pro-survival pathway that is commonly upregulated in cancers. Taken together, chloroquine shown on multiple occasions is a versatile and multi-faceted compound with numerous applications (Yang and Klionsky 2010).

Chloroquine as an Antimalarial Agent

Plasmodium: Malaria causing parasite

The discovery of the parasite now known to cause malaria, *Plasmodium*, was made in 1880 by Charles Louis Alphonse Laveran. During this time, malaria was endemic in 178 countries with very little progress in its eradication due to the occurrence of both of the World Wars. Laveran noticed spherical bodies within the blood of his malaria patients, for which he received the Nobel Prize for in 1907 (Jensen and Mehlhorn 2009). This identification allowed for the connection between the symptoms of malaria and its transmission. Both the identification of the infectious *Plasmodium* and the understanding of its life cycle facilitated the use of targeted therapies such as chloroquine, resulting in a total of 79 countries that successfully eliminated malaria by 1945. Today, malaria is now concentrated in poor tropical regions of the world with

50% of the world's population living in malaria-free areas, a significant improvement from 30% in the year 1950 (Sachs and Malaney 2002; Feachem, Phillips et al. 2010).

The life cycle of the *Plasmodium* parasite requires both humans and mosquito hosts in order to be completed (Figure 1.1). The life cycle in humans begins once an infected mosquito bites and injects sporozoites from its salivary glands into the bloodstream. Once in the body, the sporozoites localize to the liver and mature into merozoites. Merozoites are then able to continue their asexual life cycle within red blood cells. It is at this stage of the life cycle, about 10-15 days after the initial bite, that the clinical features of malaria present themselves (Miller, Baruch et al. 2002). Clinical features of malaria include headache, fever, chills, and vomiting, which are common to many conditions, thus making diagnose a challenge. If left untreated, malaria can ultimately result in death ((WHO) March 2013). A small portion of the merozoites will convert into gametocytes, completing the last stage of the life cycle within humans whereby transmission back to the mosquito takes place.

The antimalarial activity of chloroquine

The mechanism of chloroquine was uncovered when the observation was made that chloroquine is only effective against the blood stages of *Plasmodium* (Foley and Tilley 1998). During the asexual life cycle within red blood cells, the hemoglobin is ingested and degraded by the digestive vacuole, which is a modified secondary lysosome, within the *Plasmodium*. Upon treatment with chloroquine, the *Plasmodium* digestive vacuole swells and prevents digestion of hemoglobin. Over time, it has been shown that CQ is a lysosomotropic agent, meaning that it localizes to the lysosome. In the case of the *Plasmodium* digestive vacuole, CQ freely diffuses into the acidic compartment by its properties as a weak base. Upon entry, CQ is diprotonated

and becomes trapped within the compartment, simultaneously increasing the acidic pH preventing heme digestion (Foley and Tilley 1998; Bray, Ward et al. 2005). Although this is the commonly accepted mechanism of action for CQ, several other possible mechanisms of action have been proposed.   These include DNA-binding and damage, inhibition of heme polymerization, importation of CQ by a Na^+/H^+ exchanger increasing pH, and inhibition of vacuolar phospholipase (Slater 1993; Foley and Tilley 1998). It is also possible that several of these occur simultaneously and can collectively contribute to the activity of CQ.

Chloroquine has now been used safely in humans for over 70 years. However, after only a little over 10 years of use, the first cases of CQ resistance began to appear and have spread ever since (Jensen and Mehlhorn 2009). This resistance has so far only occurred in the *P. falciparum* species of the parasite, making CQ still a viable treatment for the other three strains of *Plasmodium*. Unfortunately, *P. falciparum* is also the most common and most deadly of the all species (Jensen and Mehlhorn 2009; (WHO) March 2013). Resistance to CQ has been reported to be due to mutations in the gene of a transport protein named *P*. *falciparum* chloroquine-resistant transporter (PfCRT) as well as in *P*. *falciparum* multidrug resistance gene 1 (pfmdr1), with the last one being a mutation in the P-glycoprotein homologue 1 (pgh1) (Reed, Saliba et al. 2000; Jensen and Mehlhorn 2009; Roepe 2009). Development of these mutations is thought to be due to several factors; the largest of which is: *1)* the lack of control in its treatment regimens and its distribution, and *2*) failure of people to complete a full course of CQ due minor side effects (nausea, and itching) and earlier on due to its bitter taste. These issues create resistance phenotypes similar to those that occur with antibiotics (Foley and Tilley 1998; Jensen and Mehlhorn 2009).

In response to the increasing amount of chloroquine-resistant *P. falciparum* strains, significant research efforts are now focused on the development of new antimalarial compounds. There are a large variety of chloroquine analogs available, including amodiaquine and mefloquine, two of the most commonly used analogs. In addition, the development of artemisinin compounds and their use in combination therapies (still containing chloroquine analogs) have now become the standard of care for malaria (Biamonte, Wanner et al. 2013). Regrettably, even with the development of new antimalarial agents, the concurrent development of antimalarial resistance still remains a global problem. Despite the success in malaria eradication over the past 70 years, there remain an estimated 200 to 500 million cases of malaria each year with up to 1 million deaths, most of which affect African children (Sachs and Malaney 2002; (WHO) March 2013). With the increasing number of resistant strains of *Plasmodium*, new and effective treatments are desperately needed to keep malaria under control. Fortunately, with the help of organizations such as the World Health Organization (WHO) and Medicines for Malaria Venture (MMV), there is continuing research for a potential vaccine, as well as new antimalarial agents, which are discussed in Chapter 4.

The anti-inflammatory activity of chloroquine

The use of antimalarial agents as anti-inflammatory agents began almost as soon as their use in malaria. Although immunologic diseases had been described for hundreds of years (even if actual cause was then unknown), the first successful treatment took place in 1894 by J.S. Payne when a case of lupus was treated with quinine (Lee, Silverman et al. 2011). He described the rash typically associated with lupus and prescribed quinine as a way to induce pallor, or pale the skin, believing it was caused by a form of vascular disturbance (Smith and Cyr 1988). After

this time, small cohorts of patients would be treated with quinines for lupus, but it was not until after the second World War that a larger connection was made for the treatment of rheumatic diseases with antimalarial agents (Wallace 1996). At the time, soldiers in the United States military were taking Atabrine (trade name for quinacrine) for the treatment of malaria. However, those soldiers that suffered from various rheumatic diseases, such as arthritis or lupus, reported improvements in their conditions (Lee, Silverman et al. 2011). The distribution of chloroquine in 1953 showed greater efficacy and is now used as one of the most common medications in the treatment of lupus (Wallace 1996; Lee, Silverman et al. 2011). Although the exact mechanism for the anti-inflammatory properties of chloroquine is unknown, it is hypothesized that lysosome inhibition caused by chloroquine may suppress antigen presentation, toll-like receptor signaling, and cytokine synthesis (Lee, Silverman et al. 2011). Interestingly, those suffering from lupus and treated with antimalarial medicines have not only shown improvement in their symptoms, but have also been to have a decrease risk of malignancies (Ruiz-Irastorza, Ugarte et al. 2007; Lee, Silverman et al. 2011). Until more recently, the anticancer activities of chloroquine have mostly been unexplored.

The use of chloroquine as an anti-cancer agent through autophagy inhibition

Over the past decade the crucial role autophagy plays in cancer has started to become clear. The first suggestion that autophagy may contribute to tumor suppression was the 1999 discovery that *BECN1*, a gene encoding the autophagy protein, Beclin-1, is deleted in a high proportion of cancers (Liang, Jackson et al. 1999). Levine and colleagues discovered that mono-allelic deletion of *BECN1* could promote tumorigenesis. Furthermore, with the increase in understanding of the autophagy pathway, research has shown that autophagy regulation

intersects extensively with the signaling pathways shown to be responsible in numerous cancers (Levine and Kroemer 2008). Not only does autophagy suppress tumorigenesis, but paradoxically, autophagy can be exploited for continued cell survival in established cancers (Mathew, Karantza-Wadsworth et al. 2007; Levine and Kroemer 2008; Rosenfeldt and Ryan 2009). Additionally, upregulation of autophagy can be triggered by the addition of chemotherapeutics, leading to autophagy-induced chemoresistance (Rubinsztein, Gestwicki et al. 2007; White 2012).

Autophagy pathway

Autophagy is a catabolic process derived from the Greek, "auto" (self) and "phagy" (to eat). Under normal nutrient conditions, basal autophagy is utilized for homeostasis. However, in times of stress (starvation, hypoxia, and damage), autophagy is upregulated as a cell survival pathway (Mathew, Karantza-Wadsworth et al. 2007; Mizushima, Levine et al. 2008; Mathew and White 2011). Autophagy is tightly regulated through the suppression by the mammalian target of rapamycin (mTOR), which is the mTORC1 complex (Lamb, Yoshimori et al. 2013). Initiation of autophagy through upstream signaling via mTOR results in the de-repression of ULK1 (Unc-51 Like Autophagy Activating Kinase 1) and development of a sequestering membrane called a phagophore, or isolation membrane (Figure 1.2). The formation of the phagophore requires the complex containing Beclin-1, VPS34, VPS15, and other autophagy related (ATG) proteins, that develop a double bi-lipid cup-shaped membrane that surrounds the cytosol and its constituents, isolating them from the surrounding cytosol. This process of membrane elongation is known as maturation and results in the formation of a closed double membrane vesicle called an autophagosome (Klionsky 2007).

The majority of the autophagosome formation was determined in yeast, identifying 31 ATG proteins (Longatti and Tooze 2009). Continued maturation of the autophagosome membrane is produced through two ubiquitin-related conjugation systems that are required for the expansion of the membrane. The first conjugation system results in the formation of a trimeric complex of the proteins ATG5, ATG12, and ATG16L. The second conjugation system results in the autophagosome membrane being labeled with by microtubule-associated protein 1 light chain 3 (MAP1LC3, commonly referred to as LC3) which is lipidated by phosphatidylethanolamine (PE) and referred to as LC3-II, the non-lipidated cytosolic form is known as LC3-I (Longatti and Tooze 2009). Once the autophagosome is fully formed, it fuses with the lysosome containing digestive enzymes, forming an autolysosome and initiating the terminal stage of autophagy. Additionally, endosomes are able to fuse with autophagosomes during this process, which are in turn called amphisomes, which terminate in the lysosome as well.

The lysosome is a crucial organelle within the autophagic process, as it contains the proteases and hydrolases necessary for degradation. These enzymes require an acidic pH for proper functioning. A pH between 4.5 and 5.0 is maintained within the lysosomal lumen through the use of proton pumping ATPases (Luzio, Pryor et al. 2007). More recently, the specific proteins that play a role in the interaction between the lysosomal and autophagic pathways has become more evident. Up to this point the lysosomal and endocytic pathways were shown to interact through both soluble *N*-ethylmaleimide-sensitive attachment factor receptor (SNARE) and endosomal sorting complexes required for transport (ESCRT) complexes; however their role in autophagy was unclear (Luzio, Pryor et al. 2007). It has now been shown that ESCRT mutations lead to autophagic defects (Wrighton 2011; Djeddi, Michelet et al. 2012). Further,

specific SNARE proteins, such as syntaxin 17 have been shown to be required for fusion to the lysosome (Itakura, Kishi-Itakura et al. 2012; Hegedus, Takats et al. 2013). These complexes have also been suggested to play a role in the initial curvature of the phagophore during formation which is necessary for phagophore closure (Longatti and Tooze 2009).

In addition to better understanding how the lysosome and autophagic vacuole interact directly, it has also been shown that a feed-back loop involving the upstream protein kinase mTOR take place at the lysosome. It has been shown that mTOR localizes to the lysosomal membrane where its known role of nutrient sensing takes place (Zoncu, Bar-Peled et al. 2011). Under nutrient rich conditions, mTOR inhibits autophagy and this occurs as nutrients are produced by lysosomal breakdown where localization of mTOR on the membrane allows it to sense the increases in nutrient availability, thereby inhibiting autophagy. Further, the role of mTOR is shown to lead to the reformation of lysosomes from autolysosomes (Yu, McPhee et al. 2010). As autophagy is attenuated by mTOR, proto-lysosomal tubules and vesicles form from the autolysosome and mature into functional lysosomes maintaining lysosomal homeostasis.

As autophagy is a constitutive process, a fixed snapshot for measurement is not representative of the activity within the pathway; therefore, autophagy is typically measured in terms of overall flux. Autophagic flux is determined as the rate from autophagosome formation to turnover and is most often monitored by using the classic autophagosome marker LC3 (Klionsky 2012). Due to the dynamic turnover of autophagy, a downstream inhibitor that prevents degradation by the lysosome is used to determine the amount of autophagosome accumulation over a period of time, as an indicator of flux. The most common autophagy inhibitors in the field used for measuring autophagic flux are bafilomycin A1 (BafA1), a proton pump inhibitor, and chloroquine (CQ), which is discussed extensively in this study.

As discussed earlier, chloroquine is a lysosomotropic agent and has been shown to increase lysosomal pH. It is through this mechanism that chloroquine functions as an autophagy inhibitor. Since lysosomal proteases and hydrolases are dependent on pH for functionality, increasing pH through the use of chloroquine renders these proteins non-functional. Further, as autophagy requires the use of lysosomal enzymes for degradation and to terminate the pathway, inhibition of these enzymes consequently inhibits autophagy (Levine and Kroemer 2008; White 2012).

Unfortunately, lysosome inhibitors, such as CQ, can interfere with other cellular pathways besides autophagy that also terminate in the lysosome, including endocytic trafficking and the lysosomal pathways itself. This can lead to issues when measuring autophagy, as both the endocytic and lysosomal pathways have been shown to play a role in the regulation of autophagy. In the case of lysosomes, inhibition of autophagy by mTOR on autolysosomes is needed for the reformation of lysosomes (Yu, McPhee et al. 2010). In addition, recycling endosomes are shown to be crucial in the reformation of autophagosomes (Liou, Geuze et al. 1997; Longatti, Lamb et al. 2012). Finally, lysosomal-dependent activation of mTOR signaling is responsible for autophagy inhibition (Zoncu, Bar-Peled et al. 2011; Juhasz 2012; Hegedus, Takats et al. 2013). Disruption of these pathways by a lysosomal inhibitor creates the potential for misleading results as inhibitors are required for interpretation of assays currently used to monitor autophagy. Due to this, new autophagy assays that do not require the use of an inhibitor for interpretation are needed and will be discussed in Chapter 6.

Autophagy has been implicated in many diseases, including cancer, autoimmune diseases, neurodegenerative, and inflammatory diseases. The fact that this pathway has been connected to all of these same diseases, and furthermore, that CQ has shown to be effective in

three of these such diseases, is a promising sign that efforts for new and effective therapies for one disease could hold potential for others (Mizushima, Levine et al. 2008; Yang and Klionsky 2010).

Use of chloroquine in cancer

Chloroquine was first used in cancer treatment due to its properties as a weak base rather than its autophagy inhibiting capabilities, which at that time were still relatively unknown. For example, in 1994, chloroquine was shown to reduce the cytotoxic effects of etoposide, a topoisomerase II inhibitor, by preventing DNA breaks that would otherwise occur in a non-acidic environment (Jensen, Sorensen et al. 1994). Concurrent to how CQ is now believed to function, it was argued that since tumor environments tend to be acidic, the weak basic properties of chloroquine trap it extracellularly, preventing its cytoprotection from etoposide within tumors and allowing for a more targeted treatment. It was not until 2005 that the first evidence of chloroquine mediated autophagy inhibition was uncovered and shown to reduce viability of cancer cells (Lum, Bauer et al. 2005; Amaravadi, Yu et al. 2007). Research indicated that viability of cancer cells was drastically reduced when autophagy was inhibited by chloroquine in the context of growth factor starvation (Lum, Bauer et al. 2005). In 2006, Eileen White demonstrated that autophagy in fact functions as a survival mechanism in tumor cells and that inhibition of the pathway could contribute to cell death (Degenhardt, Mathew et al. 2006; Garber 2011).

The role of autophagy was shown early on as a crucial pathway in maintaining homeostasis and preventing tumorigenesis (Liang, Jackson et al. 1999). Although somewhat contradictory, autophagy has also been shown as a critical survival pathway in established

12

tumors. Recently, a report by Eileen White demonstrated in a mouse model of non-small-cell lung cancer (NSCLC) that loss of an autophagy the gene (atg7) helped tumorigenesis early on, but was essential for the continued survival of the tumor and loss of this autophagy gene prevented further growth (Guo, Karsli-Uzunbas et al. 2013). This data helps to unite the seemingly disparate observations, in that autophagy is protective from tumorigenesis early in cancer development, but can also facilitate cancer growth after initiation.

It is now the dominant view that autophagy is responsible for cell survival and growth in established tumors and that inhibition of the pathway removes this survival advantage (Garber 2011; White 2012) (Figure 1.3). Further research has shown that the use of the autophagy inhibitor, chloroquine, is effective in reducing cancer cell survival against some of the leading causes of cancer related deaths in the country; including lung, breast, prostate, and pancreatic cancers (Han, Pan et al. 2011; Yang, Wang et al. 2011; (ACS) 2013; Boutin, Tajeddine et al. 2013; Cufi, Vazquez-Martin et al. 2013).

A universal hallmark of cancers is a dysregulated metabolism that supports the rapid proliferation of tumor cells. Most cancers have oncogenic stresses which contribute to this high metabolic demand. It has recently been hypothesized that autophagy can support this altered metabolism, making certain cancers 'addicted' to the survival advantages of promoting increased autophagy (Mathew, Karantza-Wadsworth et al. 2007; Shingu, Fujiwara et al. 2009; Mathew and White 2011). Most notably, several studies have demonstrated that cancers with oncogenic RAS activation upregulate autophagy, which is critical for their survival (Guo, Chen et al. 2011; Mathew and White 2011). Pancreatic cancer exemplifies this as 90% are driven by oncogenic KRAS and autophagy is not only beneficial, but required for continued growth (Yang and Kimmelman 2011; Yang, Wang et al. 2011). Similarly, activation of the RAS effector, BRAF,

has also been shown to upregulate autophagy. The expression of both BRAF and LC3 were shown to positively correlate in tumors and further the overexpression of BRAF in cultured cells increased LC3 levels (Maddodi, Huang et al. 2010). Furthermore, use of chloroquine was found to increase sensitivity of mutant BRAF melanoma cells to the standard of care, vemurafenib (see Chapter 4) (Goodall, Wang et al. 2013). Overall, upregulation of autophagy has been documented in tumor types where oncogenic pathways are aberrantly activated.

In addition to exploitation of autophagy by certain tumor types, many anti-cancer therapies have been shown to induce autophagy (Kondo, Kanzawa et al. 2005; Wu, Coffelt et al. 2012). Unfortunately in these cases, autophagy contributes to cell survival which represents a counterproductive consequence of treatment. Therefore, cancers that are treated with therapeutics that upregulate autophagy may be particularly vulnerable to autophagy inhibition, creating a new opportunity for combination therapy. In fact, many studies have demonstrated that both genetic and chemical inhibition of the autophagic pathway can augment the cytotoxic effects of chemotherapy (Kondo, Kanzawa et al. 2005). Loss of key autophagic machinery proteins including Beclin1, ATG5, ATG10, and ATG12, has been shown to confer sensitization to cell death (Boya, Gonzalez-Polo et al. 2005; Morselli, Galluzzi et al. 2009; Liu, Cheng et al. 2010; Wu, Coffelt et al. 2012). However, chemical inhibition of autophagy is a more viable option than genetic manipulation as a cancer treatment strategy (Apel, Herr et al. 2008).

Currently, one of the most widely used autophagy inhibitors is chloroquine. Several studies have found that tumor cells treated with chloroquine have compromised autophagy-mediated survival and are less able to withstand therapeutic treatments (Amaravadi, Yu et al. 2007; Ma, Piao et al. 2011; Yang, Wang et al. 2011). In a xenograft model of triple negative breast cancer, treatment with chloroquine and a histone deacetylase (HDAC) inhibitor decreased

tumor burden and increased animal survival, compared to the HDAC inhibitor alone (Rao, Balusu et al. 2012). Furthermore, in colon cancer, chloroquine enhanced cell death induced by topotecan, a DNA damage inducer (Li, Sun et al. 2012). These examples, and others, have contributed to evidence supporting the use of autophagy inhibitors to increase cancer cell death in conjunction with therapeutics.

Not surprisingly, there are currently over 40 clinical trials in progress investigating the use of chloroquine or hydroxychloroquine, an analogue of chloroquine, in cancer treatment; half of which are specifically investigating the inhibition of autophagy (National Library of Medicine 2013; National Library of Medicine 2013). Some findings are already showing the utility of using CQ in combination therapeutics in patients. One promising clinical trial in glioblastoma multiforme showed that combination of CQ with the conventional treatment of chemotherapy and radiotherapy prolonged the median survival of patients (Sotelo, Briceno et al. 2006). The sample size in this study was small, thereby preventing statistical significance; however, it supports the potential use of CQ as an adjuvant therapy. This is further supported by other work where increased autophagy was uncovered in glioma cells resistant to standard of care chemotherapy and radiotherapy. Importantly, treatment with an autophagy inhibitor sensitized these resistant glioma cells to therapy, supporting the role of autophagy in cell survival (Fan, Cheng et al. 2010).

Although chloroquine has proven valuable in combination with existing anti-cancer therapies, it is a relatively ineffective inhibitor and requires a large concentration (mid-micromolar range) to inhibit autophagy *in vitro* and has varying uptake viability in patients (Augustijns, Geusens et al. 1992). Therefore, small molecules that potently inhibit autophagy are needed to improve efficacy, and ultimately enhance tumor cell sensitization to therapeutics,

as discussed in Chapter 2. The use of CQ as an adjuvant in traditional chemotherapeutic regimens has shown promise in early cancer therapies allowing for the development of more potent compounds be more effective.

Rationale for this Study

The objective of this project was to develop novel, potent autophagy inhibitors that could be used to drive cancer cells toward chemotherapeutic-induced cell death. An additional objective was the development of an autophagy assay that does require the use of an inhibitor to measure autophagic flux. Through rational chemical synthesis, we were successful in developing two potent autophagy inhibitors, VATG014 and VATG032. Furthermore, we were able to show that these autophagy inhibitors were capable of greater than additive effects in oncogenic BRAF V600E mutant melanoma tumor cells when combined with the targeted standard of care chemotherapeutic, vemurafenib (PLX-4032) (Goodall, Wang et al. 2013). Furthermore, these novel compounds also show promise as potential new antimalarial agents. Finally, a new assay utilizing the autophagy protein, LC3, and the photoconvertible protein, mEOS2, was developed and shown to be highly effective in its ability to monitor autophagy.

Specific Aim 1: Develop a potent autophagy inhibitor

Hypothesis: The autophagy inhibition can be improved through rational chemical synthesis of novel chloroquine analogs.

Autophagy inhibition is an ideal target for cancer therapy; however, the commonly used autophagy inhibitor, chloroquine, is inefficient at its ability to prevent downstream blockage of this process. To pursue this concept, a collaborative project with The Translational Genomics

Research Institute (TGEN) was established to develop a more potent inhibitor of downstream autophagic flux. Autophagic flux was measured through the use of the cell based assay utilizing a tandem fluorescent GFP-RFP, tagged to the autophagy protein, LC3. Accordingly, when autophagy is inhibited at the final stage (completion), the abundance of yellow puncta is expected to increase proportionally to the level of autophagy inhibition. Cell viability in response to the novel inhibitors was concurrently monitored using CellTiter-Glo, a luminescent sensor of ATP. Furthermore, lysosomal pH was investigated using LysoTracker Red, which localizes to the lysosomes based on acidity, to determine if the novel inhibitors can also increase pH and share a similar mechanism of action with CQ. Identification of 34 autophagy inhibitors, with varying cytotoxicity profiles, were identified.

Specific Aim 2: Investigate treatment strategies combining vemurafenib and autophagy inhibition in oncogenic BRAF V600E mutant melanoma.

Hypothesis: Oncogenic BRAF V600E promotes dependency on autophagy in mutant melanoma tumor cells. Inhibition of autophagy in combination with vemurafenib will allow resensitization to therapy, therefore reducing tumor cell viability.

Autophagy has been shown to be upregulated in oncogenic BRAF V600E mutant melanoma cell lines (Maddodi, Huang et al. 2010). In addition, anti-cancer chemotherapeutics and cancers have been shown to further upregulate autophagy in some cases, making them refractory to treatment. In these cases, autophagy inhibition by chloroquine treatment has been shown to sensitize these cancers to therapeutics. Accordingly, we hypothesized that potent autophagy inhibitors, developed in Aim 1, would better sensitize cancer cells to cell death than chloroquine.

Specific Aim 3: Establish a quantitative cell based microscopy assay that can accurately measuring autophagic flux.

Hypothesis: A novel autophagy assay using a photoconvertible protein is capable of vesicle tracking and measuring autophagic vesicle turnover.

Autophagic flux reflects the turnover of autophagic vesicles over time, and is currently only estimated experimentally by use of autophagy inhibitors to prevent turnover of autophagic substrates in lysosomes. The use of autophagy inhibitors to measure autophagic flux can lead to confounding results as regulation of autophagy can occur through the lysosomes themselves (Yu, McPhee et al. 2010; Zoncu, Bar-Peled et al. 2011). To address this, a tool that could monitor two populations within the same cell was needed. Using the photoconvertible protein, mEOS2, fused to the autophagy marker LC3, one is able to measure the turnover of autophagic vesicles after photoconverting (green to red). After photoconverting to red, the appearance of new autophagosomes will appear as green and the loss of red autophagosomes can be measured, allowing for visualization of two populations simultaneously.

In summary, the results of the development and characterization of autophagy inhibitors is summarized in Chapter 2. The use of these autophagy inhibitors in sensitizing cancer cells to chemotherapeutics is discussed in Chapter 3. The repositioning of the autophagy inhibitors as potential new antimalarial agents is discussed in Chapter 4. Finally, the development of a new autophagy assay is summarized in Chapter 5. An overarching summary, conclusions, and future directions of the above projects are discussed in Chapter 6.

Figure 1.1 Life Cycle of *Plasmodium*
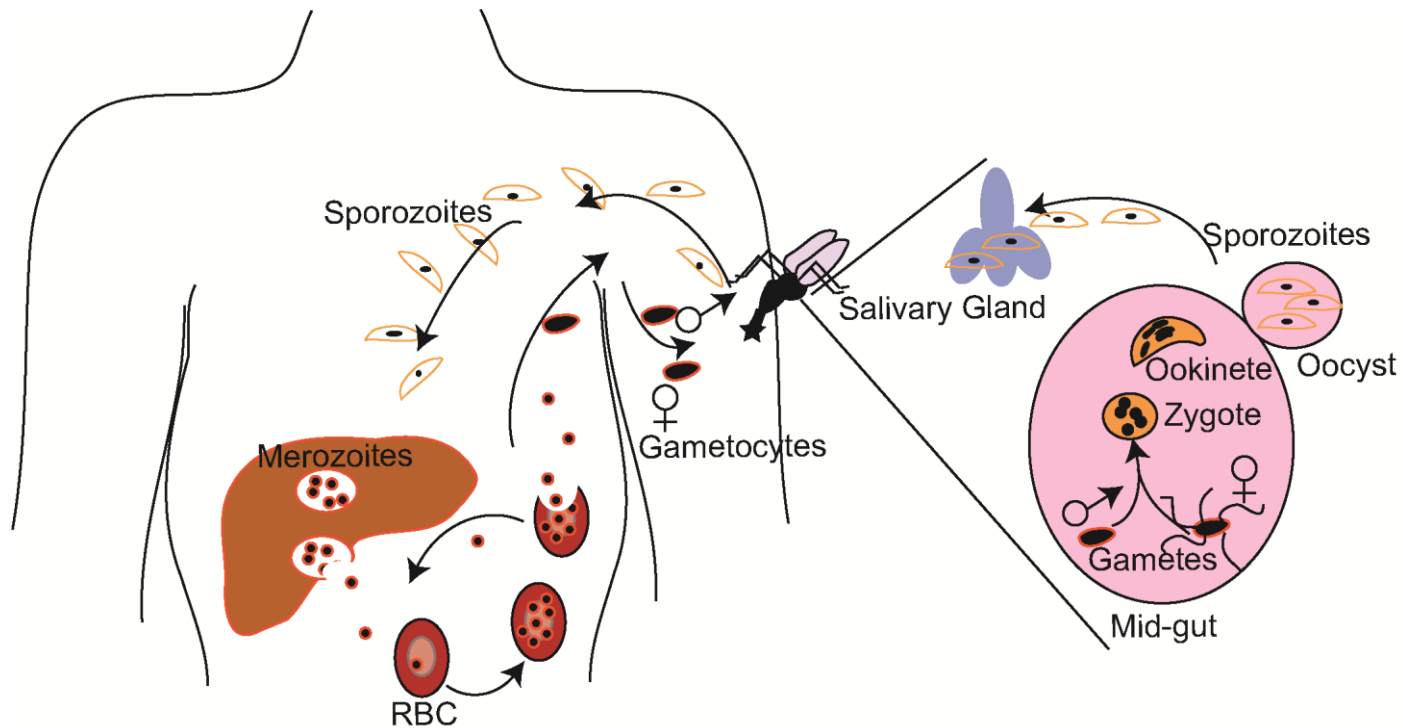
For interpretation of the references to color in this and all other figures, the reader is referred to the electronic version of this dissertation. A mosquito bite injects *Plasmodium* sporozoites into the blood stream from its salivary glands. Once in the blood stream, sporozoites localize to the liver and infect hepatocytes where the continuation of the life cycle into merozoites occurs. Approximately 10-15 days after the bite, the merozoites return to the blood stream and can continue their asexual life cycle, replicating in the red

Figure 1.2 (cont'd)

blood cells (RBCs). A few merozoites convert into gametocytes, completing the life cycle by retransmission through an additional mosquito bite. The life cycle continues in the mosquito mid gut until sporozoites localize to the salivary gland where they can be re-transmitted.

Figure 1.2 Autophagy Pathway
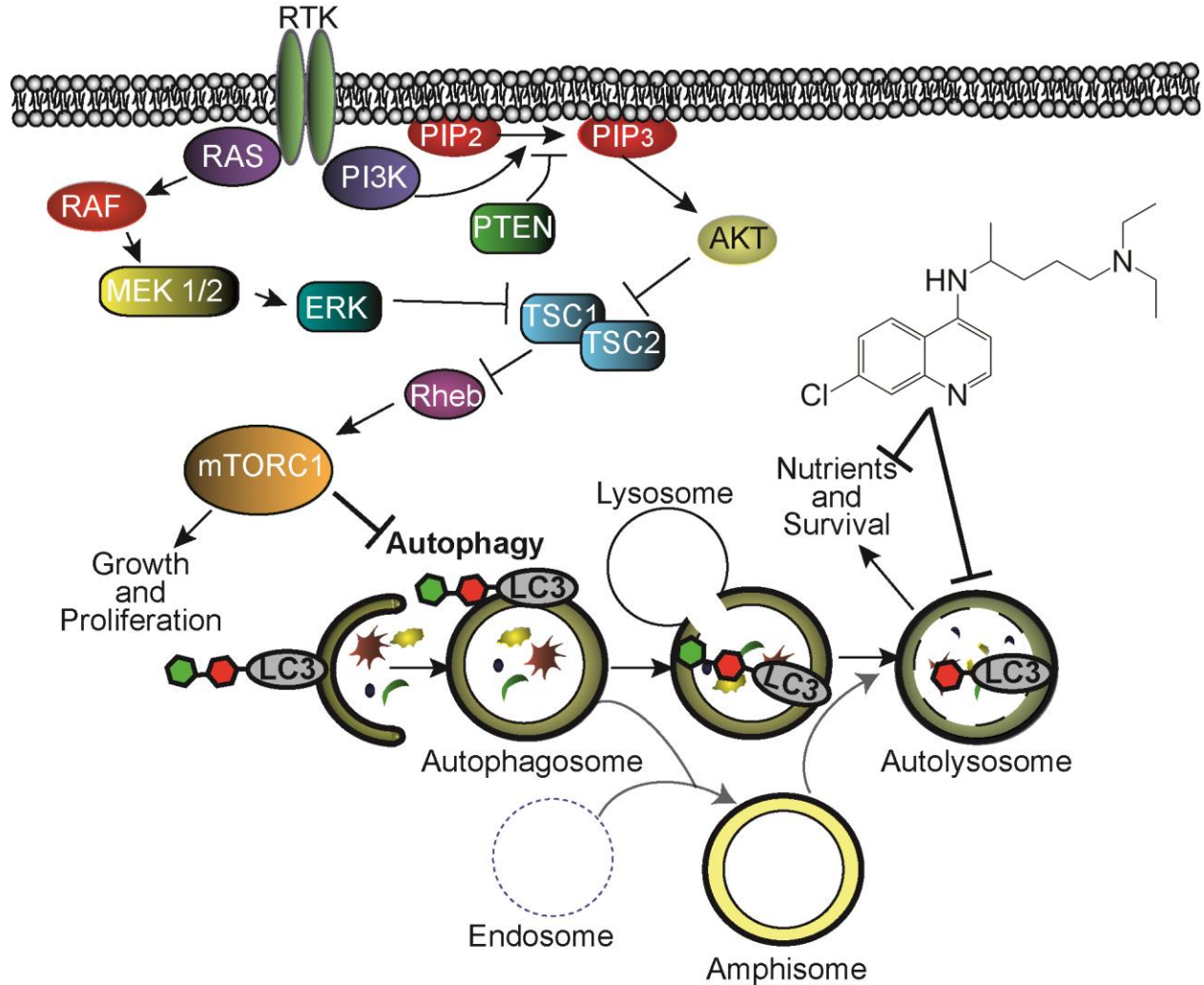
Upstream signaling through a receptor tyrosine kinase (RTK) will signal through the mammalian target of rapamycin complex 1 (mTORC1) responsible for inhibiting autophagy until times of stress, at which time, autophagy will be activated and a phagophore sequesters cytosol. A phagophore undergoes maturation into an autophagosome, a double bi-lipid membrane vesicle, and will fuse with the lysosome for degradation (forming autolysosomes). Endosomes can also fuse with autophagosomes (forming amphisomes) before fusion with the lysosome. Chloroquine increases the lysosomal pH, preventing proteases and hydrolases from functioning and inhibits lysosomal turnover, therefore inhibiting the autophagy pathway.

Figure 1.3 Role of Autophagy in Tumor Survival
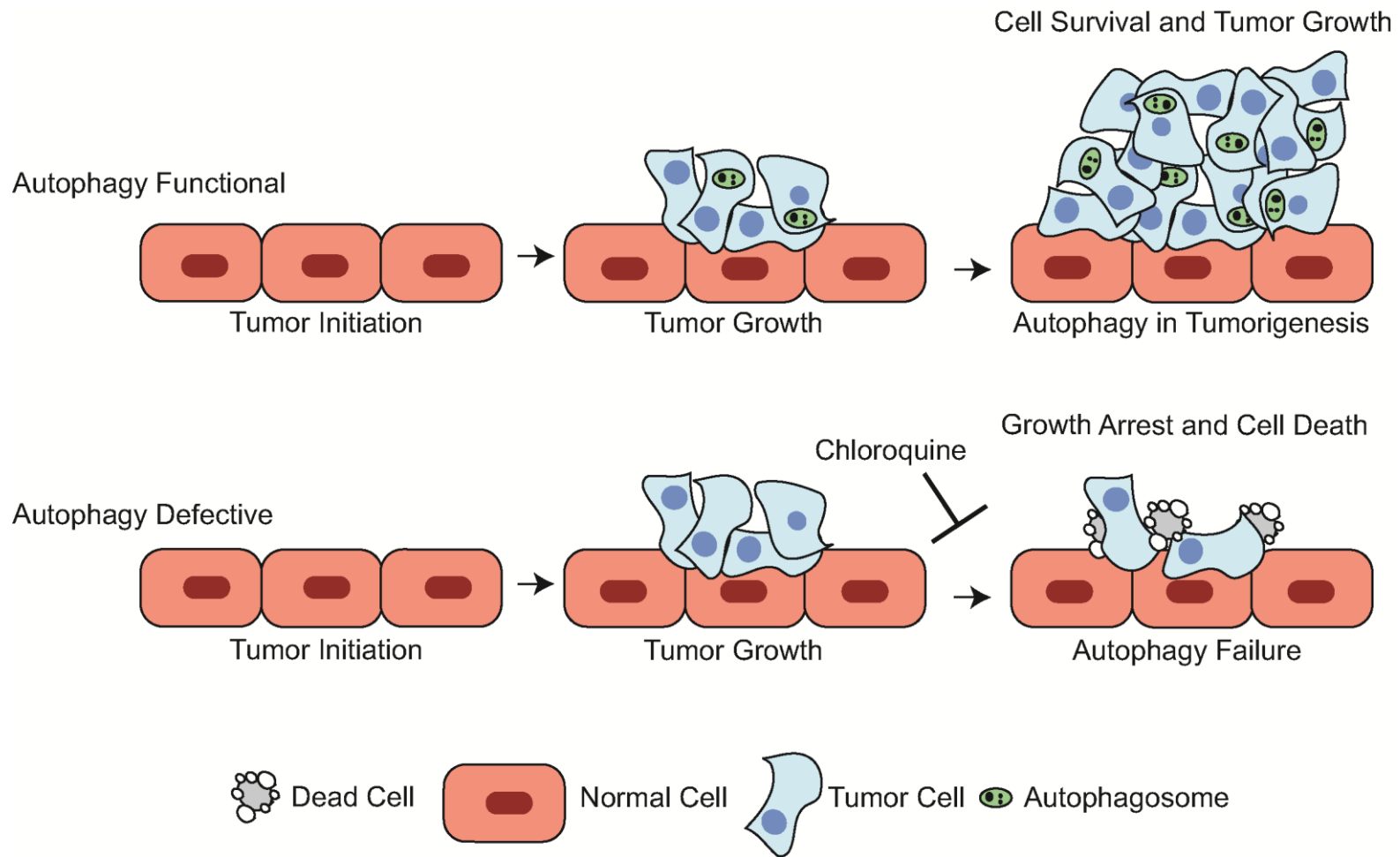
Figure 1.3 (cont'd)

Tumor cells are able to upregulate autophagy during tumor progression, allowing for continued survival and growth. However, in autophagy-defective cells, or through use of an autophagy inhibitor (i.e., chloroquine), tumor cells are unable to survive, causing growth arrest and cell death.

CHAPTER 2

SYNTHESIS AND CHARACTERIZATION OF NOVEL AND EFFECTIVE

AUTOPHAGY INHIBITORS

Modified from

And

ABSTRACT

The autophagic pathway is a conserved cellular process used to maintain homeostasis within the cell. Under times of stress (nutrient deprivation, reactive oxygen species, etc.), autophagy is upregulated in order to promote cell survival and has been shown to be exploited by cancers for cell survival. Autophagy functions by sequestering portions of the cytosol for delivery to the lysosome for recycling and can be inhibited by the widely used anti-malarial, chloroquine (CQ). Despite its activity, CQ requires high concentrations to achieve autophagy inhibition. To address this, we screened a panel of anti-malarial agents and found that quinacrine (QN) has a sixty-fold higher potency of autophagy inhibition than CQ. Despite the desired autophagy inhibiting properties of QN, it also has a higher than desired cytotoxicity profile. Therefore, we utilized synthetic chemistry to generate a novel series of QN analogues and investigated effects on autophagy inhibition and cell viability. Several analogues were created that showed reduced cytotoxicity profiles. Notably, we found that saturation of the terminal ring on the acridine backbone of QN to 1,2,3,4-tetrahydroacridine showed surprisingly little cytotoxicity while still preserving potent autophagy inhibition. Next, we determined that VATG014 and VATG032, a cytotoxic and less cytotoxic, both function through lysosomal deacidification mechanisms and ultimately disrupt autophagosome turnover.

INTRODUCTION

Autophagy is a conserved cell survival mechanism that is used to recycle damaged proteins and organelles which are targeted for reuse as cellular nutrients. This catabolic pathway segregates portions of the cytosol into an autophagosome which ultimately terminates in the lysosome for degradation of its contents (Klionsky 2007). Under normal nutrient conditions, autophagy is used to maintain homeostasis within a cell (e.g., by turning over long-lived proteins). However, under conditions of stress and starvation, autophagy can be upregulated to promote cell survival. Given its crucial role in cell function, altered autophagy has been implicated in many diseases including cancer, autoimmune, inflammatory, and neurodegenerative diseases (Mizushima, Levine et al. 2008; Yang and Klionsky 2010). In the case of cancer, autophagy can be exploited by established tumors for survival in times of metabolic, hypoxic, and therapeutic stress (Kondo, Kanzawa et al. 2005; Mathew, Karantza-Wadsworth et al. 2007; Wu, Coffelt et al. 2012).

Autophagy has been shown to be upregulated in a wide array of cancer types. In many cases, this upregulation is a consequence of mutations in proteins upstream of autophagy signaling (Kondo, Kanzawa et al. 2005; Chen, Rehman et al. 2010; Guo, Chen et al. 2011; Janku, McConkey et al. 2011; Wu, Coffelt et al. 2012). For instance, cancers characterized by oncogenic RAS activation have shown that autophagy critical for survival and often upregulated (Guo, Chen et al. 2011; Mathew and White 2011). Further evidence shows that autophagy is upregulated in cells with oncogenic BRAF (Maddodi, Huang et al. 2010). Owing to the aberrant nature of these proteins in cancer, targeted approaches to their inhibition has been actively pursued. While such treatment strategies prevent cellular growth and proliferation, many

inadvertently allow for increased autophagy. Accordingly, there is a critical need for specific autophagy inhibitors that can be used as part of cancer treatment regimens (Chen, Rehman et al. 2010).

The emerging role of autophagy in disease has garnered interest in therapeutic targeting of this pathway. Given that the autophagy pathway terminates in the lysosome, this stage represents a desirable target for inhibition. Not only would lysosomal targeting impair autophagy caused by any upstream aberration, it would prevent the regeneration of nutrients necessary for autophagy-mediated survival. This has enabled the use of chloroquine (CQ), a well-known antimalarial used clinically for over 70 years, to be effectively used as an autophagy inhibitor. CQ is known as a lysosomotropic agent that freely diffuses across the lysosomal membrane, and is then deprotonated and trapped inside as a diacidic base (Loeb 1946; Foley and Tilley 1998; Solomon and Lee 2009). The removal of free hydrogen ions by CQ increases the basicity of the lysosome and renders pH-dependent lysosomal hydrolases and proteases non-functional. The impairment of lysosomal enzymes by CQ prevents degradation of engulfed materials, thereby inhibiting the final completion stage of autophagy. Consequently, autophagy no longer contributes to cell survival and tumor cells treated with CQ are sensitized to many therapeutics (Amaravadi, Yu et al. 2007; Ma, Piao et al. 2011; Mathew and White 2011; Yang, Wang et al. 2011; Goodall, Wang et al. 2013).

A substantial number of studies have shown the potential that CQ holds as an adjuvant therapy in cancers, which has led to the initiation of several clinical trials (Chen, Rehman et al. 2010). A few of these trials have been completed and reported a moderate increase in survival and autophagy inhibition with CQ (Sotelo, Briceno et al. 2006; Amaravadi, Lippincott-Schwartz et al. 2011). Despite its promise, high concentrations (μM range) of CQ administered over the

course of weeks are needed to reach peak concentrations in the blood stream and effectively inhibit autophagy at the cellular level (Carmichael, Charles et al. 2003; Amaravadi, Lippincott-Schwartz et al. 2011). In clinical trials, this raises concerns to the effectiveness of CQ being able to achieve full autophagy inhibition. Accordingly, there is a critical a need for more potent autophagy inhibitors.

To address this need, we screened a collection of antimalarial compounds, which share similar mechanisms of action as CQ, for the ability to inhibit autophagy. Several of these compounds have been previously shown to inhibit autophagy (Sharma, Thomas et al. 2012). One antimalarial, quinacrine (QN), was particularly intriguing as it tended to be overlooked as an autophagy inhibitor. QN has been used as an antimalarial for over 60 years and has more recently been investigated as an anticancer agent (Gurova 2009). However, its use has been limited due to objectionable alternative applications, such as direct application to the reproductive organs for sterilization and having a less favorable cytotoxicity profile (Dabancens, Sokal et al. 1995; Zipper, Dabancens et al. 1995; Jensen and Mehlhorn 2009). With this in mind, we utilized medicinal chemistry using QN as a template molecule to maintain its effectiveness as an autophagy inhibitor, while lowering its cytotoxicity. Here, we report the development of a series of novel and potent lysosome-targeted autophagy inhibitors. These molecule share potent autophagy inhibiting properties yet have diverse cytotoxic profiles, suggesting they may be useful as single agents or in combination therapies.

RESULTS

Screening Anti-malarial Compounds for Autophagy Inhibition

Autophagy inhibition can be measured by fluorescent microscopy using cells expressing a tandem fluorescent (RFP-GFP) labeled MAP1LC3B (microtubule-associated protein 1 light chain 3 beta; LC3) sensor (tfLC3) (Klionsky 2012). Upon autophagosome nucleation, LC3 localizes to the autophagic membrane and the overlapping GFP and RFP fluorescence appears as yellow puncta. After the autophagosome matures, it fuses with the lysosome, forming an autolysosome. The GFP of this sensor is pH labile and becomes quenched by the acidic environment of the autolysosome. However, the RFP remains stable; therefore, autolysosomes are indicated by red puncta. Accordingly, when autophagy is inhibited at the final stage (completion) - either by an accumulation of autophagosomes or de-acidification of the autolysosome - the abundance of yellow puncta is expected to increase proportionally to the level of autophagy inhibition (Figure 1.2).

To determine if other anti-malarial compounds exist which inhibit autophagy more potently than CQ, we treated U2OS cells stably expressing tfLC3 cells with CQ or six other anti-malarial agents (amodiaquine, artemisinin, mefloquine, piperaquine, primaquine, and quinacrine) for three hours. Cells were then fixed and imaged by fluorescent microscopy (Martin, Barua et al. 2013) (Figure 2.3A). The LC3 punctae (autophagic vesicles) from these fluorescent images were quantified and used to determine the effective concentration (EC) of autophagy inhibition (Table 2.1). The EC was determined as the concentration at which cells contained a statistically significant increase in puncta number compared to the vehicle control. To identify anti-malarial compounds that inhibited autophagy more potently than CQ, the EC of each anti-malarial was

divided by the EC of CQ (EC_{CQ}) to yield a relative potency score (EC/EC_{CQ}). Accordingly, a potency score greater than one indicated a more potent autophagy inhibitor than CQ. We found that two anti-malarial compounds, mefloquine (MQ) and quinacrine (QN), were more potent autophagy inhibitors than CQ with relative potency scores of approximately 30 and 60, respectively (Table 2.1).

CQ, QN, MQ, and amodiaquine have been previously shown to inhibit autophagy, while the remaining anti-malarial agents tested (piperaquine, primaquine, and artemisinin) have not to our knowledge (Qiao, Tao et al. 2013). Although these agents showed reduced potency, we wanted to confirm that they function as autophagy inhibitors using an endogenous assay. Using immunoblotting for endogenous LC3, we demonstrated that each agent induced the accumulation of LC3-II (the form of LC3 localized to the autophagic membrane), both basally and in response to rapamycin-induced autophagy induction (Figure 2.1). This data suggests that autophagy inhibition may be a common activity of anti-malarial agents.

Next, we wanted to carefully characterize the autophagy inhibition of QN, the most potent autophagy inhibitor, in comparison with CQ. To this end, we treated U2OS-tfLC3 cells with ten-point concentration gradients of QN of CQ and again, imaged LC3 puncta. While QN treatment increased the amount of LC3 puncta at nearly all doses, the same doses of CQ failed to achieve an appreciable number of puncta (Figure 2.2A). In order to quantitatively confirm the results, we used image analysis software to determine the mean intensity of puncta at each dose of compound. We found that mean intensity was a more accurate indicator of autophagy in these experiments compared to puncta number due to the large abundance of puncta that become individually indistinguishable at higher inhibitor concentrations. This autophagosome accumulation prevents accurate separation of objects, rendering puncta number less reliable.

30

Mean intensity proved to correlate well with number of puncta, and importantly, was not negatively affected at high concentrations (Figure 2.3B-D). Treatment with QN significantly increased the mean intensity of autophagic puncta at 0.25 μM. However, CQ treatment was only able to produce a significant increase in mean intensity at 15 μM, a 60-fold higher concentration (Figure 2.2B).

Synthesis and Screening of Novel Compounds

Next, we produced a series of novel chemical compounds using the general synthetic route shown in Scheme 1 for backbone synthesis (Figure 2.4). Moderate yields were achieved for most of the substrates. All compounds were then prepared as hydrochloride salts and reconstituted in DMSO stock solutions. Cells were treated with each compound in 10-point concentration responses and dually measured for cytotoxicity and autophagy inhibition. Autophagy inhibition was measured using the ptfLC3 sensor and quantitative microscopy, as described above. Cytotoxicity was measured using a luminescent sensor of cellular ATP, CellTiter-Glo, and the concentration of compound which reduced the viability of cells by 50% (LD_{50}) was determined. The cLogP values, a measure of hydrophilicity or how the compound will partition between water and oil, were also determined. cLogP values are important for understanding the initial pharmacodynamics and pharmacokinetics of a compound and therefore its expected behavior once in the body.

Modification of the 1,4-butyldiamino and Cyclized Amino Groups

Initial analogue chemistry focused on altering the 1,4-butyldiamino group on QN, followed by further alterations of cyclized terminal amino groups, as outlined in Scheme 2

(Figure 2.5; Table 2.2). Little change was observed in either cytotoxicity or autophagy inhibition with removal of the methyl group (VATG001). However, further removal of the methoxy group on the acridine backbone greatly reduced cytotoxicity (LD_{50} 6 μM) (VATG002). Tertiary relocation of the methyl group onto the primary amine substantially reduced autophagy inhibition (10-fold), likely due to the alteration of the basicity of the N and steric hindrance (VATG003).

Exploration of the terminal diethylamine group with either methoxy or dimethylamine showed little change in autophagy inhibition or cytotoxicity (VATG004 and VATG005), with bulkier terminal replacements of sulfonamide or *tert*-butyl groups (VATG007 and VATG008) showing substantially poorer autophagy inhibition (EC 50 μM). However, a terminal acetamide allowed for potent autophagy inhibition, while still having low cytotoxicity (VATG006). Terminal cyclopropane groups also maintained desirable autophagy inhibition (EC 0.25 μM) (VATG009-011) with VATG009, which contains a terminal methyl group instead of ethyl group, having a sharply higher cytotoxicity than its counterparts (LD_{50} 0.2 μM). This suggests that the cytotoxicity was very sensitive to the change in terminal alkyl groups.

To address sensitivity based on alkyl groups, cyclized terminal amino groups were examined next. A morpholine group drastically attenuated both autophagy inhibition and cytotoxicity (VATG013). Compounds containing a cyclopentylamine and methyl piperazine group (VATG012 and VATG014) both had higher cytotoxicity (LD_{50} 0.5 μM and 0.7 μM, respectively), with very potent autophagy inhibition being observed with the methylpiperazine (EC 0.1 μM).

Modification of Side Chain Length and Rigidity Alternatives

Despite the progress made with the side chain optimization and the discovery of some improved compounds, the 1, 4-butyldiamino group presented potential problems as flexible carbon chains were known to be associated with metabolic instability, high hydrophobicity, and inferior binding affinity due to conformational entropy penalty (Gurova 2009). With these considerations in mind, we went forward to explore *1)* alterations in chain length (Table 2.3 and Figure 2.6) and *2)* structurally rigid alternatives (Table 2.4 and Figure 2.7). Notably, the length of the side chain was previously found to affect the activity of CQ analogues (Natarajan, Alumasa et al. 2008; Hocart, Liu et al. 2011).

Firstly, a reduction in chain length initially to a 1,3-propyldiamino moiety (VATG015) showed to be detrimental to autophagy inhibition (EC 2.5 µM), while a 1,2-ethyldiamino moiety (VATG016) inversely maintained potent autophagy inhibition with lower cytotoxicity (LD_{50} 7 µM). A longer chain ether linkage (VATG017) did not change autophagy inhibition and also produced lower cytotoxicity (LD_{50} 4 µM). Contradictory, a methoxyethylamine group (VATG018) reversed the biological properties with high cytotoxicity and low autophagy inhibition (EC 5 µM and LD_{50} 0.2 µM). The potent autophagy inhibition from methyl piperazine observed from earlier was next investigated with the promising 1,2-ethyldiamino moiety. Potent autophagy inhibition was maintained even with structural halide modifications on the acridine ring (VATG019-VATG022).

Secondly, the more rigid system was explored by centering on 3-aminopyrrolidine and 4-aminopiperdine groups (Table 2.4 and Figure 2.7). In contrast to the five membered 3-

amniopyrrolidine group (VATG023), the six membered 4-aminopiperdine group, either substituted with methyl (VATG024) or ethyl (VATG025), was more favorable for autophagy inhibition (EC 0.25 μM). Further manipulation of the core demonstrated that small group halide substitutions were required at both X_1 and X_2 to slightly alter cytotoxicity and autophagy inhibition (VATG026 to VATG030).

Modification of the Acridine Backbone

In spite of obtaining a number of new compounds with effective autophagy inhibiting concentrations of ≤ 0.25 μM, our attempts to reduce the cytotoxicity of these autophagy inhibitors was not as successful as hoped. A few compounds, such as VATG006 and VATG029, had lower cytotoxicity profiles than QN (LD_{50} 12.5 μM for both compounds); however, we sought to further reduce cytotoxicity. To address this, we first compared the structures of QN and CQ, given the significantly lower cytotoxicity of CQ. QN shares many common structural features with CQ, including the exact same basic side chain, but it has a tricyclic core rather than the bicyclic core of CQ (Figure 2.1).

Using this knowledge, the acridine backbone of QN was replaced with either aza-acridine or 1,2,3,4-tetrahydroacridine using a short or rigid side chain (Table 2.5 and Figure 2.8). Replacement of the acridine backbone with aza-acridine (VATG031-VATG033) produced greater cytotoxicity (LD_{50} 0.5 μM), while the 1,2,3,4-tetrahydroacridine successfully reduce cytotoxicity (LD_{50} 27 μM), 10-fold that of QN (VATG032 and VATG034). Releasing the constraint of the fused tricyclic system, as in acridine or aza-acridine, the saturated terminal ring of 1,2,3,4-tetrahydroacridine likely adopted a twist-chair conformation. Since a planar

34

conformation of multi-cyclic aromatic systems is mandatory for DNA binding (Denny 2002), the conformation change of VATG032 and VATG034 could be the reason for their diminished cytotoxic effects. In addition to the potent autophagy inhibition and reduced cytotoxicity, both VATG32 and VATG34 showed much better biophysical property as anticipated. Furnished with the *N*-ethylpiperdine-4-amino and 2-(4-methylpiperazine)ethanamino groups, both VATG32 and VATG34 became much less hydrophobic than QN and their cLogPs dropped to 4.2 and 5.5, respectively.

Detailed characterization of VATG014 and VATG032

While moderate changes in autophagy inhibition and viability were seen with most chemical alterations, a few key changes had considerable impacts on cell viability (LD_{50}) and/or EC. From the most potent autophagy inhibitors, we chose two molecules for further evaluation, each with divergent effects on cell viability (LD_{50}). While compound VATG032 (EC = 5 μM), was less cytotoxic than QN with an LD_{50} equal to 27 μM, VATG014 (EC = 0.1 μM) was considerably more cytotoxic with an LD_{50} of 0.7 μM. The autophagy inhibition and cell viability effects of VATG014 and VATG032 were carefully quantified across a concentration gradient, as described above, and compared to that of both CQ and QN (Figure 2.9A-C and Table 2.6). We found VATG032 was 3-fold more potent at autophagy inhibition than CQ, yet 10 times less cytotoxic than QN (Table 2.6). The potent autophagy inhibition coupled with low cytotoxicity makes VATG032 a candidate compound for adjuvant therapy. We also found VATG014 to be 150-fold more potent at autophagy inhibition than CQ (and 2x more potent than QN); however, it was also 3.5-fold more cytotoxic than QN. To confirm autophagy inhibition

independent of a fluorescent reporter, we performed a concentration response and measured endogenous LC3 processing by immunoblotting (Figure 2.10). Compounds VATG014 and VATG032 both showed increased accumulation of LC3-II, consistent with the tfLC3 observations (Martin, Barua et al. 2013) (Figure 2.9 and Figure 2.10). Cytotoxicity of each compound was tested for caspase-3 activation at 3 μM and demonstrated that the cytotoxic compounds QN and VATG014 reduction in cell viability is at least partially the result of apoptotic cell death (Figure 2.9D).

To determine whether the cytotoxicity of CQ, QN, VATG014, and VATG032 was dependent on autophagy, concentration gradients were repeated in cells transfected with siRNAs to ATG5/12 and ULK1, core proteins required for autophagy. Effective knockdown of ATG5, ATG12, and ULK1 was measured by quantitative real-time PCR (qRT-PCR) and autophagy impairment was confirmed as a lack of LC3 lipidation by immunoblotting (Figure 2.11). Knockdown of neither ATG5/12 nor ULK1 (in comparison to a non-targeting (NT) control siRNA), did not significantly alter the cytotoxicity induced by compounds, suggesting that autophagy does not play a role in the acute cytotoxicity of these compounds. Moreover, caspase-3 activation did not change with knockdown of either ATG5/12 or ULK1, further demonstrating that reduction in acute cell viability is more likely the result of apoptotic cell death (Figure 2.12).

Mechanism of Action—Lysosomal Inhibition

Since both CQ and QN are both known to inhibit autophagy by deacidifying lysosomes and preventing the turnover of their constituents, we hypothesized that these VATG compounds function by the same mechanism. To test this, we first visualized lysosomes using transmission electron microscopy (TEM). We treated U2OS cells with a CQ concentration above the effective dose (100 μM) for 3 hours as a positive control, fixed and imaged cells. While few vesicles were

observed in vehicle-treated cells, we found an accumulation of large, electron-dense and electron-lucent vesicles, consistent with lysosomes and endosomes, upon addition of CQ (Figure 2.13A). Once this phenotype was established, we treated cells with a lower concentration (3 μM) of CQ to compare to cells treated with each compound at the same concentration. This dose was previously shown to inhibit autophagy for QN, VATG014, or VATG032, but not CQ (Figure 2.2). As expected, we found that 3 μM CQ was insufficient to cause a noticeable increase in either vesicle size or number compared to the vehicle control. However, 3 μM treatments with QN, VATG014, and VATG032 caused a statistically significant increase in the number of electron-lucent and electron-dense vesicles detected (Figure 2.13B-C). In addition, VATG014 and VATG032 treatment resulted in the appearance of several electron-opaque structures, consistent with lipid droplets, which are known to be broken down by autophagy (Figure 2.13B) (Singh, Kaushik et al. 2009; Velikkakath, Nishimura et al. 2012).

Deacidification of lysosomes would be expected to not only prevent the maturation and turnover of the early lysosomes to late lysosomes, but also affect the functionality of lysosomal enzymes and consequently, the turnover of lysosomal constituents. To determine if lysosomal activity was inhibited, we measured pro and active forms of the lysosomal protease cathepsin B, by immunoblotting (Figure 2.13D). Lysates were harvested from cells were treated with CQ, QN, VATG014, and VATG032 at either 3 μM or 30 μM for 6 hours. QN and VATG014 showed a nearly complete loss of active cathepsin B at 30 μM, while VATG032 showed a significant decrease at the same dose. In contrast, CQ showed little effect on active cathepsin B at either dose. Taken together, this suggests that the acridine derivatives are considerably more potent than CQ at blocking lysosomal activity and turnover.

Next, we sought to confirm the inhibition of lysosomal turnover induced by VATG compounds by evaluating the abundance of endogenous lysosomal protein, LAMP1. In addition, we assessed lysosome acidity by co-staining cells with LysoTracker Red, a dye that localizes to the lysosome based on the low pH. Cells were treated with 3 μM CQ, QN, VATG014, or VATG032 for 3 hours, with LysoTracker Red supplemented for the final hour. Following, cells were fixed and stained with endogenous LAMP1 antibodies and both LAMP1 and LysoTracker Red imaged. We found that CQ failed to yield an appreciable change in LAMP1 positive membranes and LysoTracker Red staining at 3 μM (Figure 2.14A and 2.15B). In contrast, QN, VATG014, and VATG032 treatments all caused substantial increases in LAMP1 staining and essentially eliminated LysoTracker Red staining (Figure 2.14A-B). To quantify this phenotype, the colocalization of LAMP1 and LysoTracker Red was measured using image analysis software. The ratio of intensity of each signal across pixels of individual vesicles was measured and displayed using a colorimetric scale, where red indicates the presence of LAMP1-only, purple indicates the presence of LysoTracker Red-only, and green indicates the presence of both (Figure 2.15). In addition, Mander's colocalization coefficient (MCC) values were determined for each treatment (Figure 2.14C). Mander's colocalization coefficient measures pixel by pixel the co-occurrence of each channel or the proportion of pixels with positive values for both channels (Dunn, Kamocka et al. 2011). We confirmed that not only does the presence of LAMP1-positive membranes increase, but the intensity of LAMP1 staining also increases with QN, VATG014, and VATG032 treatment (Figure 2.14). We also show the inverse holds true for LysoTracker Red staining; treatment with QN, VATG014, or VATG032 decreased LysoTracker Red staining more so than CQ, suggesting a more substantial loss of lysosomal acidity at these

lower concentrations. Collectively, these results suggest that these compounds function by deacidifying lysosomes and impairing their turnover.

DISCUSSION

Through the use of quantitative microscopy and rational chemical synthesis, we have further identified novel autophagy inhibitors with up to a 50-fold increase in autophagy inhibition compared to that of CQ and 10-fold to that of QN, successfully synthesizing QN analogues that not only retain autophagy inhibiting properties, but have further increased potency. Overall, alterations of the acridine backbone to 1,2,3,4-tetrahydroacridine in two compounds (VATG032 and VATG034) showed the most drastic decrease in cytotoxicity. The saturated terminal ring is thought to be the reason for their diminished cytotoxic effects, since this would diminish their ability to bind DNA shown to be partially be responsible for the cytotoxicity of QN (Denny 2002). This suggests that these compounds may also potentially allow for safer toxicity profiles *in vivo* and are of particular excitement as they preserve the effective autophagy inhibiting properties of QN (while being non-toxic), allowing for more effective autophagy inhibition than is currently achieved with CQ (EC 50 μM).

Alteration of the side chain to more rigid systems using 3-aminopyrrolidine or 4-aminopiperdine groups was also more favorable for autophagy inhibition. These alterations likely prevented the flexible carbon chains, known to be associated with metabolic instability, as well as decreasing the hydrophobicity and inferior binding affinity due to conformational entropy penalty. To simplify, the rigid groups likely prevent the conformation entropy by decreasing the promiscuous binding to other proteins that can occur before reaching the lysosome with the 1,4-butyldiamino group on CQ and QN. Further, the rigid groups are also more hydrophobic in nature than CQ, but less hydrophobic than QN (Hydrophobic > QN > 3-aminopyrrolidine and 4-aminopiperdine > CQ > hydrophilic), allowing for more favorable hydrophobicity for entry into

the lysosome due to the charge on the lysosomal membrane (Steinberg, Huynh et al. 2010). This side group alteration allows for a more favorable entry into the molecules intended organelle of action, the lysosome, and is likely the cause for their increased autophagy inhibiting effectiveness. To confirm this, a detailed characterization of both a highly (VATG014) and lowly (VATG032) cytotoxic autophagy inhibitor containing these rigid side groups were shown to have similar mechanisms of action to that of CQ and QN - increased lysosomal pH, reduced lysosomal enzyme activity, and impaired vesicle turnover.

Several studies have explored the development of CQ analogs; however, these analogs were primarily investigated for efficacy in malaria treatments and have not been explored as cancer therapeutics (De, Krogstad et al. 1998; Iwaniuk, Whetmore et al. 2009). Consequently in addition to the therapeutic potential in these analogues hold in cancer, these novel autophagy inhibitors may prove useful in the treatment of malaria (see Chapter 4). Malaria is endemic in several regions of the world and resistance to current anti-malarial drugs, including CQ, is an ever growing problem (Anderson, Nkhoma et al. 2011; Muregi, Wamakima et al. 2012). The development of new treatment strategies effective for such resistant strains is critical for the management of this disease. Accordingly, these modified analogues can be explored for cancer therapeutics and additionally be investigated for activity against malaria strains resistant to current therapeutics.

MATERIALS AND METHODS

Chemistry

Anti-malarial drugs shown in Table 1 were purchased commercially: amodiaquine (Chempacific, Corp. 35393), artemisinin (Sigma, 361593), chloroquine (Sigma, C6628), mefloquine (Amplachem, Inc., AA-90157), primaquine (OChem, Inc., 598P906), piperaquine (AK Scientific, H853), and quinacrine (TCI America, Q0056). Unless otherwise indicated, all reagents and solvents were purchased from commercial sources and were used without further purification. Moisture or oxygen sensitive reactions were conducted under an atmosphere of argon or nitrogen gas. ^{1}H nuclear magnetic resonance spectra were recorded on a Varian or Bruker 300 or 400 MHz with Me_4Si, DDS, or signals from residual solvent as the internal standard. Chemical shifts are reported in ppm, and signals are described as s (singlet), d (doublet), t (triplet), q (quartet), m (multiplet), b (broad singlet), and dd(double–doublet). Chemical purities were >95% for all final compounds, as assessed by LCMS analysis at UV 220 nm or ^{1}H NMR.

General procedure for synthesis of backbone (compounds 1 to 34):

A mixture of **starting material 1** (**2-chloro-R$_1$-benzoic acid**) and **starting material 2** (**pR$_2$-aniline)** was heated at 130°C in presence of Cu, K_2CO_3, and isoamyl alcohol generating **intermediate 1**. **1** was mixed with $POCl_3$ at 130°C yielding **intermediate 2** (**9-chloro-2-R$_1$-6-R$_2$-dimethylacridine**) which was mixed with phenol and heated to 100°C under a nitrogen

atmosphere and stirred for 1 hour. To this mixture, amine HNRR' as added (see Schemes 2-4

for comprehensive view of all R groups synthesized). The reaction was stirred at 100°C for 5

hours, cooled to room temperature, and diluted with dichloromethane. The mixture was washed

twice with sodium hydroxide solution (1 N) and twice with ammonium chloride solution. The

organic layer was dried and concentrated. The residue was purified by C18 reverse phase

Biotage column chromatography to give compounds 1-30 (yield: 17% to 85%). The backbone

was further modified in the 2 and 6 positions, substituting alternative halides.

A mixture of **starting material 3** (**2,4-dichlorobenzoic acid**) and **starting material 4**

(**cyclohexylamine)** was heated at 130°C in presence of Cu, K_2CO_3, and isoamyl alcohol

generating **intermediate 2**. **2** was mixed with $POCl_3$ at 130°C yielding **intermediate 2** (**9-

chloro-1,2,3,4-tetrahydroacridine**) which was mixed with phenol and heated to 100°C under a

nitrogen atmosphere and stirred for 1 hour. To this mixture, amine HNRR' was added (see

Schemes 5 for comprehensive view of all R groups synthesized). The reaction was stirred at

100°C for 5 hours, cooled to room temperature, and diluted with dichloromethane. The mixture

was washed twice with sodium hydroxide solution (1 N) and twice with ammonium chloride

solution. The organic layer was dried and concentrated. The residue was purified by C18

reverse phase Biotage column chromatography to give compounds 31-34 (yield: 17% to 85%).

43

High-Performance Liquid Chromatography (HPLC) Results

N[1]-(6-chloro-2-methoxyacridin-9-yl)-N[4],N[4]-diethylbutane-1,4-diamine (VATG001)

^{1}H NMR (CD$_3$OD, 400 Hz) δ: 8.26-8.24 (d, *J* = 9.2 Hz, 1H), 7.87-7.83 (m, 2H), 7.52 (s, 1H), 7.43-7.41 (d, *J* = 9.2 Hz, 1H), 7.30-7.27 (d, *J* = 9.2 Hz, 1H), 3.98 (s, 3H), 3.87-3.83 (t, *J* = 6.8 Hz, 2H), 2.45-2.37 (m, 6H), 1.79-1.72 (m, 2H), 1.54-1.46 (m, 2H), 0.95 (t, *J* = 6.8 Hz, 6H). *m/z* = 386 [M + H]$^+$

N[1]-(3-chloroacridin-9-yl)-N[4],N[4]-diethylbutane-1,4-diamine (VATG002)

^{1}H NMR (CD$_3$OD, 400 Hz) δ: 8.34-8.31 (m, 2H), 7.89-7.86 (m, 2H), 7.74-7.69 (m, 1H), 7.42-7.37 (m, 1H), 7.32-7.28 (m, 1H), 3.98-3.93 (t, *J* = 8.8 Hz, 2H), 2.51-2.41 (m, 6H), 1.86-1.77 (m, 2H), 1.59-1.49 (m, 2H), 0.98-0.94 (t, *J* = 9.2 Hz, 6H). *m/z* = 356.0 [M + H]$^+$

N[1]-(6-chloro-2-methoxyacridin-9-yl)-N[4],N[4]-diethyl-N[1]-methylbutane-1,4-diamine (VATG003)

^{1}H NMR (CD$_3$OD, 300 Hz) δ: 8.28-8.25 (d, *J* = 9.3 Hz, 1H), 8.03 (s, 1H), 7.99-7.96 (d, *J* = 9.3 Hz, 1H), 7.50-7.44 (m, 3H), 4.00 (s, 3H), 3.69-3.65 (t, *J* = 6.9 Hz, 2H), 3.35 (s, 1H), 2.41-2.30 (m, 6H), 1.72-1.62 (m, 2H), 1.49-1.40 (m, 2H), 0.90-0.86 (t, *J* = 6.9 Hz, 6H). *m/z* = 400 [M + H]$^+$

6-chloro-2-methoxy-N-(4-methoxybutyl)acridin-9-amine (VATG004)

^{1}H NMR (CD$_3$OD, 400 Hz) δ: 8.51-8.49 (d, J = 9.2 Hz, 1H), 7.85-7.83 (m, 2H), 7.80-7.77 (d, J = 9.2 Hz, 1H), 7.71-7.69 (d, J = 9.2 Hz, 1H), 7.54-7.52 (d, J = 9.2 Hz, 1H), 4.22-4.20 (t, J = 7.2 Hz, 2H), 4.03 (s, 3H), 3.51-3.48 (t, J = 5.8 Hz, 2H), 2.11-2.07 (m, 2H), 1.79-1.75 (m, 2H). m/z = 345.2 [M + H]$^+$

N^1-(6-chloro-2-methoxyacridin-9-yl)-N^4,N^4-dimethylbutane-1,4-diamine (VATG005)

^{1}H NMR (CD$_3$OD, 400 Hz) δ: 8.21-8.18 (d, J = 9.2 Hz, 1H), 7.78 (s, 1H), 7.76-7.74 (d, J = 9.2 Hz, 1H), 7.46 (s, 1H), 7.35-7.32 (d, J = 9.2 Hz, 1H), 7.22-7.20 (d, J = 9.2 Hz, 1H), 3.88 (s, 3H), 3.79-3.75 (t, J = 7.2 Hz, 2H), 2.19-2.16 (t, J = 7.6 Hz, 2H), 2.04 (s, 6H), 1.72-1.65 (m, 2H), 1.48-1.41 (m, 2H). m/z = 358 [M + H]$^+$

N-(4-(6-chloro-2-methoxyacridin-9-ylamino)butyl)-N-ethylacetamide (VATG006)

^{1}H NMR (CD$_3$OD, 400 Hz) δ: 8.34-8.31 (d, J = 10.4 Hz, 1H), 7.90-7.86 (m, 2H), 7.60 (s, 1H), 7.48-7.46 (d, J = 9.2 Hz, 1H), 7.36-7.34 (d, J = 9.6 Hz, 1H), 4.00 (s, 3H), 3.92-3.91 (b, 2H), 3.30-3.21 (m, 4H), 2.04 (s, 2H), 1.94 (s, 1H), 1.81-1.77 (m, 2H), 1.64-1.61 (m, 2H), 1.11-1.07 (t, J = 6.8 Hz, 2H), 1.01-0.97 (t, J = 6.8 Hz, 1H). m/z = 400.0[M + H]$^+$

N-(4-(6-chloro-2-methoxyacridin-9-ylamino)butyl)-N-ethylmethanesulfonamide (VATG007)

^{1}H NMR (CD$_3$OD, 400 Hz) δ: 8.52-8.49 (d, J = 9.6 Hz, 1H), 7.86 (s, 1H), 7.83 (s, 1H), 7.80-7.77 (d, J = 9.2 Hz, 1H), 7.70-7.67 (d, J = 9.6 Hz, 1H), 4.24-4.20 (t, J = 7.2 Hz, 2H), 4.04 (s, 3H),

3.33-3.25 (m, 4H), 2.86 (s, 3H), 2.11-2.03 (m, 2H), 1.83-1.76 (m, 2H), 1.22-1.81 (t, J = 7.2 Hz, 3H). m/z = 436.0 [M + H]$^+$

N^1-tert-butyl-N^4-(6-chloro-2-methoxyacridin-9-yl)butane-1,4-diamine (VATG008)

^{1}H NMR (CD$_3$OD, 400 Hz) δ: 8.56-8.53 (d, J = 9.6 Hz, 1H), 7.94 (s, 1H), 7.85 (s, 1H), 7.82-7.79 (d, J = 9.2 Hz, 1H), 7.71-7.69 (d, J = 9.2 Hz, 1H), 7.56-7.54 (d, J = 9.2 Hz, 1H), 4.28-4.25 (t, J = 6.4 Hz, 2H), 4.06 (s, 3H), 3.10-3.06 (t, J = 7.2 Hz, 2H), 2.16-2.13 (m, 2H), 1.89-1.87 (m, 2H), 1.40 (s, 9H). m/z = 386.0 [M + H]$^+$

N^1-(6-chloro-2-methoxyacridin-9-yl)-N^4-(cyclopropylmethyl)-N^4-methylbutane-1,4-diamine (VATG009)

^{1}H NMR (CDCl$_3$, 300Hz) δ: 8.05-7.94 (m, 3H), 7.40-7.36 (m, 1H), 7.26-7.23 (m, 2H), 3.93 (s, 3H), 3.75-3.71 (t, 2H, J = 6Hz), 2.48-2.43 (t, 2H, J = 6Hz), 2.29-2.22 (m, 5H), 1.85-1.78 (m, 2H), 1.76-1.65 (m, 2H), 0.87-0.85 (m, 1H), 0.50-0.45 (d, 2H, J = 2.4Hz), 0.09-0.05 (d, 2H, J = 4.8Hz). m/z = 397.3 [M + H]$^+$

6-chloro-2-methoxy-N-(4-(pyrrolidin-1-yl)butyl)acridin-9-amine (VATG012)

^{1}H NMR (CD$_3$OD, 400 Hz) δ: 8.34-8.32 (d, J = 9.6 Hz, 1H), 7.89 (s, 1H), 7.87-7.85 (d, J = 9.2 Hz, 1H), 7.61 (s, 1H), 7.49-7.46 (d, J = 9.2 Hz, 1H), 7.37-7.34 (d, J = 9.2 Hz, 1H), 4.04 (s, 3H), 3.95-3.91 (t, J = 7.0 Hz, 2H), 2.63-2.61 (m, 6H), 1.89-1.82 (m, 6H), 1.69-1.61 (m, 2H). m/z = 384.1 [M + H]$^+$

6-chloro-2-methoxy-N-(4-morpholinobutyl)acridin-9-amine (VATG013)

^{1}H NMR (CD$_3$OD, 400 Hz) δ: 8.32-8.29 (d, J = 9.2 Hz, 1H), 7.89 (s, 1H), 7.88- 7.85 (d, J = 9.2 Hz, 1H), 7.57 (s, 1H), 7.46-7.44 (d, J = 9.2 Hz, 1H), 7.34-7.31 (d, J = 9.2 Hz, 1H), 4.00 (s, 3H), 3.91-3.88 (t, J = 6.8 Hz, 2H), 3.60 (b, 4H), 2.33-2.29 (m, 6H), 1.84-1.78 (m, 2H), 1.60-1.53 (m, 2H). m/z = 400.0 [M + H]$^+$

6-chloro-2-methoxy-N-(4-(4-methylpiperazin-1-yl)butyl)acridin-9-amine (VATG014)

^{1}H NMR (CD$_3$OD, 400 Hz) δ: 8.32-8.30(d, J = 9.2 Hz, 1H), 7.89 (s, 1H), 7.88-7.85(d, J = 9.2 Hz, 1H), 7.57 (s, 1H), 7.46-7.44 (d, J = 9.2 Hz, 1H), 7.34-7.31 (d, J = 9.2 Hz, 1H), 4.00(s, 3H), 3.91-3.88 (t, J = 6.8 Hz, 2H), 2.41-31(m, 10H), 2.25(s, 3H), 1.84-1.77(m, 2H), 1.60-1.53(m, 2H). m/z = 413.0 [M + H]$^+$

N^1-(6-chloro-2-methoxyacridin-9-yl)-N^3,N^3-diethylpropane-1,3-diamine (VATG015)

^{1}H NMR (CD$_3$OD, 400 Hz) δ: 8.56-8.54 (d, J = 9.6 Hz, 1H), 7.97 (s, 1H), 7.87 (s, 1H), 7.83-7.81 (d, J = 9.2 Hz, 1H), 7.73-7.71 (d, J = 9.2 Hz, 1H), 7.58-7.56 (d, J = 9.2 Hz, 1H), 4.34-4.31 (t, J = 7.2 Hz, 2H), 4.08(s, 3H), 3.37-3.27(m, 6H), 2.51-2.43(m, 2H), 1.38-1.35(t, J = 7.2 Hz, 6H). m/z = 372 [M + H]$^+$

N^1-(6-chloro-2-methoxyacridin-9-yl)-N^2,N^2-diethylethane-1,2-diamine (VATG016)

^{1}H NMR (DMSO-d_6, 400Hz) δ: 8.59-8.53 (d, J = 9.6 Hz, 1H), 8.19 (s, 1H), 7.97 (s, 1H), 7.89-7.82 (d, J = 9.2 Hz, 1H), 7.73-7.66 (m, 1H), 7.52-7.45 (d, J = 9.2 Hz, 1H), 4.50 (m, 2H), 3.98 (s, 3H), 3.63 (m, 2H), 3.20 (b, 4H), 1.25-1.21 (t, J = 7.2 Hz, 6H). m/z = 358 [M + H]$^+$

6-chloro-2-methoxy-N-(2-(4-methylpiperazin-1-yl)ethyl)acridin-9-amine (VATG019)

^{1}H NMR (CD$_3$OD, 400 Hz) δ: 8.35-8.33 (d, J = 9.2 Hz, 1H), 7.90-7.86 (m, 2H), 7.50-7.47 (m, 2H), 7.36-7.34 (d, J = 9.2 Hz, 1H), 4.01 (s, 3H), 3.97-3.94 (t, J = 6.0 Hz, 1H), 2.76-2.73 (t, J = 6.0 Hz, 2H), 2.51-2.30 (m, 8H), 2.25 (s, 3H). m/z = 385 [M + H]$^+$

3-chloro-N-(2-(4-methylpiperazin-1-yl)ethyl)acridin-9-amine (VATG020)

^{1}H NMR (CD$_3$OD, 400 Hz) δ: 8.35-8.30 (m, 2H), 7.91-7.86 (m, 2H), 7.78-7.73 (m, 1H), 7.45-7.42 (m 1H), 7.35-7.33 (d, 1H), 4.03-4.00 (t, J = 6.0 Hz, 2H), 2.78-2.76 (t, J = 6.0 Hz, 2H), 2.54-2.41 (m, 8H), 2.25 (s, 3H). m/z = 355.1 [M + H]$^+$

6-chloro-2-fluoro-N-(2-(4-methylpiperazin-1-yl)ethyl)acridin-9-amine (VATG021)

^{1}H NMR (CDCl$_3$, 300 Hz) δ: 8.15-8.08 (m, 3H), 7.82-7.77 (m, 1H), 7.56-7.53 (m, 1H), 7.35-7.32 (m 1H), 3.88-3.84 (t, J = 5.7 Hz, 2H), 2.73-2.71 (t, J = 5.7 Hz, 2H), 2.63 (m, 8H), 2.39 (s, 3H). m/z = 373 [M + H]$^+$

6-fluoro-2-methoxy-N-(2-(4-methylpiperazin-1-yl)ethyl)acridin-9-amine (VATG022)

^{1}H NMR (CDCl$_3$, 300 Hz) δ: 8.24-8.19 (m, 1H), 8.03-8.00 (d, *J* = 9.3 Hz, 1H), 7.71-7.67 (m, 1H), 7.48-7.41 (m 1H), 7.35 (s, 1H), 7.18-7.14 (m, 1H), 3.85 (b, 2H), 2.88-2.43 (m, 10H), 2.42 (s, 3H). *m/z* = 369.1 [M + H]$^+$

6-chloro-N-(1-ethylpiperidin-4-yl)-2-methoxyacridin-9-amine (VATG025)

^{1}H NMR (CD$_3$OD, 400 Hz) δ: 8.29-8.27 (d, *J* = 8.8 Hz, 1H), 7.94 (s, 1H), 7.91-7.88 (d, *J* = 9.2 Hz, 1H), 7.56 (s, 1H), 7.51-7.49 (d, *J* = 9.2 Hz, 1H), 7.43-7.41 (d, *J* = 9.2 Hz, 1H), 4.01(s, 3H), 3.92 (b, 1H), 3.13- 3.10 (m, 2H), 2.59-2.56 (q, *J* = 6.8 Hz, 2H), 2.23- 2.21 (m, 2H), 2.12- 2.09 (m, 2H), 2.00- 1.91 (m, 2H), 1.18-1.14(t, *J* = 6.8 Hz, 3H). *m/z* = 370 [M + H]$^+$

N-(1-ethylpiperidin-4-yl)-6-fluoro-2-methoxyacridin-9-amine (VATG026)

^{1}H NMR (CD$_3$OD, 300 Hz) δ: 8.39-8.34 (m, 1H), 7.91-7.89 (d, *J* = 9.3 Hz, 1H), 7.58-7.53 (m, 2H), 7.50-7.46 (m, 1H), 7.34-7.27 (m, 1H), 4.01(s, 3H), 3.88-3.79 (m, 1H), 3.06- 3.02 (m, 2H), 2.50-2.43 (q, *J* = 7.2 Hz, 2H), 2.10-2.03 (m, 4H), 1.98- 1,84 (m, 2H), 1.15-1.11 (t, *J* = 7.2 Hz, 3H). *m/z* = 354.1 [M + H]$^+$

N-(1-ethylpiperidin-4-yl)-2-methoxyacridin-9-amine (**VATG027**)

^{1}H NMR (CD3OD, 400Hz) δ: 8.29-8.27(d, *J* = 8.8 Hz, 1H), 7.96-7.94 (d, *J* = 8.8 Hz, 1H), 7.92-7.89 (d, *J* = 9.6 Hz, 1H), 7.70-7.66 (m, 1H), 7.53 (m, 1H), 7.46-7.43 (m, 2H), 3.98 (s, 3H), 3.90-3.80 (m, 1H), 3.02-3.8 (bm, 2H), 2.46-2.41(q, 2H, *J* = 7.2 Hz), 2.05-2.00 (m, 4H), 1.93-1.83 (m, 2H), 1.11-1.08(t, 3H, *J* = 7.2 Hz). *m/z* = 336 [M + H]$^+$

N-(1-ethylpiperidin-4-yl)acridin-9-amine VATG028)

^{1}H NMR (CD3OD, 400Hz) δ: 8.35-8.33 (d, J = 8.8 Hz, 2H), 8.00-7.98 (d, J = 8.8 Hz, 2H), 7.78-7.74 (m, 2H), 7.49-7.45 (m, 2H), 4.02-3.97 (m, 1H), 3.05-3.02 (m, 2H), 2.50-2.44 (q, J = 7.2 Hz, 2H), 2.11-2.05 (m, 4H), 1.95-1.87 (m, 2H), 1.15-1.12 (t, J = 7.2 Hz, 3H). m/z = 306.1 [M + H]$^+$

6-chloro-N-(1-ethylpiperidin-4-yl)-2-fluoroacridin-9-amine (VATG029)

^{1}H NMR (CD3OD, 300Hz) δ: 8.29-8.26 (d, J = 9.3 Hz, 1H), 8.05-8.00 (m, 2H), 7.95 (s, 1H), 7.64 (m, 1H), 7.43-7.39 (m, 1H), 3.97-3.83 (m, 1H), 3.06-3.02 (m, 2H), 2.51-2.44 (q, J = 7.2 Hz, 2H), 2.13-2.05 (m, 4H), 1.91-1.87 (m, 2H), 1.16-1.11 (t, J = 7.2 Hz, 3H). m/z = 358.0 [M + H]$^+$

3-chloro-N-(1-ethylpiperidin-4-yl)acridin-9-amine (VATG030)

^{1}H NMR (CD$_3$OD, 400Hz) δ: 8.32-8.30 (m, 2H), 7.94 (s, 2H), 7.78-7.74 (m, 1H), 7.49-7.45 (m, 1H), 7.40-7.38 (d, J = 9.2 Hz, 1H), 4.01-3.96 (m, 1H), 3.04-3.01 (m, 2H), 2.49-2.44 (q, J = 7.2 Hz, 2H), 2.08-2.06 (b, 4H), 1.94-1.86 (m, 2H), 1.15-1.11 (t, J = 7.2 Hz, 3H). m/z = 340 [M + H]$^+$

7-chloro-2-methoxy-N-(2-(4-methylpiperazin-1-yl)ethyl)benzo[β][1,5]naphthyridin-10-amine (**VATG031**)

^{1}H NMR (DMSO-d_6, 400Hz) δ: 8.43-8.41(d, 1H, J = 9.2 Hz), 8.12-8.10 (d, 1H, J = 9.2 Hz), 7.87 (b, 1H), 7.2(s, 1H), 7.2.9-7.27(d, 1H, J = 9.2 Hz) 7.25-7.24(d, 1H, J = 9.2 Hz), 4.10 (m, 2H), 4.06 (s, 3H), 2.70-2.68 (m, 2H), 2.33 (b, 8H), 2.14 (s, 3H). m/z = 386 [M + H]$^+$

6-chloro-N-(2-(4-methylpiperazin-1-yl)ethyl)-1,2,3,4-tetrahydroacridin-9-amine

(**VATG032**)

^{1}H NMR (CDCl$_3$, 300Hz) δ: 7.97-7.95(m, 2H, J = 9 Hz), 7.95-7.91 (d, 1H, J = 9 Hz), 7.28-7.25(m, 1H), 5.25 (b, 1H), 3.58-3.49 (m, 2H), 3.05 (m, 2H), 3.73 (m, 2H), 2.63-2.59(m 10H), 2.39(s, 3H), 1.94-1.90(m, 4H). m/z = 359 [M + H]$^+$

7-chloro-N-(1-ethylpiperidin-4-yl)-2-methoxybenzo[β][1,5]naphthyridin-10-amine

(**VATG033**)

^{1}H NMR (DMSO-d_6, 400Hz) δ: 8.43-8.42(d, J = 9.2 Hz, 1H), 8.11-8.10 (d, 1H, J = 9.2 Hz), 7.84(s, 1H), 7.37-7.35(d, 1H, J = 9.2 Hz) 7.25-7.23(d, 1H, J = 9.2 Hz), 6.95 (b, 1H), 4.98 (b, 1H), 4.00 (s, 3H), 2.85 (b, 2H), 2.30 (b, 2H), 2.02-1.99 (m, 4H), 1.00-1.97 (t, 3H, J = 7.2 Hz). m/z = 371 [M + H]$^+$

6-chloro-N-(1-ethylpiperidin-4-yl)-1,2,3,4-tetrahydroacridin-9-amine (**VATG034**)

^{1}H NMR (DMSO-d_6, 400Hz) δ: 8.07-8.05 (d, J = 9.2 Hz, 1H), 7.71 (d, , J = 2.0 Hz, 1H), 7.36-7.33(dd, J = 9.2, 2.0 Hz, 1H), 3.26 (b, 5H), 2.88-2.85 (m, 4H), 2.69-2.66 (m, 4H), 1.84-1.72 (m, 6H), 1.06 (b, 3H). m/z = 344 [M + H]$^+$

Autophagy Inhibition Screen

U2OS cells stably expressing tfLC3 (Addgene, plasmid 21074) (Kimura, Noda et al. 2007) were seeded at 5,000 cells per well in 5A McCoy's medium (Invitrogen, 16600-082) with 10% fetal bovine serum [FBS (CellGro, 35-101-CV)] in 96-well glass bottom tissue culture

plates for 24 hours at 37 $^\circ$C and 5% CO_2. Cells were treated with a selection of commonly used anti-malarial compounds (amodiaquine, artemisinin, chloroquine, mefloquine, primaquine, piperaquine, and quinacrine) in a 6-point concentration curve for three hours, fixed with 3.7% formaldehyde, and nuclei were stained with Hoechst 33342 (2 µg/mL: Invitrogen, H1399). Cells were visualized using a 60x oil-immersion objective on a Nikon Eclipse Ti fluorescent microscope. Images were qualitatively scored for effective concentration (EC), defined as the concentration at which there was a significant accumulation of tfLC3-labeled puncta over vehicle controls. Cells were later treated with novel VATG compounds in a 6-point dose response for three hours, fixed, and visualized. An EC was established for each VATG compound.

Detailed Autophagy Inhibition Curves

U2OS cells stably expressing tfLC3 were seeded at 50,000 cells per well in 5A McCoy's with 10% FBS on number 1.5 coverglass. Cells were treated with VATG compounds after 24 hours at concentrations of 0.1 µM, 0.25 µM, 0.5 µM, 1 µM, 5 µM, 15 µM, 25 µM, and 50 µM for three hours. Cells were washed with 1x PBS, fixed with 3.7% formaldehyde, and nuclei were stained with Hoechst 33342 (2 µg/mL). Using mounting gel, coverglass was inverted onto microscope slides. Cells were imaged using a 60x oil-immersion objective on a Nikon Eclipse Ti fluorescent microscope and 10 images at each concentration were taken for quantification. Image processing and quantification were completed with the NIS Elements software (Nikon). Representative images were chosen for each concentration and the lookup table (LUT) brightness' were set based on the mean intensity of the DMSO control. All other settings (gain, exposure time, and lamp strength) were kept the constant all conditions. Puncta number was used to determine an effective dose (EC), which is the significant increase in RFP-LC3 labeled

punctae number compared to DMSO control. Auto-fluorescence was tested using wild-type U2OS cells confirming that compound auto-fluorescence did not interfere with ptfLC3 quantification (Figure 2.16).

Quantification of Autophagy Inhibition

U2OS cells stably expressing tfLC3 were seeded at 50,000 cells per well in 5A McCoy's with 10% FBS on number 1.5 coverglass in 24-well tissue culture dishes. After 24 hours, cells were treated with rapamycin [100 nM] (Millipore, 553210-10mg), bafilomycin A1 [100 nM] (AG Scientific, B-1183), AZD-8055 [100 nM] (Selleck Chemicals, S1555), or CQ [50 µM] as well as autophagy inhibitors (CQ, QN, VATG-014, and VATG-032) at doses of 0.1 µM, 0.25 µM, 0.5 µM, 1 µM, 5 µM, 15 µM, 25 µM, and 50 µM for three hours. Cells were washed with 1x PBS, fixed with 3.7% formaldehyde, and nuclei were stained with Hoechst-33342 (2 µg/mL). Coverglass was inverted onto microscope slides using mounting gel. Cells were imaged using a 60x oil-immersion objective on a Nikon Eclipse Ti fluorescent microscope and 10 images at each concentration were taken for quantification. Image processing and quantification were completed with NIS Elements software (Nikon). To quantify, images were deconvolved using a 2D blind deconvolution function with one iteration and settings of normal cell thickness and normal noise level. Regions of interest (ROI) were drawn around the edges of each cell. Intensity thresholds were set to include all pixels equal to or greater than the intensity of the mean background fluorescence using the separation feature and restrictions set for puncta size (Figure 2.3). Objects within the threshold for each ROI were quantified using an automated object count function and exported for analysis. Although other parameters were also collected, the mean intensity of the objects was averaged between the 10 images of each concentration, or

approximately 50 cells (Figure 2.3B and 2.4C). Representative images were chosen for each concentration and the lookup table (LUT) brightness' were set based on the mean intensity of the DMSO control (Figure 2.2A and 2.9A). The mean intensity of each image was divided by the mean intensity of the DMSO control to control for brightness and the LUTs were adjusted by the percent difference to avoid background and for consistent visualization. All other settings (gain, exposure time, and lamp strength) were kept the same across all conditions. Punctae number was used to determine an effective dose (EC), using a two-tailed student t-test the statistically significant (p-value $\leq$ 0.05) increase in RFP- LC3 labeled punctae number compared to DMSO control. Mean intensity was further chosen for quantification as it accurately represents both the increase in puncta number and area when the accumulation of autophagosomes partially fuse (Figure 2.3C and 2.4D). Quantification of the red channel (RFP-LC3 puncta) was performed to determine the total autophagic vesicle population (both autophagosomes and autolysosomes). Auto-fluorescence of each compound was tested using wild-type U2OS cells to confirm that compound auto-fluorescence did not interfere with ptfLC3 quantification (Figure 2.16).

Cell Viability (LD$_{50}$) Screen

U2OS cells were seeded at 500 cells per well in 5A McCoy's with 10% FBS in 96-well clear bottom, black-walled tissue culture plates. After 24 hour incubation, cells were treated with VATG compounds in triplicate with a 10-point half log concentration curve from 0.001 µM to 1000 µM for 24 and 48 hours. Medium was removed and 2x CellTiter-Glo (Promega, G7571) reagent mixed 1:1 with Opti-MEM (Invitrogen, 31985062) was added at 100 µL per well and incubated at room temperature for 15 minutes while rocking. 75 µL per well was moved to a white-walled 96-well plate and luminescence quantified using the 96 LUM program on an

EnVision plate reader (PerkinElmer) and exported for analysis. All triplicate data points were averaged and luminescent readings for each treatment were normalized to vehicle control for change in viability.

Fluorescence-Activated Cell Sorting (FACS) Analysis

U2OS cells were seeded in a 6 well plate in 5A McCoy's with 10% FBS at 100,000 cells per well. After 24 or 48 hours incubation, cells were treated at 1 μM, 3 μM, 10 μM, and 30 μM with CQ, QN, VATG014, or VATG032 for 48 hours. Media was collected and spun down to collect floating cells, discarding the supernatant. Wells were treated with 250 μL 0.25% Trypsin-EDTA and cells were again collected, spun down, and supernatant discarded. Cells were then fixed in 5 mL of 70% ethanol and stored at -20°C for 24 hours. Cells were centrifuged at 300g for 5 min and resuspended in 1 mL 90% chilled methanol. After 30 minutes, cells were washed twice in 3 mL incubation buffer (0.5g BSA in 100mL 1xPBS) and resuspended in 100 μL incubation buffer for 10 minutes. Cells were then incubated with the primary cleaved caspase-3 antibody (Cell Signal Technology, 9661S) at 1:1000 in incubation buffer for one hour. Cells were washed (incubation buffer) and secondary anti-rabbit alexa 546 antibody added 1:1000 for 30 minutes. Cells were then washed and resuspended in 100 μL 1xPBS and acquired using a FACS-Calibur (BD Biosciences).

ATG5/12 and ULK1 Knockdown

U2OS cells were seeded for either the cell viability screen or FACS analysis in 5A McCoy's with 10% FBS. The next day, cells were transfected with either control (non-targeting) siRNA (Qiagen, 1027281) or a pool of two siRNAs targeting ATG5 (ATG5: Qiagen SI00069251 and SI02655310), ATG12 (ATG12: Qiagen SI00298018 and SI02655289), or ULK1 (ULK1:

Qiagen SI02223270 and SI02223277) at a final concentration of 50 nM (total siRNA) using 2 μg

Oligofectamine (Invitrogen,12252-011) per 1 mL transfection volume and Opti-MEM

(Invitrogen, 31985-062) in 5A McCoy's with 10% FBS. Cell viability assays and FACS analysis

were completed as described above after 24 hours transfection. Knockdown was measured using

RNA extracts from siRNA-transfected cells and qRT-PCR with ATG5, ATG12, and ULK1

specific primers and an endogenous HPRT control. Delta-Delta Ct method was used to

determine relative mRNA levels from control, ATG5/12, and ULK1 siRNA-transfected cells.

Transmission Electron Microscopy

U2OS cells were seeded in 10 cm plates in 5A McCoy's with 10% FBS at 1×10^6 cells per

plate. After 24 hours incubation, cells were treated with DMSO (vehicle control), CQ (3 or 100

μM), quinacrine (3 μM), VATG014 (3 μM), or VATG032 (3 μM) for three hours. Following,

cells were trypsinized, washed, pelleted, and resuspended in 2% glutaraldehyde fixative (Sigma,

G5882). Cell pellets were embedded in 2% agarose, post-fixed in osmium tetroxide, and

dehydrated with an acetone series. Cell samples were infiltrated and embedded in Poly/Bed 812

resin and polymerized at 60°C for 24 hours. Ultrathin sections of 70nm were generated with a

Power Tome XL (Boeckeler Instruments) and placed on copper grids. Sections were examined

using a JEOL 100Cx Transmission Electron Microscope at 100kV. Lysosomal structures were

identified by a single membrane structure both containing and lacking cytosolic components, in

addition to lipid droplets that are electron-opaque (Figure 2.12). Transmission electron

microscopy services were performed by Michigan State University Center for Advanced

Microscopy (East Lansing, MI).

Lysosome Analysis by Fluorescent Microscopy

U2OS cells were seeded at 5×10^4 cells per well in 5A McCoy's with 10% FBS on number 1.5 coverglass discs in 24-well tissue culture dishes. After 24 hours, cells were treated with 3 μM CQ, QN, VATG014, or VATG032 for three hours. An hour prior to fixation, media was supplemented with LysoTracker Red DND-99 added at 100 nM (Invitrogen, L7528). Cells were washed with 1x PBS, fixed with 3.7% formaldehyde, permeabilized with 0.2% Triton-X 100, and blocked with 3% bovine serum albumin (BSA) in PBS. LAMP1 antibody (Santa Cruz, sc-18821) was added at 1:1000 for 16 hours at 4°C followed by Alexa-Fluor-488-conjugated anti-mouse IgG (Invitrogen, A11008) 1:5000 for 1 hour at room temperature. Nuclei were stained with Hoechst-33342 (2 μg/mL). Coverglass discs were inverted onto a microscope slide using mounting gel. The microscope slides were imaged using a 60x oil-immersion objective on a Nikon Eclipse Ti fluorescent microscope. Intensity of the red and green channels were visualized using the intensity plot on the Nikon NIS Elements software (Figure 2.13B). Colocalization was determined by using the ratio feature which ratios the intensity of the green channel (LAMP1) over the red channel (LysoTracker Red) per pixel and displays it on a colorimetric scale (Figure 2.14). The RGB threshold of only the color (green) indicating both LAMP1 and LysoTracker Red positivity was performed and data for analysis. The Mander's colocalization coefficient was produced from the Nikon NIS Elements software.

Immunoblotting Analyses

For immunoblotting, U2OS cells were seeded in 10 cm plates in 5A McCoy's with 10% FBS at 1×10^6 cells per plate. After 24 hours, cells were treated with CQ, QN, VATG014, or

VATG032 in a concentration response of 0.3 μM, 1 μM, 3 μM, 10 μM, and 30 μM for three hours. After treatment, cells were lysed [10mM KPO_4, 1mM EDTA, 10mM $MgCl_2$, 5mM EGTA, 50mM bis-glycerophosphate, 0.5% NP_40, 0.1% Brij35, 0.1% sodium deoxycholate, 1mM $NaVO_4$, 5mM NaF, 2mM DTT, and complete protease inhibitors (Sigma, P8340-5mL)] and 50 μg of protein was resolved by SDS-PAGE. Proteins were transferred to PVDF membranes and probed with primary antibodies [LC3 (Sigma, L7543-200UL), α-tubulin (Sigma, T6199), cathepsin B (Santa Cruz, sc-13985)] for 16 hours at 4^0C followed by a secondary antibody [HRP-linked rabbit or mouse IgG (GE Healthcare, NA934 or NA931) or Odyssey IRDye 680CW Goat anti-rabbit IgG (LI-COR, 926-32221) or IRDye 800CW Goat anti-mouse IgG (LI-COR, 926-32210)] for 1 hour at room temperature. Proteins were detected with enhanced chemiluminescence or using an Odyssey imager (LI-COR) and quantified.

ACKNOWLEDGEMENTS

TABLES

Table 2.1. Relative autophagy inhibition for each anti-malarial compound
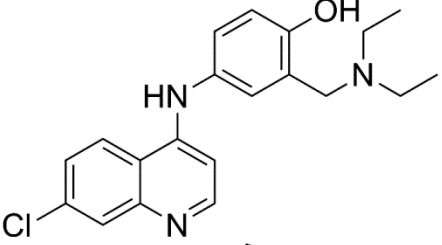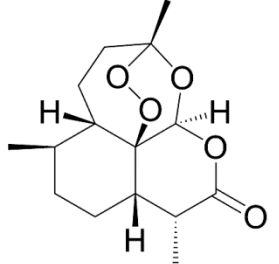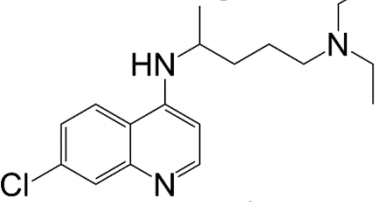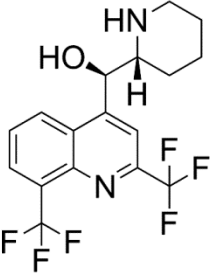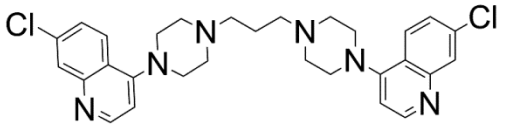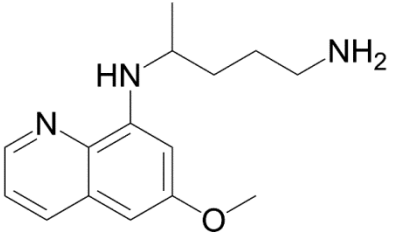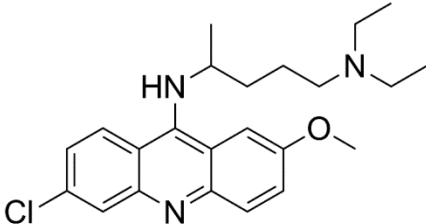
Anti-malarial		Effective Concentration (EC)	Potency (EC/EC$_{CQ}$)
Amodiaquine		15µM	1
Artemisinin		15µM	1
Chloroquine		15µM	1
Mefloquine		0.5µM	30
Piperaquine		50µM	0.25
Primaquine		50µM	0.25

Table 2.1 (cont'd)

Anti-malarial		Effective Concentration (EC)	Potency (EC/EC$_{CQ}$)
Quinacrine		0.25µM	60

U2OS cells were treated in a concentration curve with each anti-malarial and effective concentrations (EC) were determined as a significant increase of punctae above background. Potency was determined by comparing the EC to the EC of CQ.

Table 2.2 Structural overview of Scheme 2.
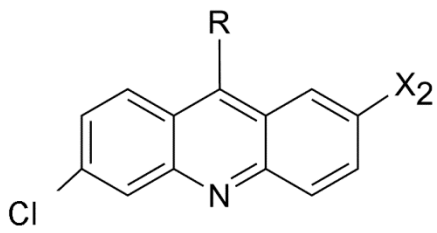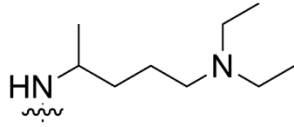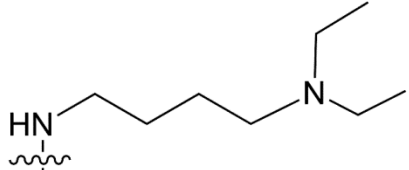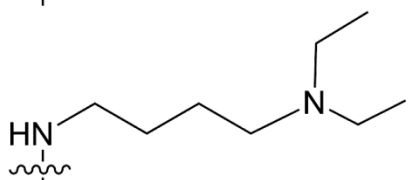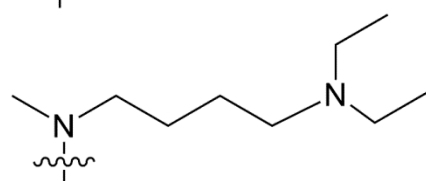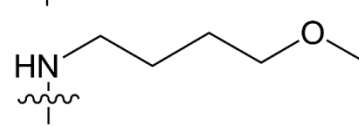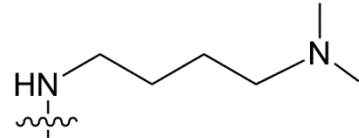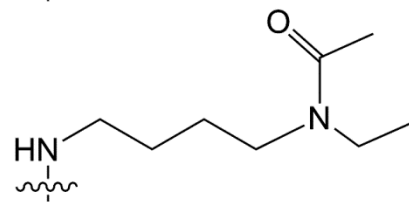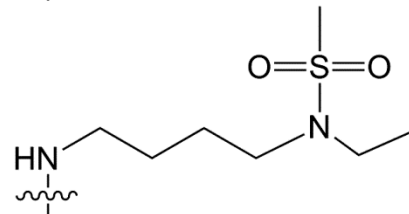
Compound	R	X	LD50	EC50
Quinacrine		methoxy	2.5 μM	0.2 μM
VATG001		methoxy	1 μM	0.25 μM
VATG002		-H	6 μM	0.25 μM
VATG003		methoxy	4 μM	2.5 μM
VATG004		methoxy	1 μM	0.25 μM
VATG005		methoxy	1 μM	0.25 μM
VATG006		methoxy	12.5 μM	0.25 μM
VATG007		methoxy	3 μM	5 μM

Table 2.2 (cont'd)
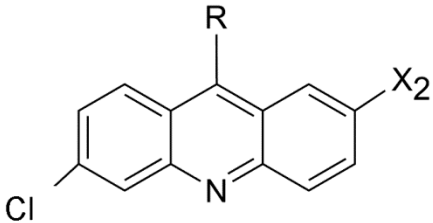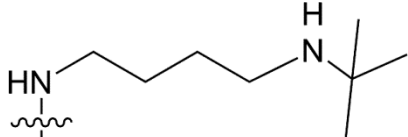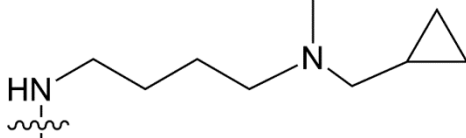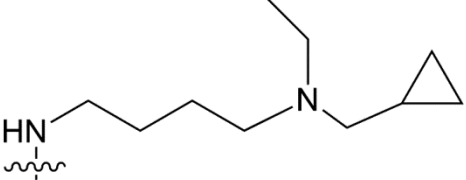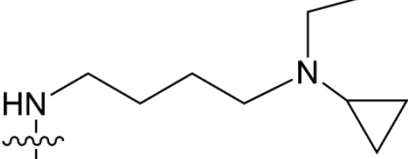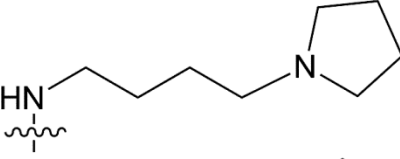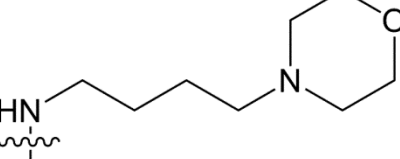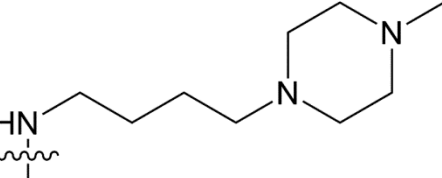
Compound	R	X	LD$_{50}$	EC$_{50}$
VATG008		methoxy	3.5 μM	5 mM
VATG009		methoxy	0.2 μM	0.25 μM
VATG010		methoxy	1.5 μM	0.25 μM
VATG011		methoxy	2 μM	0.5 μM
VATG012		methoxy	0.5 μM	0.25 μM
VATG013		methoxy	12.5 μM	2.5 μM
VATG014		methoxy	0.7 μM	0.1 μM

Table 2.3. Structural Overview of Scheme 3.
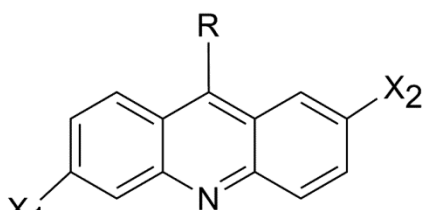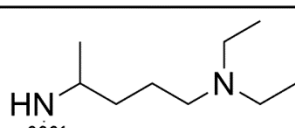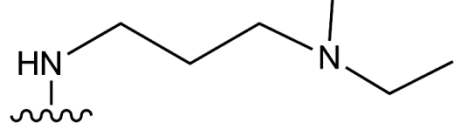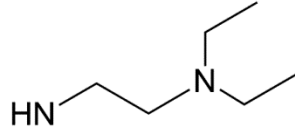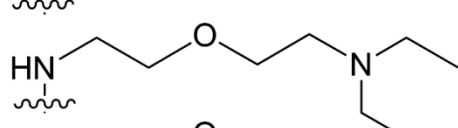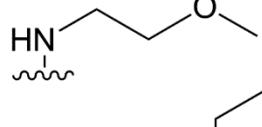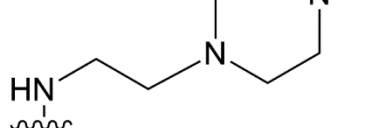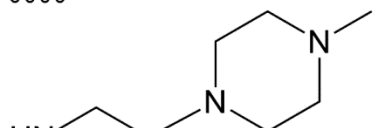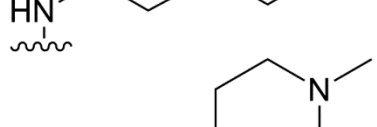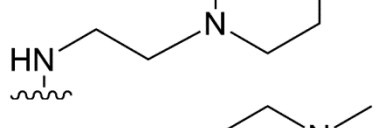
Compound	R	X1	X2	LD50	EC50
Quinacrine		-Cl	methoxy	2.5 μM	0.2 μM
VATG015		-Cl	methoxy	1.5 μM	2.5 μM
VATG016		-Cl	methoxy	7 μM	0.25 μM
VATG017		-Cl	-H	4 μM	0.25 μM
VATG018		-Cl	methoxy	0.25 μM	5 μM
VATG019		-Cl	methoxy	0.5 μM	0.25 μM
VATG020		-Cl	-H	0.5 μM	0.5 μM
VATG021		-Cl	-F	0.5 μM	0.5 μM
VATG022		-F	methoxy	0.5 μM	0.5 μM

Table 2.4 Structural overview of Scheme 4.
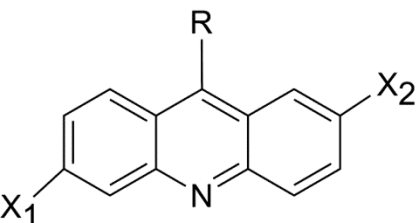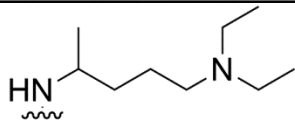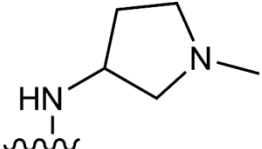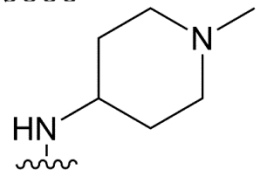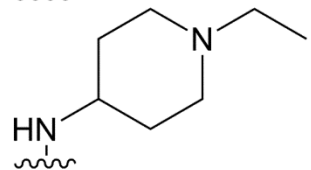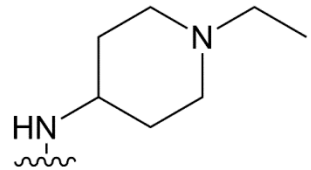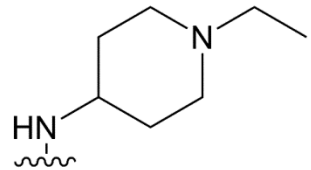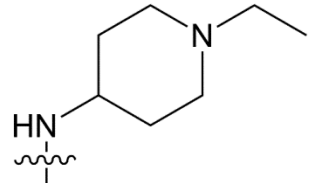
Compound	R	X1	X2	LD50	EC50
Quinacrine		-Cl	methoxy	2.5 μM	0.2 μM
VATG023		-Cl	methoxy	4 μM	0.5 μM
VATG024		-Cl	methoxy	2.5 μM	0.25 μM
VATG025		-Cl	methoxy	3 μM	0.25 μM
VATG026		-F	methoxy	4μM	0.5 μM
VATG027		-H	methoxy	0.5 μM	0.25 μM
VATG028		-H	-H	0.5 μM	0.5 μM

Table 2.4 (cont'd)
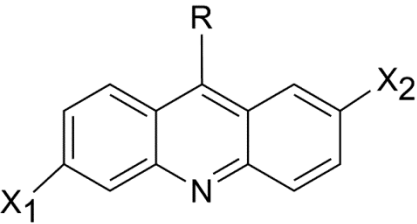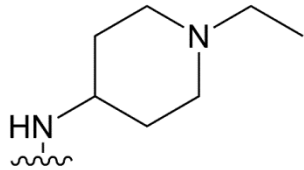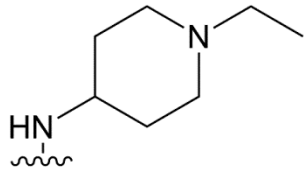
Compound	R	X$_1$	X$_2$	LD$_{50}$	EC$_{50}$
VATG029	HN—(4-(1-ethylpiperidinyl))	-Cl	-F	12.5 μM	0.5 μM
VATG030	HN—(4-(1-ethylpiperidinyl))	-Cl	-H	0.5 μM	0.5 μM

Table 2.5 Structural overview of Scheme 5.
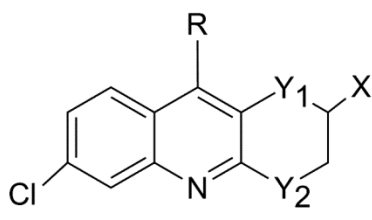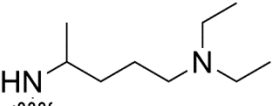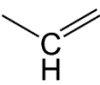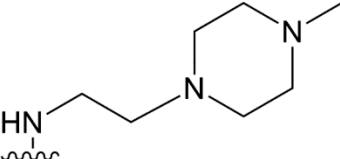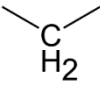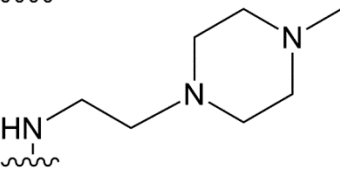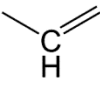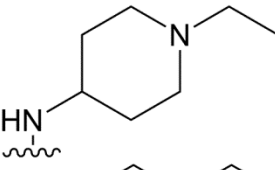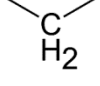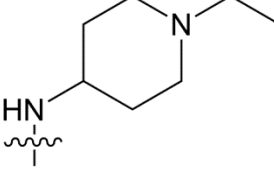
Compound	Y1	Y2	R	X	LD50	EC50
Quinacrine	——	——		methoxy	2.5 μM	0.2 μM
VATG031	N=	=CH		methoxy	0.5 μM	0.25 μM
VATG032	CH2	CH2		-H	27 μM	0.5 μM
VATG033	N=	=CH		methoxy	0.5 μM	0.5 μM
VATG034	CH2	CH2		-H	27 μM	0.25 μM

Table 2.6. Relative autophagy inhibition (EC), cytotoxicity (LD$_{50}$), and chemical structure of two selected novel autophagy inhibitors.

Compound	Y$_1$	Y$_2$	R	X	Effective Concentration	Potency	IC$_{50}$
Chloroquine	methoxy	—		—	15 μM	1	75 μM
Quinacrine				methoxy	0.25 μM	60	2.5 μM
VATG-014				methoxy	0.1 μM	150	0.7 μM
VATG-032				-H	5 μM	3	27 μM

Figure 2.1 Anti-malarial compounds function as autophagy inhibitors.
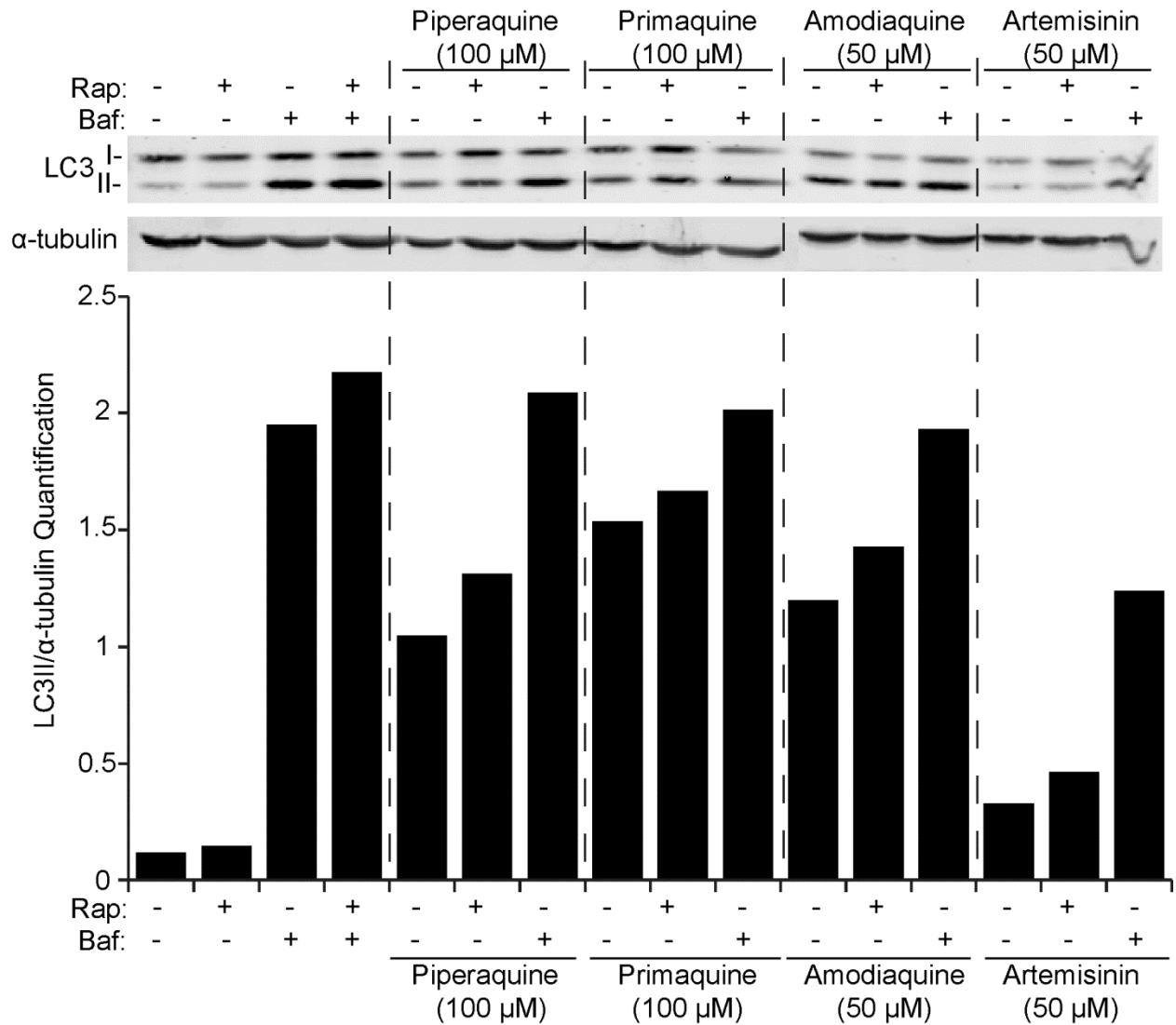
(A) Immunoblot of U2OS cells treated with effective concentrations of piperaquine (100 μM), primaquine (100 μM), amodiaquine (50 μM), and artemisinin (50 μM) for three hours (+) with and without (-) rapamycin (Rap; 100 nM) or bafilomycin A1 (BafA1; 100 nM). Cell lysates were probed by immunoblotting for endogenous LC3 (LC3-I: cytosolic; LC3-II: membrane-bound).

Figure 2.1 (cont'd)

Alpha-tubulin was included as a loading control. Quantification was performed using the Odyssey infrared imaging system and values of LC3-II/α-tubulin determined.

Figure 2.2. Quinacrine inhibits autophagy more potently than chloroquine.
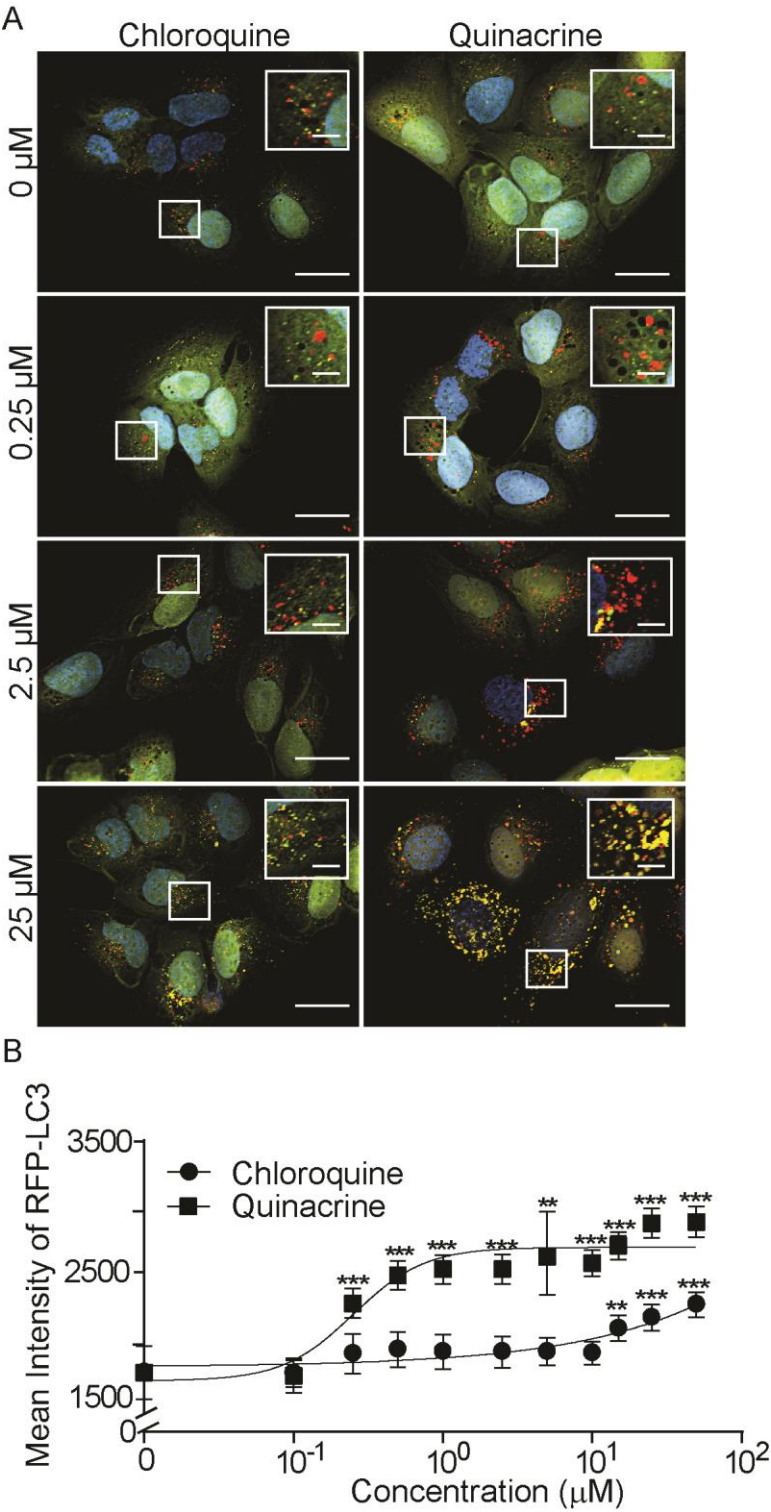
Figure 2.2 (cont'd)

(**A**) U2OS cells expressing tandem fluorescent LC3 (tfLC3) were treated for 3 hours with chloroquine or quinacrine at the concentrations indicated, fixed, and imaged at 60x magnification. Green: GFP-LC3B; Red: RFP-LC3B, Blue: Hoechst (nuclei). Scale bars are 20 μm. Insets are at 2x magnification with scale bars set at 5 μm. (**B**) Mean intensity of RFP-LC3B-positive puncta was quantified using image analysis software on an average of 50 cells following treatment with chloroquine (filled circles) or quinacrine (open circles) at the indicated concentrations. Error bars indicate standard deviation. Two-tailed student t-test was used to determine significant p-value of < 0.05 (*), 0.01(**), and 0.001(***).

Figure 2.3. Autophagic vesicle quantification method utilized to determine the effective dose of autophagy inhibition.

A

2D Deconvolution → Define Region of Interest (ROI) Single Cell → Threshold/Mean Intensity of ROI → Automated Measurements Exported to Excel for Quantification
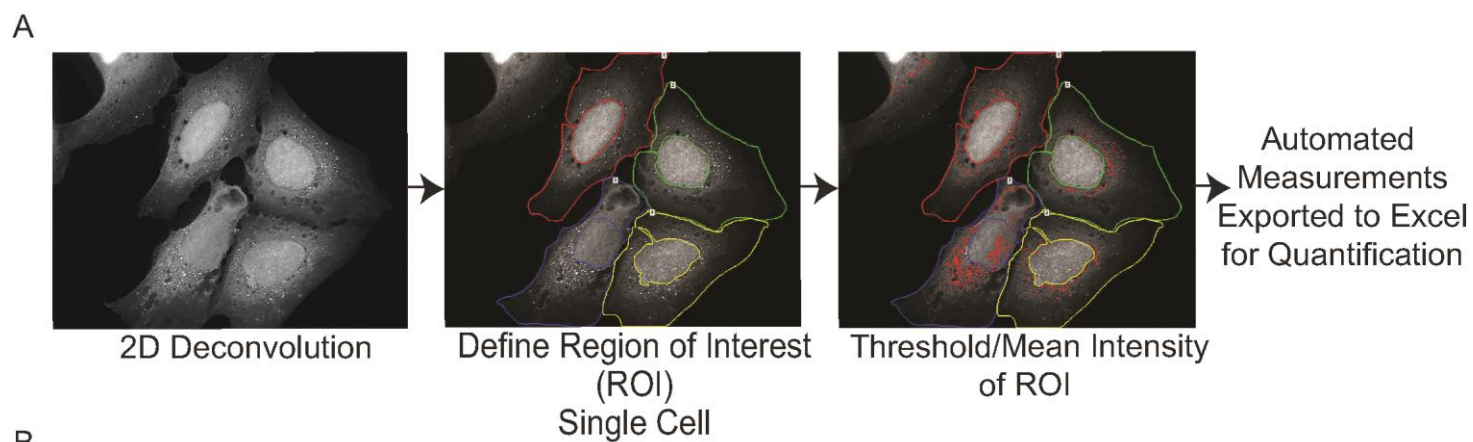
B

Compound	Puncta Number	Mean Intensity	Cell Number	Total Intensity/Cell	Puncta/Cell
Control	2934	1186	49	72882	60
CQ	7546	1411	63	171160	120
AZD	8231	1436	62	205497	133
AZD.CQ	11349	1450	67	249413	170
Rap	6326	1323	53	155428	119
Rap.CQ	9912	1533	52	270529	190

Figure 2.3 (cont'd)

C

D
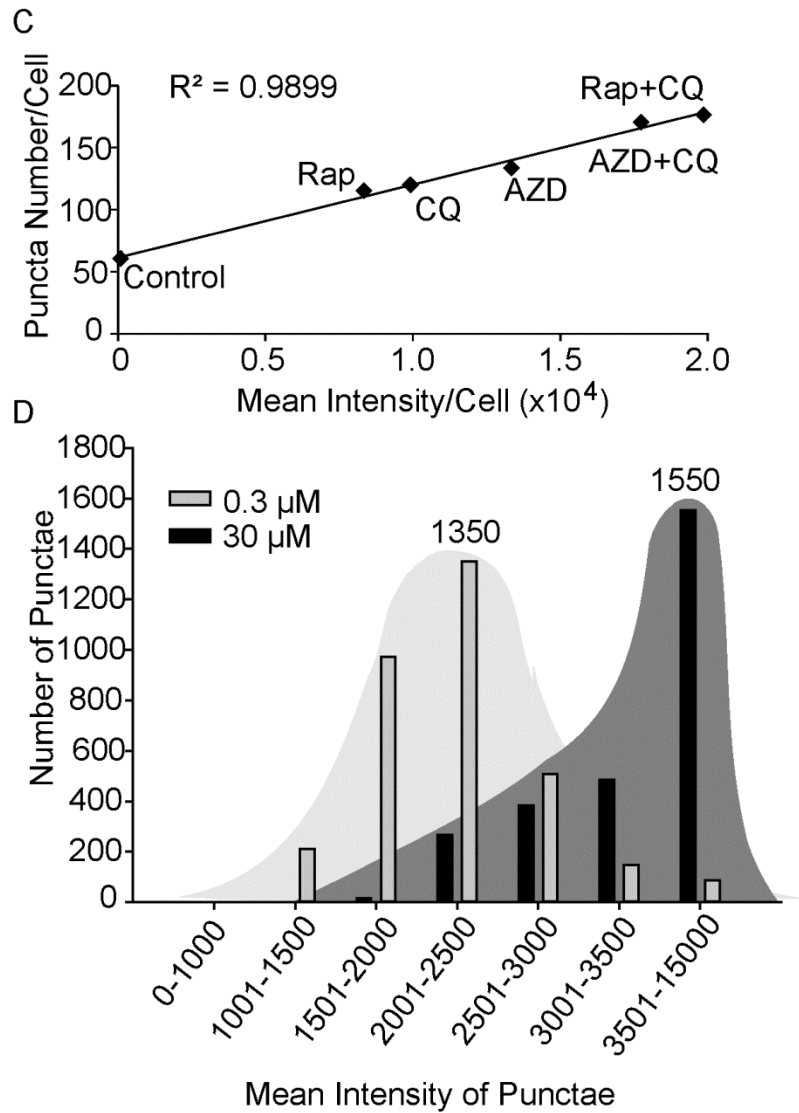
(**A**) Images of U2OS-tfLC3 cells were first processed using a 2D blind deconvolution step within image analysis software. Regions of interest (ROIs) were then drawn around each cell. An intensity threshold was defined to include bright RFP-LC3-postive objects while minimizing background. The binary images created from thresholding are shown in red. Object data within the ROIs that is above the threshold indicates an autophagosome. Data collected includes number of objects, in which ROI an object resides, mean

Figure 2.3 (cont'd)

object intensity, and mean object area. (**B**) Raw data of known autophagy inducers (rapamycin

and AZD-8055) and inhibitor (CQ) showing puncta number, mean intensity, cell number,

average intensity per cell, and puncta per cell values compared to a control. (**C**) Association plot

of the mean intensity of RFP-LC3-positive puncta per cell against the puncta number per cell.

The correlation coefficient (R^2) was determined to be 0.9899. (**D**) Relationship between number

of puncta and puncta mean intensity (RFP-LC3) after VATG-027 treatment. The X-axis

contains mean intensity bins while the Y-axis is the number of puncta. The light grey bars

indicate the 0.3 µM concentration with the light grey area denoting distribution and the black

bars indicate the 30 µM concentration with the dark grey area denoting distribution. The

numbers above the bars are the total number of puncta. The higher concentration of VATG-027

shows a distribution of puncta with a higher mean intensity.

Figure 2.4. Scheme 1: Chemical Synthesis of Backbone for Compounds VATG001-030

Reagents and conditions: i) Cu, K_2CO_3, isoamyl alcohol, $130^{\circ}C$; ii) $POCl_3$, $130^{\circ}C$; iii)

$HNRR'$, $100^{\circ}C$, Phenol

Figure 2.5. Scheme 2: R group Synthesis of Compounds VATG001-014 Shown in Table 1.

1: R_3 = diethylamine

2: R_3 = diethylamine R_2 = H

3: R_3 = diethylamine X_1 = methyl

4: R_3 = methoxy

5: R_3 = dimethylamine

6: R_3 = *N*-ethylacetamide
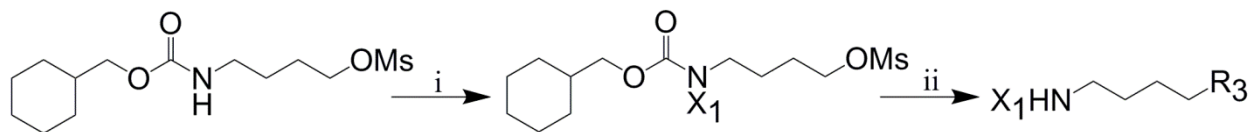
7: R_3 = *N*-ethylmethanesulfonamide

8: R_3 = 2-methylpropan-2-amine

9: R_3 = 1-cyclopropyl-*N*-methylmethanamine

10: R_3 = *N*-(cyclopropylmethyl)ethanamine

11: R_3 = *N*-ethylcyclopropanamine

12: R_3 = pyrrolidine

13: R_3 = morpholine

14: R_3 = 1-methylpiperazine

Reagents and Conditions: i) THF, heat, HR$_3$; ii) H$_2$, Pd/C, MeOH

All compounds contain R_1 = Cl and R_2 = methoxy, unless otherwise noted.

Figure 2.6. Scheme 3: R group Synthesis of Compounds VATG015-022 Shown in Table 2
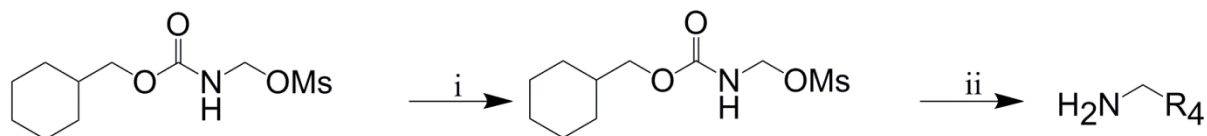
15:R_4 = triethylamine   **19:**R_4 = 1,4-dimethylpiperazine

16:R_4 = *N*-ethyl-*N*-methylethanamine **20:**R_4 = 1,4-dimethylpiperazine R_2 = H

17:R_4 = N,N-diethyl-2-methoxyethan **21:**R_4 = 1,4-dimethylpiperazine R_2 = F

     -1-amine R_2 = H   **22:**R_4 = 1,4-dimethylpiperazine R_1 = F

18:R_4 = methoxymethane

Reagents and Conditions: i) THF, heat, HR_4; ii) H_2, Pd/C, MeOH

All compounds contain R_1= Cl and R_2=methoxy, unless otherwise noted.

Figure 2.7. Scheme 4: R group Synthesis of Compounds VATG023-030 Shown in Table 3
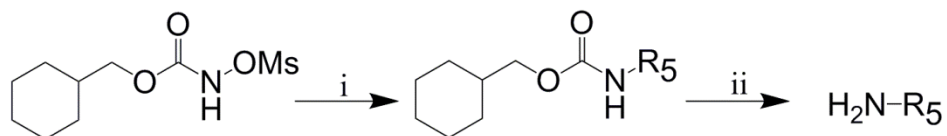
23:R_1 = Cl R_2 = methyl R_5 = 1,3-dimethylpyrrolidine

24:R_1 = Cl R_2 = methyl R_5 = 1,4-dimethylpiperidine

25:R_1 = Cl R_2 = methyl R_5 = 1-ethyl-4-methylpiperidine

26:R_1 = F R_2 = methyl R_5 = 1-ethyl-4-methylpiperidine

27:R_1 = H R_2 = methyl R_5 = 1-ethyl-4-methylpiperidine

28:R_1 = H R_2 = H R_5 = 1-ethyl-4-methylpiperidine

29:R_1 = Cl R_2 = F R_5 = 1-ethyl-4-methylpiperidine

30:R_1 = Cl R_2 = H R_5 = 1-ethyl-4-methylpiperidine

Reagents and Conditions: i) THF, heat, HR_5; ii) H_2, Pd/C, MeOH

Figure 2.8. Scheme 5: Chemical Synthesis of Backbone and R groups of Compounds

VATG031-034 Shown in Table 4

Starting Material   Intermediate
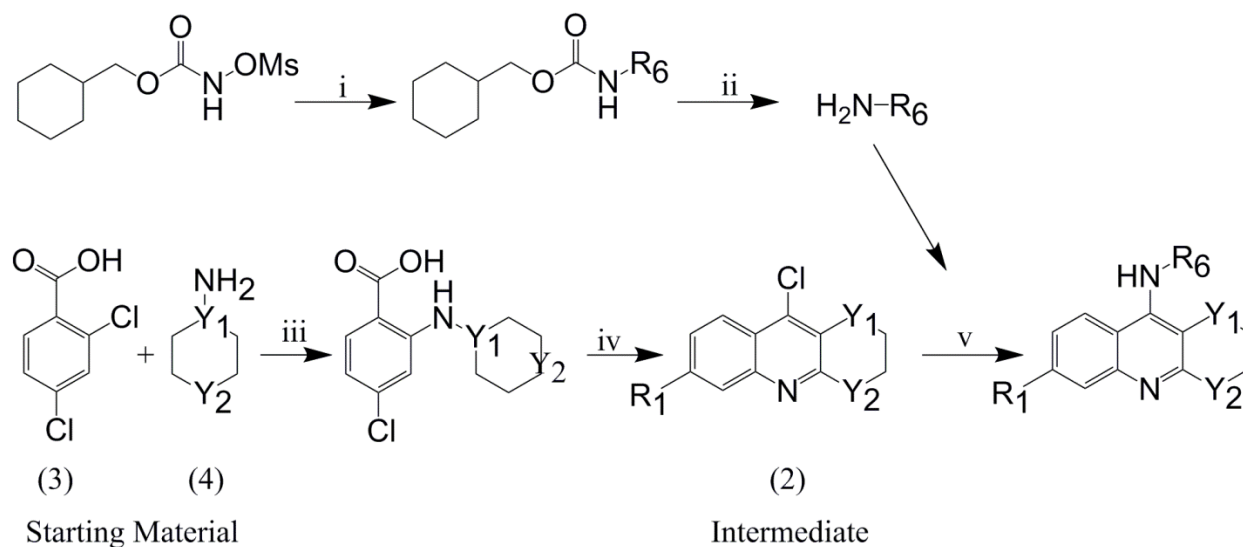
31: Y_1 = *N*-methylmethanimine Y_2 = prop-1-ene R_6 = 1-ethyl-4-methylpiperazine

32: Y_1 = propane Y_2 = propane R_6 = 1-ethyl-4-methylpiperazine

33: Y_1 = *N*-methylmethanimine Y_2 = prop-1-ene R_6 = 1-ethyl-4-methylpiperidine

34: Y_1 = propane Y_2 = propane R_6 = 1-ethyl-4-methylpiperidine

Reagents and Conditions: i) THF, heat, HR_6; ii) H_2, Pd/C, MeOH; iii) Cu, K_2CO_3, isoamyl alcohol, 130°C; iv) $POCl_3$, 130°C; v) H_2NR_6, 100°C, Phenol

All compounds contain R_1= Cl, unless otherwise noted.

Figure 2.9. VATG014 and VATG032 show greater autophagy inhibition than chloroquine.
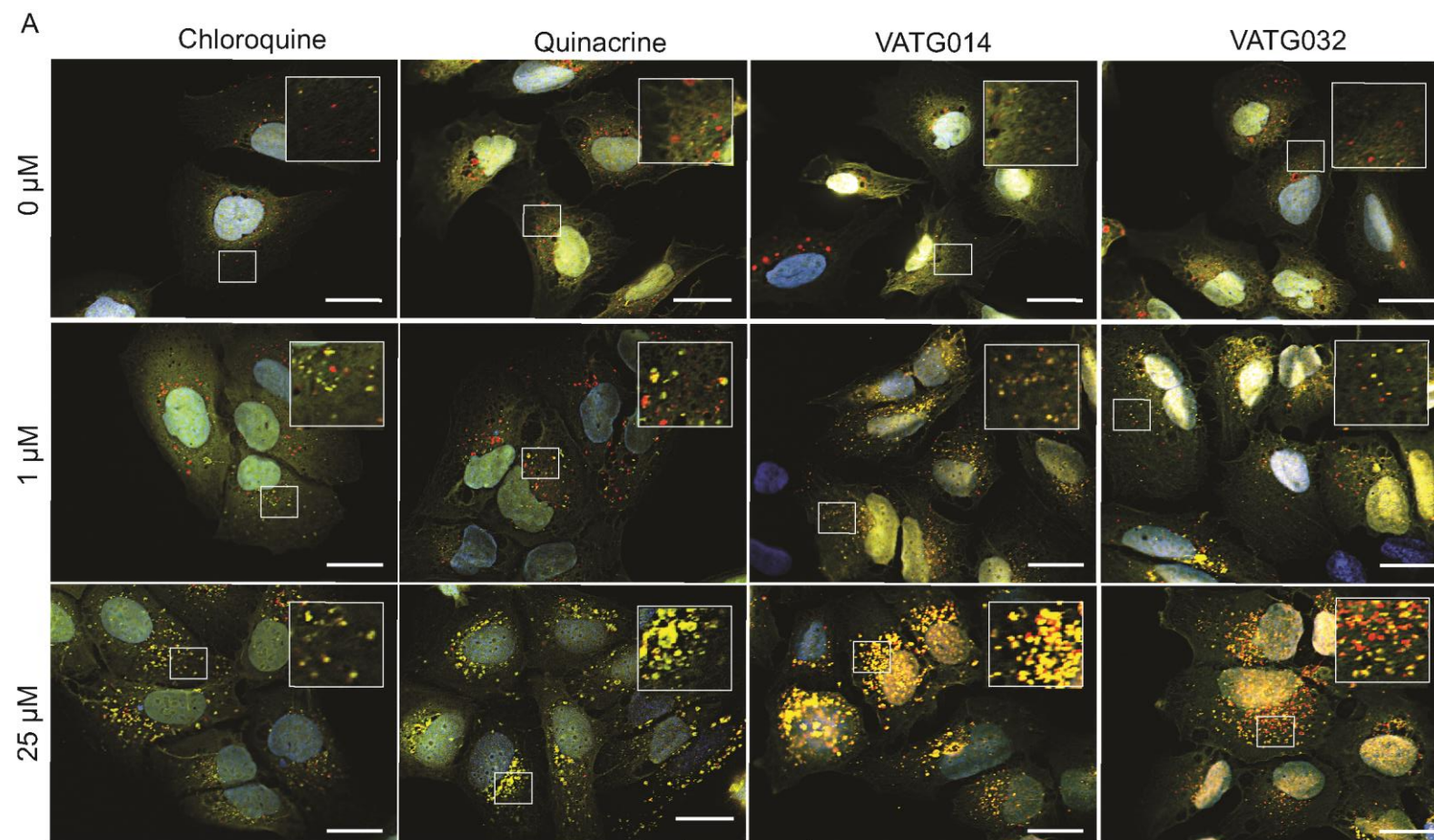
Figure 2.9 (cont'd)
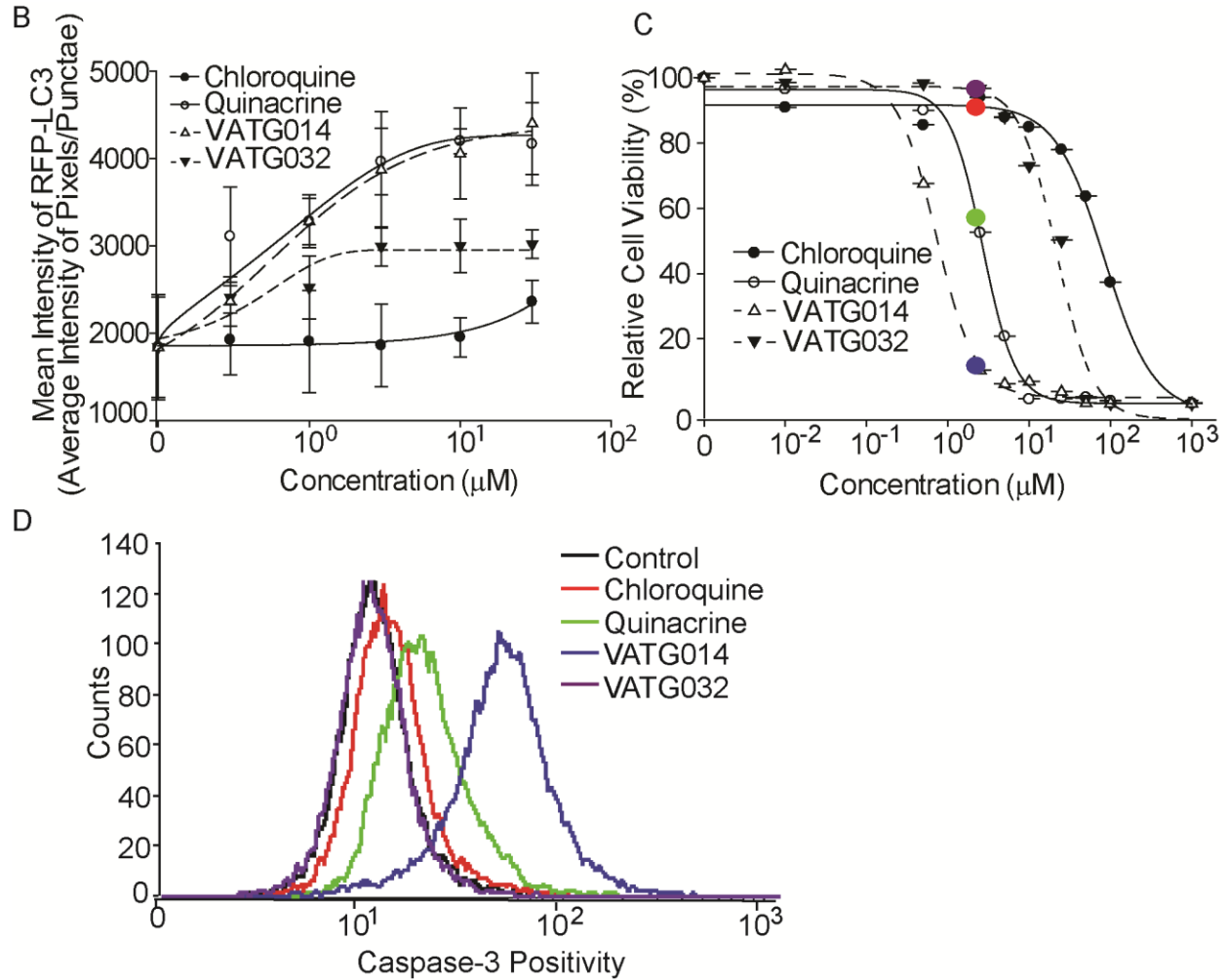
(**A**) U2OS cells expressing tfLC3 were treated for 3 hours with chloroquine, VATG014, or VATG032 at the indicated concentrations, fixed, and imaged at 60x magnification. Green: GFP-LC3; Red: RFP-LC3; Blue: Hoechst (nuclei). Scale bars are 20 μm. Insets are at a 2.5x magnification with scale bars set at 8 μm. (**B**) Mean pixel intensity of RFP-LC3 (red) puncta over a concentration curve with chloroquine (filled circles, solid line), VATG014 (closed triangles, dashed line), and VATG032 (open triangles, dashed line). Error bars indicate standard deviation. Two-tailed student t-test determined significant p-values < 0.05 (*), 0.01 (**), and 0.001 (***). (**C**) Percentage of cell viability compared to a DMSO control determined by

Figure 2.9 (cont'd)

CellTiter-Glo after 48 hours of treatment with chloroquine, quinacrine, VATG014 or VATG032. Error bars indicate standard deviation. Colored circles highlight the viability of each compound treatment used in D. (**D**) FACS analysis of cleaved caspase-3 after treatment with 3 μM chloroquine, quinacrine, VATG014, and VATG032.

Figure 2.10. Quantification of autophagy inhibition using endogenous LC3 after quinacrine, VATG014, and VATG032 treatment.

A
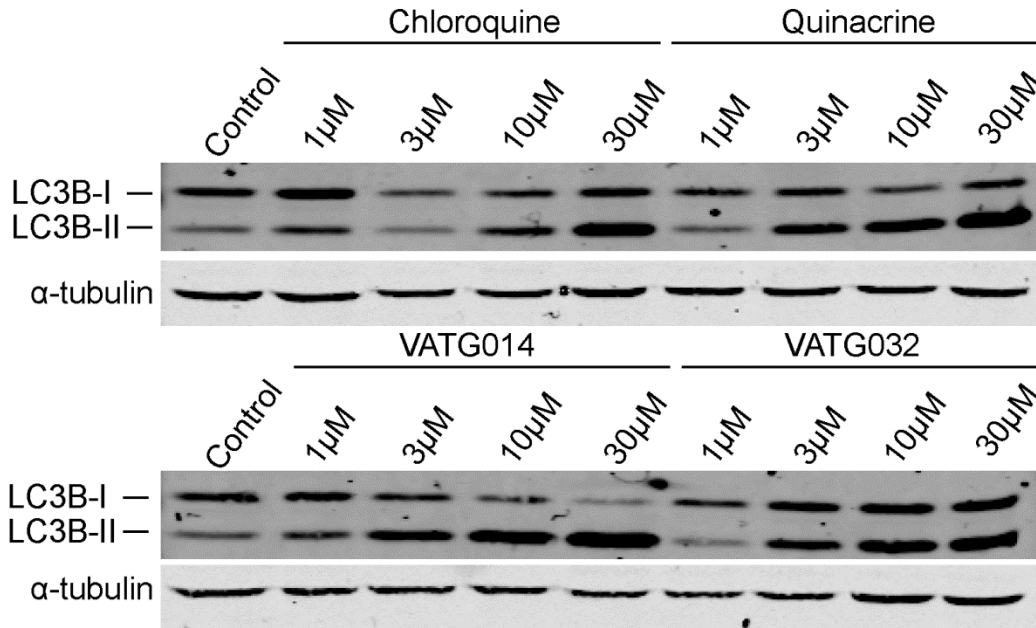
B
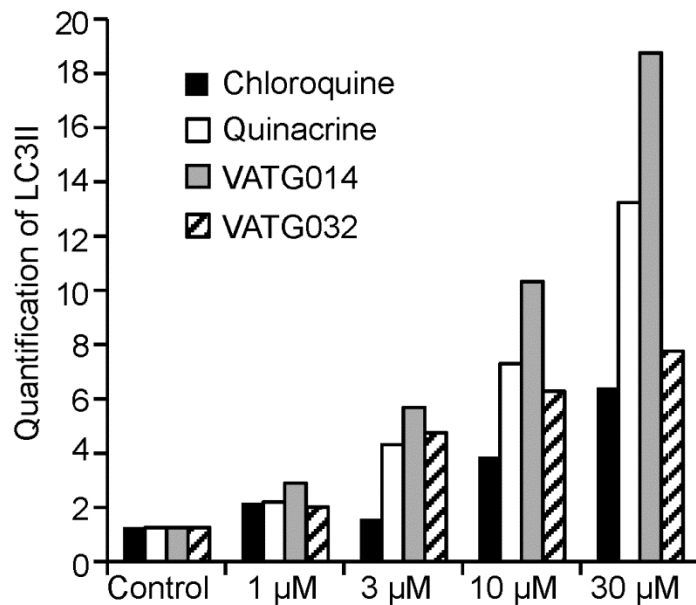
(A) immunoblot of U2OS cells treated with 1 μM, 3 μM, 10 μM and 30 μM of chloroquine, quinacrine, VATG014, or VATG032 for three hours. Cell lysates were probed by immunoblotting for endogenous LC3 (LC3-I: cytosolic; LC3-II: membrane-bound). Alpha-

Figure 2.10 (cont'd)

tubulin was included as a loading control. (**B**) Quantification of LC3-II immunoblot bands from

above after normalized to α-tubulin.

Figure 2.11. Chloroquine, quinacrine, VATG014, and VATG032 cytotoxicity is independent of autophagy.

Figure 2.11 (cont'd)

B

C
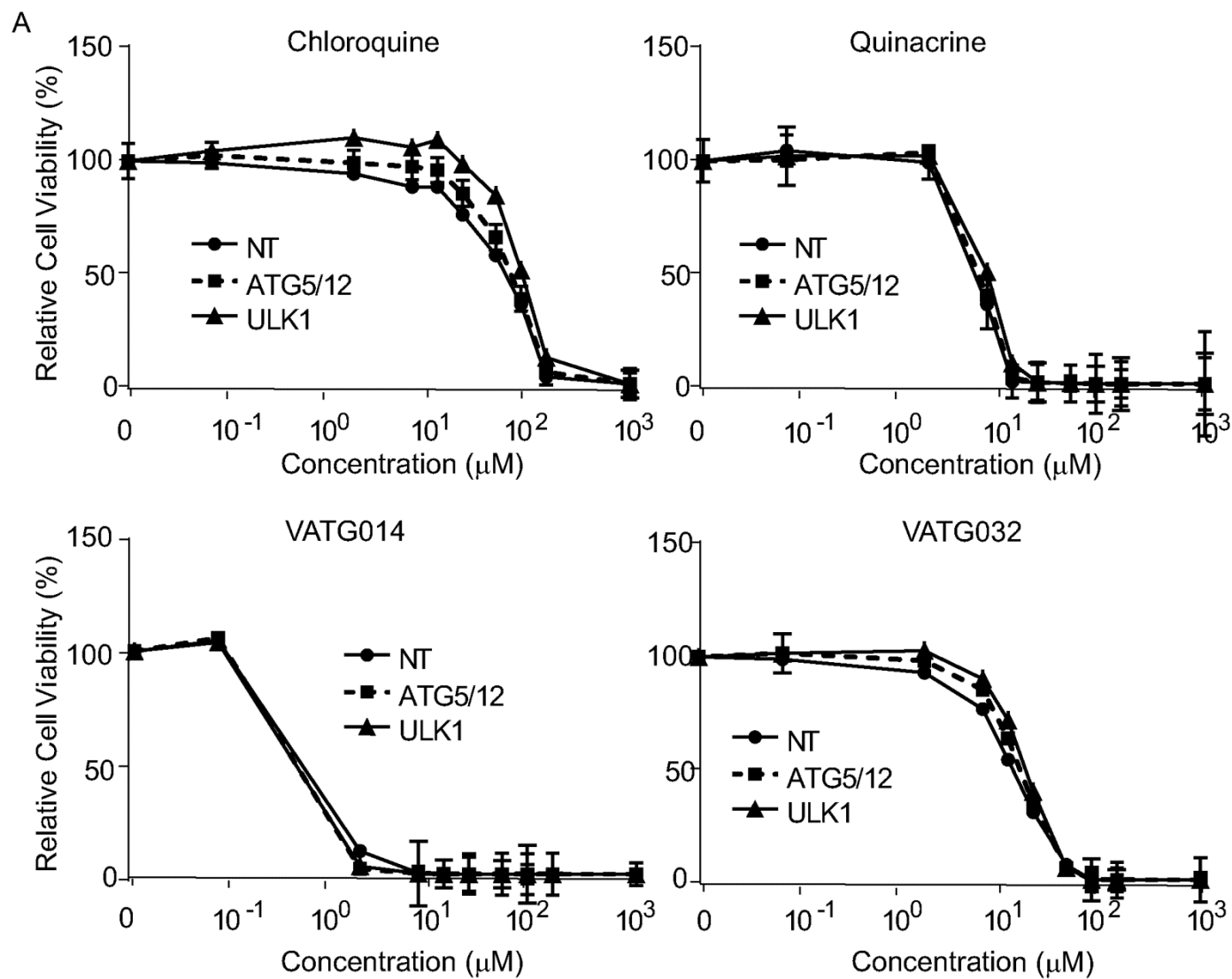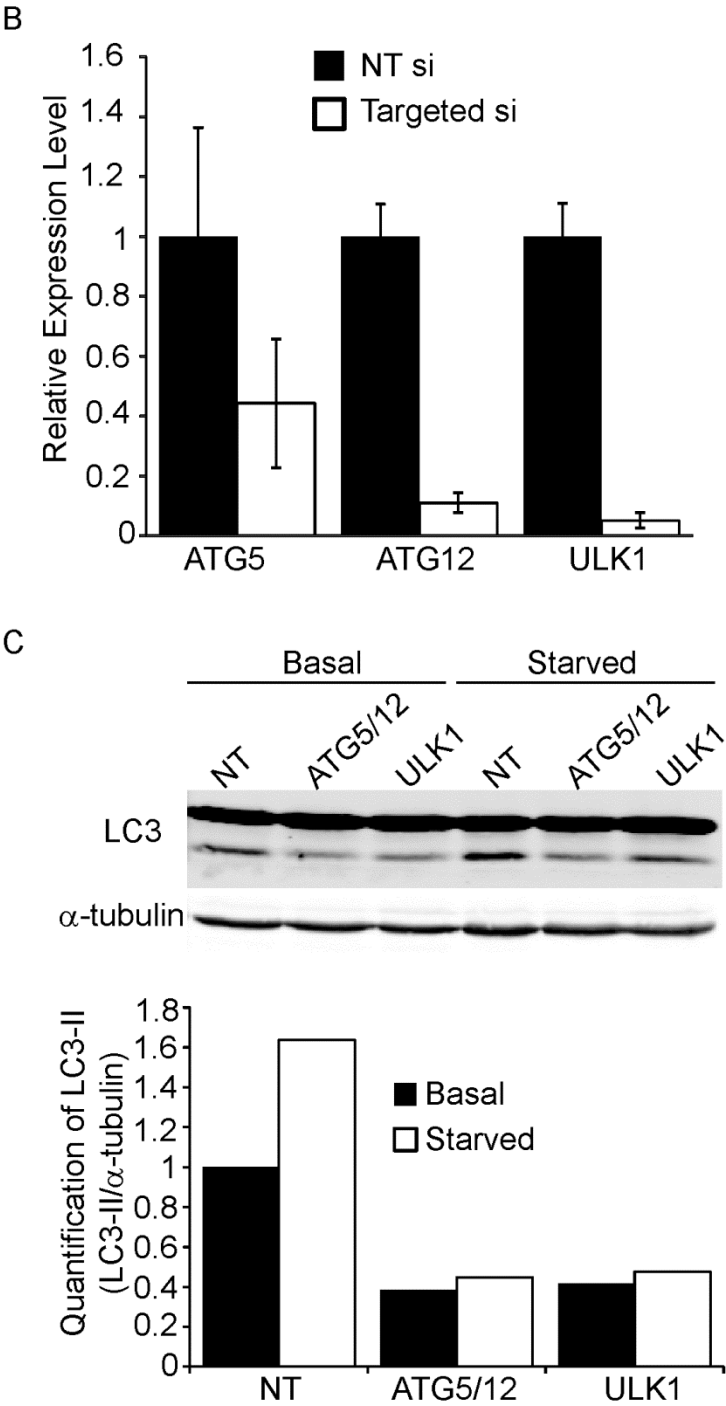
(**A**) Percentage of cell viability compared to a DMSO control determined by CellTiter-Glo after

48 hours of treatment with chloroquine, quinacrine, VATG014 or VATG032 with non-targeting

Figure 2.11 (cont'd)

(NT) siRNA compared to siRNA targeting ATG5/12 or ULK1. Error bars indicate standard deviation. (**B**) qRT-PCR showing relative change in mRNA transcripts after treatment with ATG5/12 or ULK1 siRNA compared to NT siRNA. (**C**) Immunoblot of U2OS cells treated with NT siRNA compared to siRNA targeting ATG5/12 or ULK1 under both basal and starved nutrient conditions. Cell lysates were probed by immunoblotting for endogenous LC3 (LC3-I: cytosolic; LC3-II: membrane-bound). Alpha-tubulin was included as a loading control and was quantified along with LC3-II.

Figure 2.12. Chloroquine, quinacrine, VATG014, and VATG032 cytotoxicity is independent of autophagy.
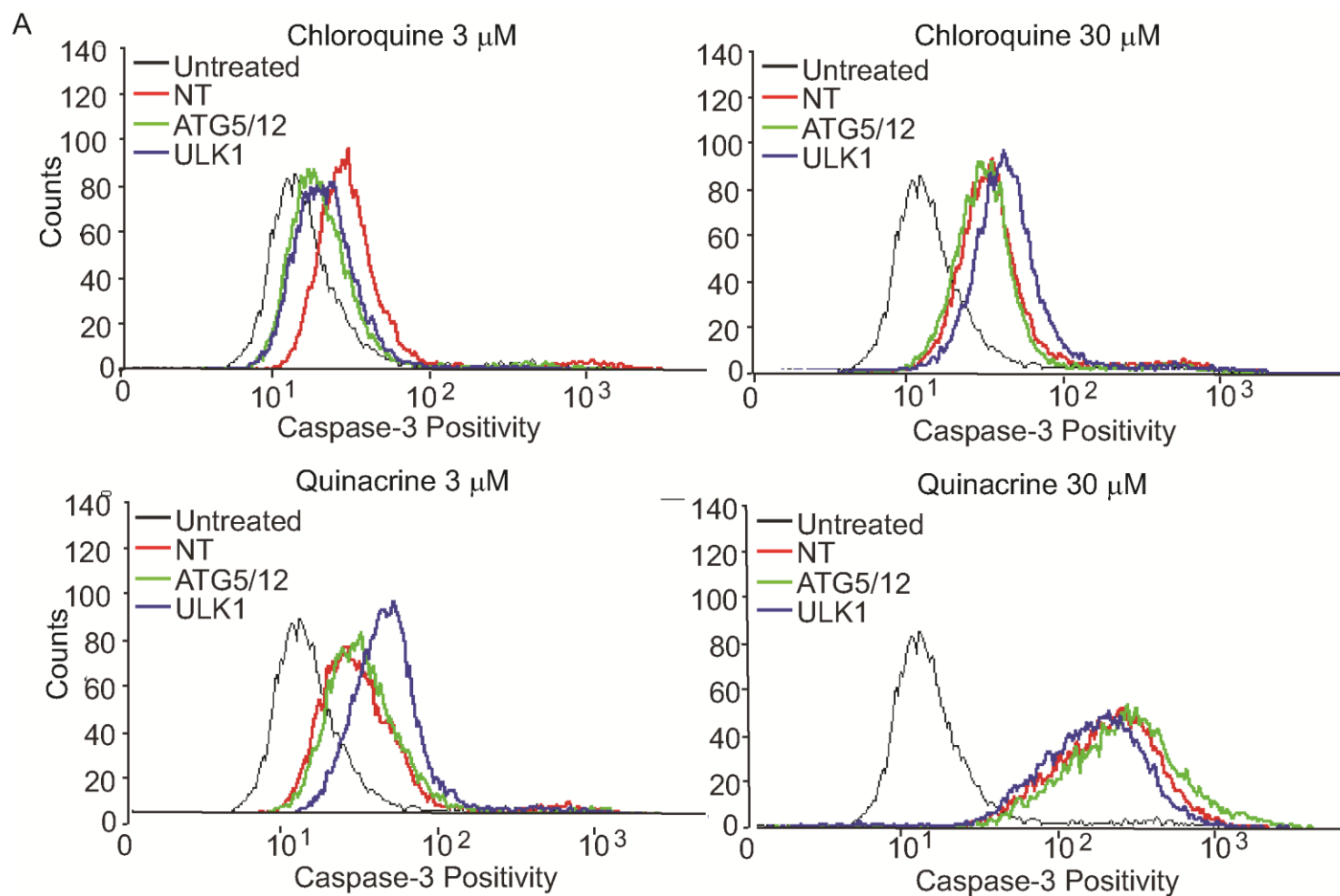
Figure 2.12 (cont'd)

B
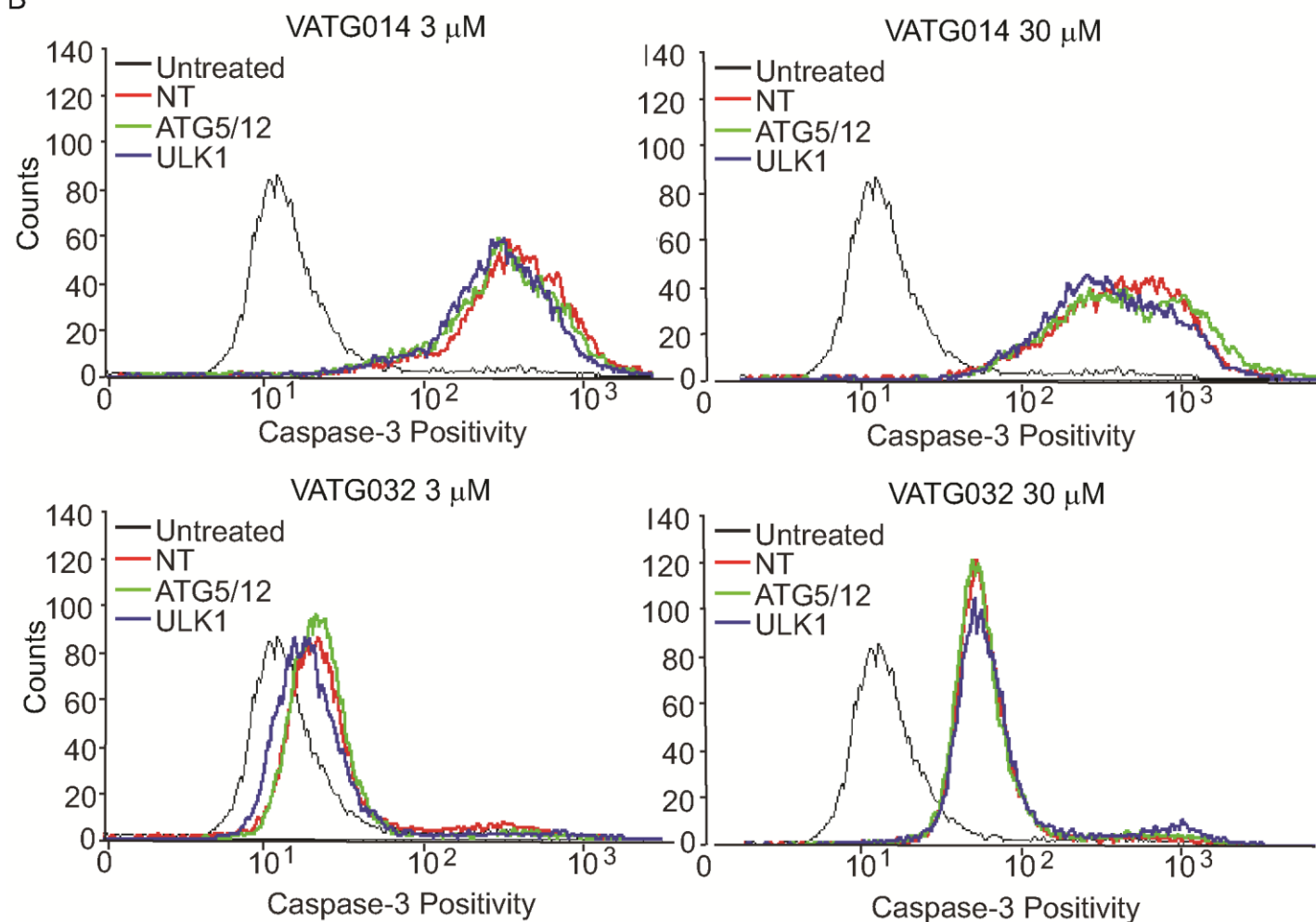
(**A**) FACS analysis of cleaved caspase-3 after treatment with 3 μM or 30 μM chloroquine and quinacrine for 48 hours, following 24

hour treatment with non-targeting (NT) siRNA or siRNA targeting ATG5/12 or ULK1 (total 72 hours knockdown) or untreated

90

Figure 2.12 (cont'd)

control. Caspase-3 positive cells show a shift in fluorescence from untreated control at $\log 10^1$ to $\log 10^2$, while counts is the total number of cells detected. (**B**) FACS analysis of cleaved aspase-3 after treatment with 3 μM or 30 μM VATG014 and VATG032 for 48 hours following 24 hour treatment with NT siRNA or siRNA targeting ATG5/12 or ULK1 (total 72 hours knockdown) or untreated control. Caspase-3 positive cells show a shift in fluorescence from untreated control at $\log 10^1$ to $\log 10^2$, while counts is the total number of cells detected.

Figure 2.13. Autophagy inhibitors inactivate lysosomes and cause accumulation of cytosolic vesicles.
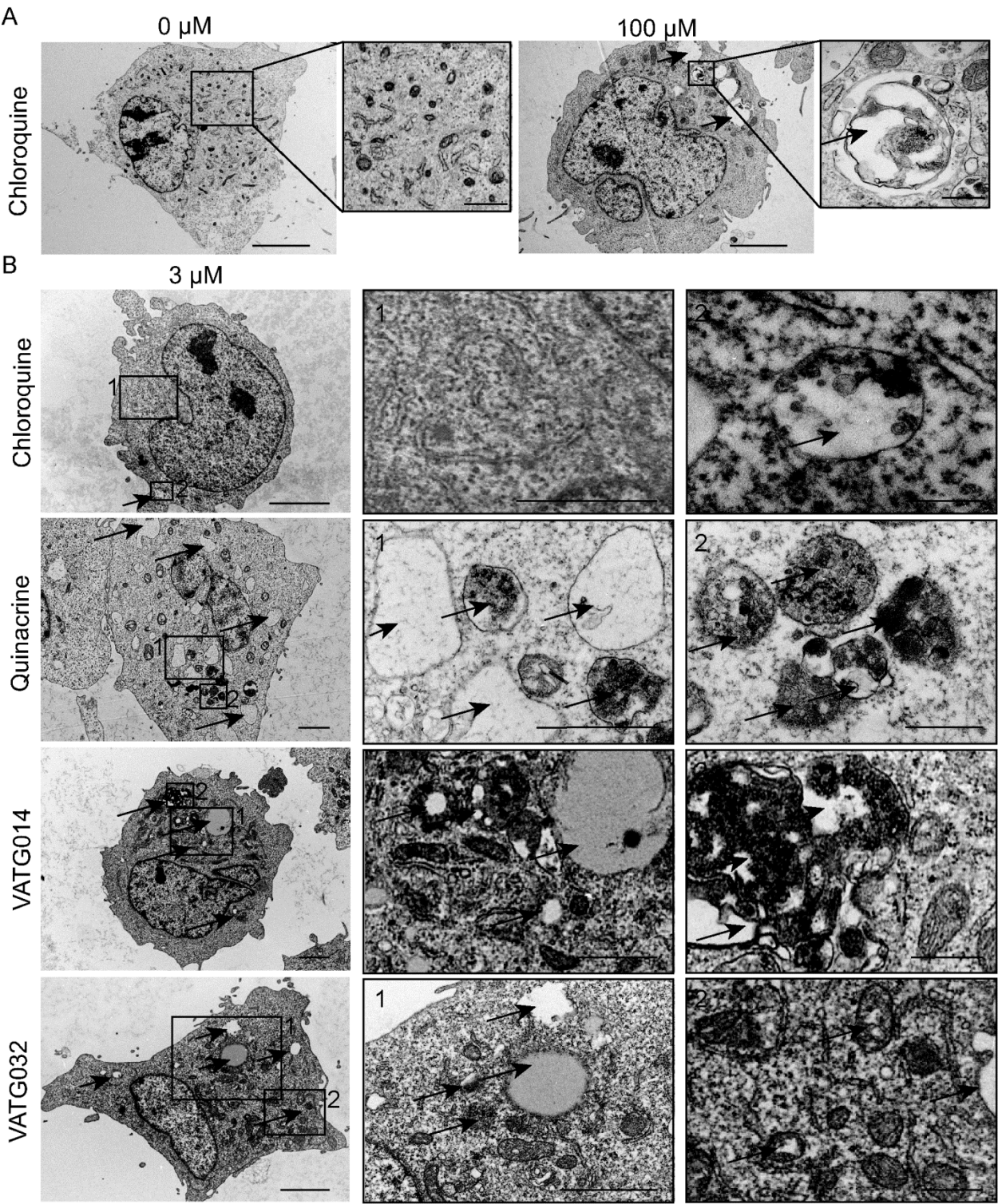
Figure 2.13 (cont'd)
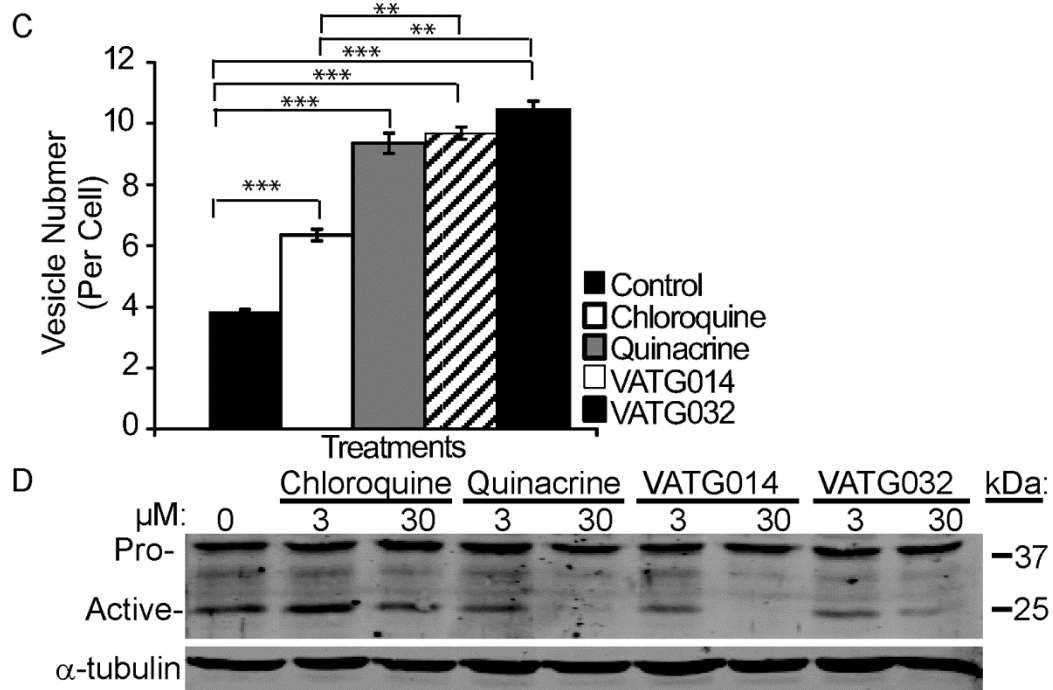
(A) U2OS cells were treated for 3 hours with a vehicle control or 100 μM chloroquine, fixed, and analyzed by transmission electron microscopy (TEM). Accumulation in both size and number of electron dense and lucent vesicles, consistent with lysosomes and endosomes (black arrows), is observed following chloroquine treatment. Scale bar indicates 2 μm. Panels on the right are magnifications of the boxed regions (scale bars are 1.14 μm and 500 nm, respectively). **(B)** U2OS cells were treated for 3 hours with 3 μM of chloroquine, quinacrine, VATG014, or VATG032, fixed, and analyzed by TEM. Electron-dense and electron-lucent vesicles are indicated with black arrows. Scale bar indicates 2 μm in the images on the left. Panels on the right are magnified images of the boxed regions indicated by number (scale bars are 1.2 μm and 500nm, respectively for panels 1 and 2). **(C)** Mean values of the quantification of vesicle accumulation as shown in B across 20 images. Error bars indicate standard deviation and significant p-values < 0.01 (**) and 0.001 (***) as compared to control and CQ determined by a

93

(B) Figure 2.13 (cont'd)

two-tailed student t-test. (**D**) Immunoblot of U2OS cells treated with 3 μM and 30 μM of chloroquine, quinacrine, VATG014, and VATG032 for 6 hours. Cell lysates were probed using immunobloting for pro and active forms of cathepsin B. Alpha-tubulin was included as a loading control.

Figure 2.14 Autophagy inhibitors decrease lysosomal pH and impair lysosomal turnover.
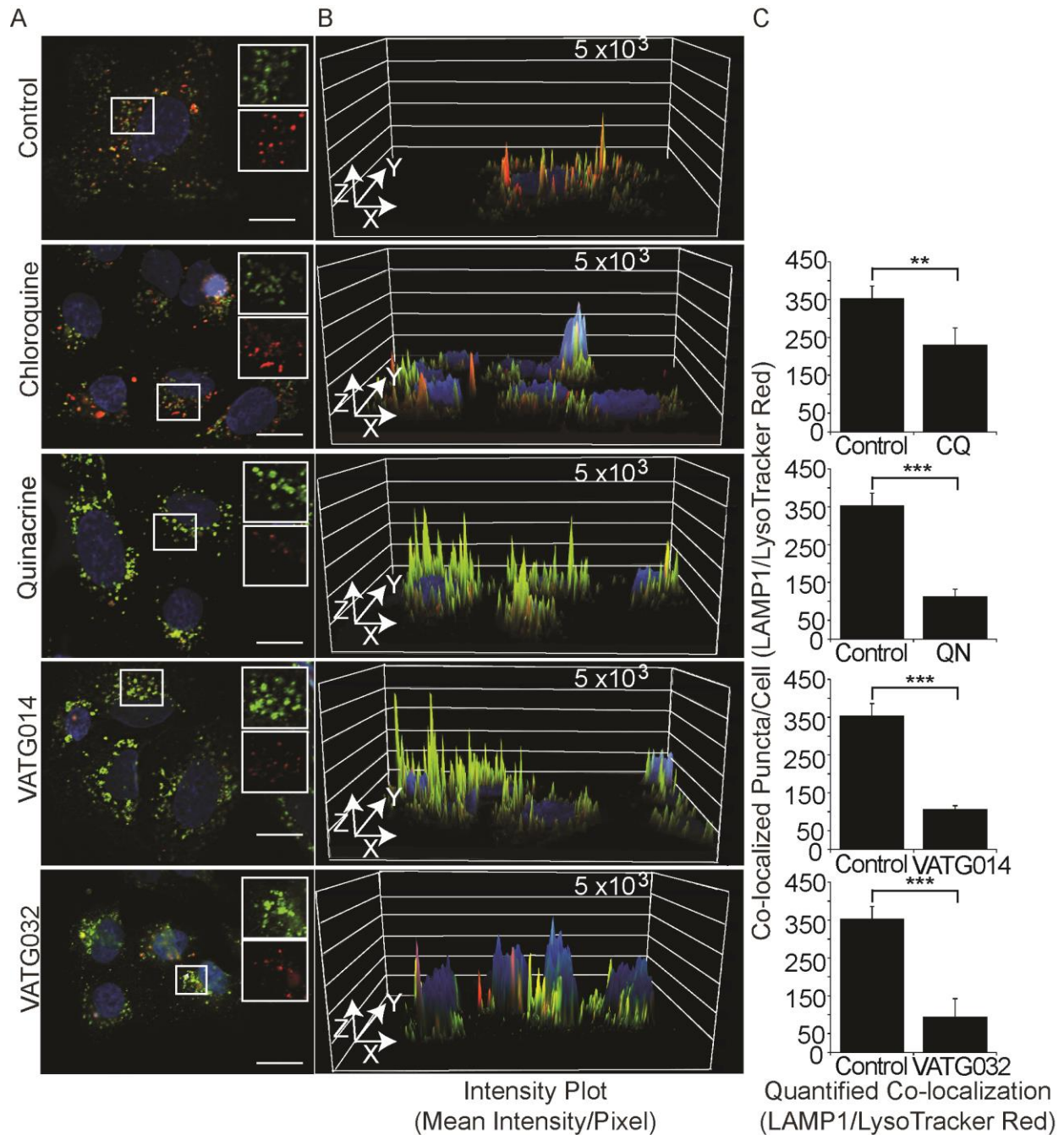
Intensity Plot
(Mean Intensity/Pixel)

Quantified Co-localization
(LAMP1/LysoTracker Red)

(A) U2OS cells were treated for 3 hours with vehicle control or 3 μM autophagy inhibitor (chloroquine, quinacrine, VATG014, or VATG032). Cells were stained with 100 nM LysoTracker Red for one hour prior to fixation, shown in red. Cells were stained by immunofluorescence with endogenous LAMP1 antibody and fluorescently conjugated secondary

Figure 2.14 (cont'd)

antibody (green), followed by Hoechst staining (blue nuclei), then imaged at 60x magnification.

Scale bars are 20 μm. Smaller insets show the red and green channels separated and magnified

1.5x. (**B**) Intensity plots were generated using image analysis software and the intensities of red

and green channels are displayed on the Z axis (peaks) of a 3D representation of the images in A.

(**C**) Quantification of co-localized LAMP1/LysoTracker Red as described in *Materials and*

Methods. Two-tailed student t-test determined significant p-values < 0.01 (**) and 0.001 (***)

and Mander's co-localization coefficient (MCC).

Figure 2.15. Quantification of co-localization of LAMP1/LysoTracker Red.
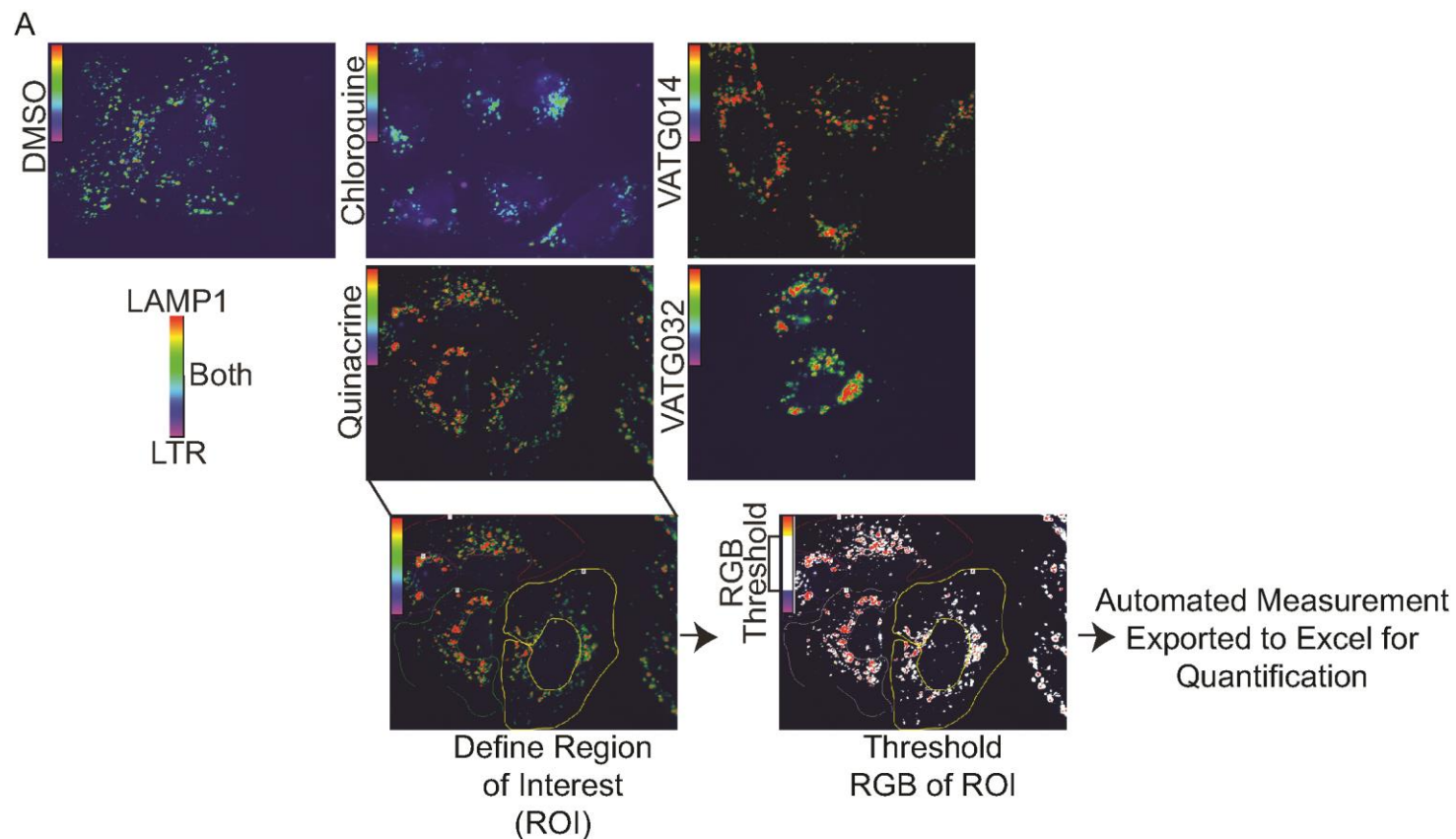
(**A**) U2OS cells were treated for 3 hours with vehicle control or 3 μM autophagy inhibitors (chloroquine, quinacrine, VATG014, and VATG032). Cells were stained with 100 nM LysoTracker Red for one hour prior to fixation and after fixation, were stained by immunofluorescence with endogenous LAMP1 antibody and fluorescently conjugated secondary antibody. Following, cells were stained with Hoechst (blue; nuclei) and imaged at 60x magnification. The ratio of LAMP1/LysoTracker Red was displayed on a

Figure 2.15 (cont'd)

colorimetric scale with red indicating only LAMP1 present, purple indicating only LysoTracker

Red present, and green indicating both stains present. Images were then thresholded on the RGB

scale to include only those puncta containing both LAMP1 and LysoTracker Red (green) and

displayed in white. White puncta data were then exported and quantified.

Figure 2.16. Testing autofluorescence of VATG compounds.

U2OS cells were treated with 30 μM of chloroquine, quinacrine, VATG014, or VATG032. Cells were stained with Hoechst (blue) and imaged in the red, green, and blue channels using the look-up table (LUT) settings for Figures 2.3 and 2.9. Representative images using VATG014 in U2OS and tfLC3 cells at standard LUT settings and high LUT settings are shown for comparison.

CHAPTER 3

THE AUTOPHAGY INHIBITOR VATG014 FUNCTIONS AS AN ANTIMALARIAL AGENT

ABSTRACT

Malaria is a deadly parasitic disease affecting millions of people each year. Although some success has been made in its eradication, it is still endemic in poor, tropical regions of the world. Major advances in antimalarial medications have been made with the lysosomotropic agent, chloroquine and its analogs. Chloroquine impedes the blood stage in the life cycle of the protozoans responsible for malarial infections. Unfortunately, the development of resistance to these agents by *Plasmodium* species is becoming extremely problematic. To generate new compounds with properties similar to chloroquine, we implemented rational chemical synthesis and developed a series of novel analogues. Two of these chemicals, VATG014 and VATG032, were shown to potently deacidify lysosomes and impair autophagy, a vesicular pathway that culminates in the lysosome (see Chapter 2). We hypothesized that these molecules might harbor antimalarial activity, specifically to chloroquine-resistant strains. To test this, we treated blood cultures containing parasite with VATG014 and VATG032 and found that both were effective in reducing viability, demonstrating antimalarial properties in both chloroquine-sensitive and chloroquine-resistant strains of *P. falciparum.* Additionally, both compounds maintained well-tolerated cytotoxicity profiles in mammalian cells as they did not kill at concentrations that were sufficient for parasite toxicity, allowing for an acceptable therapeutic window *in vitro* to continue into a murine model. Using mice parasitized with murine *P.burghei*, we determined that VATG014 is effective at reducing parasitemia, or parasite blood load, to be considered curative.

INTRODUCTION

Despite significant progress in the treatment of malaria over the past century, it still remains a major health risk, especially in developing countries. In 2010, the World Health Organization (WHO) estimated that there were 219 million cases resulting in 660 thousand deaths, 80% of which affected African children ((WHO) March 2013). Malaria is transmitted through the injection of *Plasmodium* sporozoites by mosquito bites. There are four strains of *Plasmodium* known to cause malaria in humans: *P.falciparum, P.vivax, P.malariae,* and *P.ovale. P.falciparum* is the most common and also the most deadly (Miller, Baruch et al. 2002; (WHO) March 2013). Once in the blood stream, *Plasmodium* sporozoites travel and localize to the liver where the asexual life cycle continues, eventually returning to the blood stream as merozoites. These merozoites continue to replicate in red blood cells or leave through additional mosquito bites (Figure 1.1). Symptoms begin to present 10 to 15 days after the mosquito bite, at the time that the asexual parasite begins to multiply in the red blood cells (Miller, Baruch et al. 2002; (WHO) March 2013). These symptoms, which include headache, fever, chills, and vomiting, are not unique to malaria and therefore make diagnosis challenging. Unfortunately, if left untreated, malaria can ultimately result in death.

Antimalarial compounds, such as chloroquine (CQ), have been used safely in humans for over 70 years. A wide variety of antimalarial medicines are now available; however, *Plasmodium* strains have developed dramatic resistance to many of these drugs. Antimalarial medicines display diverse activities and prevent *Plasmodium* infection by many different mechanisms (Biamonte, Wanner et al. 2013). Notably, CQ functions by deacidifying the *Plasmodium* digestive vacuole, which is required for heme digestion and survival (Slater 1993). The current malaria standard of care is a combination therapy that includes the sesquiterpene

lactone, artemisinin (artemisinin-based combination therapies; ACTs), which functions through the creation of free radicals (Bray, Ward et al. 2005; Biamonte, Wanner et al. 2013). Common drug combinations in this therapy include lumefantrine and piperaquine, a chloroquine derivative. Although artemisinin is effective at parasite clearing, it has a very short half-life and is not effective at clearing residual parasites (Biamonte, Wanner et al. 2013). The ACTs therefore, require the chloroquine derivative compounds for their longer half-lives. Ultimately, a more effective antimalarial with a longer half-life would be ideal. Unfortunately, a malaria vaccine does not exist, which together with the increasing abundance of antimalarial resistant strains of *Plasmodium*, underscores the desperate need for new antimalarial agents (Roepe 2009; Stanisic, Barry et al. 2013).

To address this, we utilized rational chemical synthesis and cell-based assays to develop a series of novel compounds using the chloroquine analog, quinacrine (QN), as a template (see Chapter 2). These molecules showed a similar, yet more potent, mechanism for autophagy inhibition as compared to CQ and QN. We hypothesized that these compounds would also be effective antimalarial agents. Here, we show antimalarial activity using VATG014 and VATG032 in two strains of *P.falciparum*, NF54 (CQ sensitive) and K1 (CQ resistant), with both having cytotoxicity profiles allowing for a therapeutic window. However, VATG014 met acceptable *in vitro* dosing concentrations of < 10 nM as determined by the Medicines for Malaria Venture (MMV) to continue into a murine model (Burrows, van Huijsduijnen et al. 2013). VATG014 was also shown to be effective at reducing the parasitemia load in the murine malaria model of malaria, *P. berghei.* Thus, this compound remains promising for use as a new antimalarial agent in CQ resistant strains. This work was completed with key collaborators and expertise from the MMV.

RESULTS

VATG014 and VATG032 demonstrate antimalarial activity *in vitro*

To determine whether the novel quinacrine analogs, VATG014 and VATG032, displayed anti-malarial activity, we investigated their effects on *in vitro* blood cultures of the malaria-causing parasite *Plasmodium falciparum*. Two-fold dilution curves of both VATG014 and VATG032 were assayed against the CQ-sensitive *Plasmodium falciparum* NF54 strain, and the CQ-resistant K1 strain. Compounds were scored as having no activity: $IC_{50} > 1000$ ng/mL; low activity: IC_{50} 50-1000 ng/mL; or good activity: $IC_{50} < 50$ ng/mL. In the CQ-sensitive NF54 strain, VATG014 and VATG032 showed antimalarial activity with IC_{50} values of 4 nM (good activity) and 323 nM (low activity), respectively (Table 3.1). Similar results were observed with the CQ-resistant K1 strain, in which VATG014 and VATG032 showed antimalarial activity with IC_{50} values of 23 nM (good activity) and 131 nM (low activity), respectively (Table 3.1).

Cytotoxicity of VATG014 and VATG032 allow for a therapeutic window

Next, we wanted to determine if there is a therapeutic window for VATG014 and VATG032 in the treatment of *P. falciparum*. A therapeutic window for *P. falciparum* treatment is defined as a 10-fold differential between the *in vitro* cytotoxicity (LD_{50}) within a mammalian cell line and the antimalarial IC_{50} (LD_{50}/IC_{50}) as defined by the MMV. Using the rat skeletal muscle L6 mammalian cell line, dose-response curves for VATG014 and VATG032 were performed and the LD_{50} determined. The LD_{50} of VATG014 is approximately 1.9 μM and VATG032 is 26 μM, making the therapeutic windows for both compounds more than sufficient

at >10-fold in each *Plasmodium* strain (Table 3.1). VATG014 showed the greatest therapeutic window with a fold-change of 475 in the NF54 strain (CQ sensitive) and a fold-change of 82 in the K1 strain (CQ resistant). However, MMV experience with successful compounds shows that those compounds with an *in vitro* activity against the laboratory strains of *P. falciparum* at < 10 nM have the most success, predicating the continuation of only VATG014 *in vivo* (Burrows, van Huijsduijnen et al. 2013).

VATG014 demonstrates antimalarial activity against *P.berghei in vivo*

The potent anti-malarial activity of VATG014, combined with its therapeutic window *in vitro*, led us to explore its activity *in vivo* using a murine model of malaria. Mice are infected with the murine specific *Plasmodium*, *P.berghei*, after which an antimalarial treatment regimen is given. VATG014 was given at 50 mg/kg at times 4, 24, 48, and 72 hours post-infection of mice already infected with *P.berghei*. The reduction in parasitemia, measured as the total blood load of the *P.berghei* parasite, was compared to an infected control group for the percent reduction of parasite on day 4 (96 hours post-infection). VATG014 was shown to be effective in reducing parasitemia by 99% compared to the infected control group after 4 days, making it an effective antimalarial in these preclinical models.

DISCUSSION

The current success of malaria elimination has relied heavily on the cooperation of multiple factors working together in concert; biological, parasitological, social, and environmental factors (Alonso, Brown et al. 2011). However, despite the large success in the reduction of malaria, antimalarial resistance remains a sizeable issue. Resistance occurs through the failure of people to complete a full course of their antimalarial allowing *Plasmodium* to develop mutations in genes that can efflux drugs or counteract their mechanisms of action (Foley and Tilley 1998; Jensen and Mehlhorn 2009). With increasing cases of resistance occurring, a need for new antimalarial medicines is growing.

In this study, we characterized the antimalarial activity of two novel compounds; VATG014 and VATG032, which were derived from quinacrine (see Chapter 2). We discovered that both VATG014 and VATG032 have antimalarial effects on the malaria-causing *P.falciparum* strains, NF54 (chloroquine sensitive) and K1 (chloroquine resistant). Moreover, these compounds have appropriate cytotoxicity profiles to ensure therapeutic windows in malaria treatment and moreover, VATG014 showed promise in the murine malaria model, *P.berghei*. These novel compounds not only fill a need for new antimalarial compounds, but have shown better autophagy inhibiting properties than chloroquine, making them potentially more effective as antimalarial agents.

With the rise in chloroquine resistant strains of *Plasmodium* in the world, the promise of new therapeutic options for malaria, such as these, brings hope. Further, as these compounds have been shown to inhibit autophagy (see Chapter 2), it raises the question of whether other autophagy inhibitors that also impair the lysosome could be used for malaria treatment. Since these more potent autophagy inhibitors share a common mechanism of action and malaria-

inhibiting properties with chloroquine, the investigation into their effectiveness in other diseases that chloroquine has been shown to be beneficial in, such as in auto-immune disorders, could prove to be beneficial.

Since these compounds are based on an antimalarial agent that has been used in the population, it does stand to reason that resistance could be developed to these compounds as well. However, current ACTs have shown to reduce the rate at which resistance arises to antimalarial agents by the combination of multiple modes of action at once. As our compounds are still unused in a human population, the ability to use them in ACTs will reduce the rate at which resistance will develop. With a lower rate of resistance developing, the eradication of more areas with endemic malaria is feasible. Further, if efforts are in place for large scale distribution and control, results have shown to be promising at decreasing the incidence of malaria with other antimalarial agents, bringing optimism that these compounds could be very effective.

MATERIALS AND METHODS

In vitro compound screen of *Plasmodium falciparum* asexual blood stage

Compounds VATG014 and VATG032 were dissolved in DMSO at 10 mg/mL and 4x compound dilutions were prepared in screening medium [RPMI 1640 with no hypoxanthine, HEPES (5.94 g/L), $NaHCO_3$ (2.1 g/L), Neomycin (100 μg/mL), and Albumax II (5 g/L)]. Human red blood cells were prepared without and with stock cultures of *P.falciparum* strains, NF54 (CQ sensitive) and K1 (CQ resistant), to a parasitemia of 0.3% and hematocrit of 2.5%. Using a 96-well plate, 100 μL/well of red blood solution was added along with a 2-fold serial dilution of VATG014 and VATG032. Plates were incubated at $37^{\circ}C$ with 93% N_2, 4% CO_2, and 3% O_2 for 48 hours, after which 50 μL of [^{3}H]-hypoxanthine (0.5 μCi) was added to each well. After 24 hours, plates were harvested with a Betaplate TM cell harvester (Wallac, Zurich Switzerland) which transferred the red blood cells onto a glass fiber filter and washed with distilled water. Dried filters were inserted into a plastic foil with 10 mL of scintillation fluid and counted in a Betaplate^{TM} liquid scintillation counter (Wallac, Zurich Switzerland). Results were in counts per minute (cpm) per well at each concentration. The 50% inhibitory concentration (IC_{50}) value was evaluated by Logit regression analysis. Compounds were scored as no activity: $IC_{50} > 1000$ ng/mL; low activity: IC_{50} 50-1000 ng/mL; or good activity: $IC_{50} < 50$ ng/mL.

Evaluation of *in vitro* cytotoxicity (LD_{50})

L6 cells were seeded at 4×10^4 cells per well in a 96-well microtiter plate with each well containing 100 μL of RPMI 1640 medium, supplemented with 1% L-glutamine (200 mM), and

10% fetal bovine serum. Serial drug dilutions of VATG014 and VATG032 with seven 3-fold dilution steps, covering a range from 90 to 0.12 µg/mL, were prepared. After 72 h of incubation, the plates were inspected under an inverted microscope to ensure growth of the controls and sterile conditions. Alamar Blue (10 µL, 12.5 mg of resazurin dissolved in 100 mL of double-distilled water) was then added to each well, and the plates were incubated for another 2 hours. Plates were read with a microplate fluorometer using an excitation wavelength of 536 nm and an emission wavelength of 588 nm. Data were analyzed using microplate reader software. Podophyllotoxin was used as a standard (L6 IC_{50} = 0.04 µg/mL).

In vivo compound efficacy in *Plasmodium berghei*

Mice were infected intravenously with parasitized red blood cells on day 0 (2×10^7 parasitized erythrocytes per mL). Experimental mice were treated at 4, 24, 48, and 72 hours post-infection with an oral dose of VATG014 at 50 mg/kg and were compared to an infected control group for the % reduction in parasitaemia on day 4 (96 hours post-infection) and for mean survival (monitored up to 30 days post-infection). A compound was considered curative if the animal survived to day 30 after infection with no detectable parasites.

ACKNOWLEDGEMENTS

TABLES

Table 3.1. Antimalarial activity (IC_{50}) against P.*falciparum* NF54 and K1 *in vitro*, cytotoxicity (LD_{50}) in L6 cells, and their fold difference of LD_{50}/IC_{50} (therapeutic window).

Compound	P.*falciparum* NF54 (CQ sensitive)	P.*falciparum* K1 (CQ resistant)	Cytotoxicity in L6 Cells (LD_{50})	NF54 Fold	K1 Fold
Chloroquine	68 nM $\pm$ 1 nM	196 nM $\pm$ 31 nM	–	–	–
VATG014	4 nM $\pm$ 1.3 nM	23 nM $\pm$ 2.5 nM	1.9 μM + 0.01 nM	475	82
VATG032	323 nM $\pm$ 78 nM	131 nM $\pm$ 8 nM	26 μM $\pm$ 1 nM	80	19

CHAPTER 4

POTENT AUTOPHAGY INHIBITORS THAT SENSITIZE ONCOGENIC BRAF (V600E) MUTANT MELANOMA TUMOR CELLS TO VEMURAFENIB

Modified from

ABSTRACT

Autophagy is a dynamic cell survival mechanism by which a double membrane vesicle, or autophagosome, sequesters portions of the cytosol for delivery to the lysosome for recycling. This process can be inhibited using the common anti-malarial chloroquine (CQ), which impairs lysosomal function and prevents autophagosome turnover. Here, we characterized a novel acridine derivative (VATG014) and a 1,2,3,4-tetrahydroacridine derivative (VATG032), generated by chemical synthesis for autophagy inhibitory effects using the antimalarial quinacrine (QN) as a template, as discussed in Chapter 2. However, the role of autophagy in cancer cells depends on tumor type, tumor stage, and genetic context. To evaluate the genetic context in which these compounds may be effective, we tested these inhibitors in patient-derived melanoma cell lines driven by oncogenic BRAF. We discovered that both VATG014 and VATG032 sensitized melanoma cells to the BRAF-V600E inhibitor, vemurafenib (PLX-4032). Overall, these autophagy inhibitors provide a means to effectively block autophagy-mediated cell survival in melanoma with lower toxicity and have the potential to sensitize cancers to first line therapies.

INTRODUCTION

Macroautophagy (autophagy) is a catabolic salvaging pathway that cells use to segregate portions of the cytosol, including proteins and organelles, for delivery to the lysosome for degradation (Klionsky 2007). Autophagy is an ordered process executed in four distinct steps; initiation, nucleation, elongation, and completion (Kohli and Roth 2010). Following initiation, a phagophore, or a cup-shaped double bi-lipid membrane, is nucleated at the initiation site. The membrane subsequently elongates and eventually closes, sequestering the constituents into a mature double-membrane autophagosome. Lastly, the autophagosome fuses with a lysosome, or endocytic vesicle destined for the lysosome, for degradation of its contents and completion of the pathway (Rosenfeldt and Ryan 2009; Simonsen and Tooze 2009).

While autophagy is utilized to maintain homeostasis under nutrient-rich conditions, it is also activated during times of stress as a survival mechanism (Mathew and White 2011; White 2012). Given this pivotal role in cell fate, autophagy has been implicated in many diseases including cancer, autoimmune, inflammatory, and neurodegenerative diseases (Mizushima, Levine et al. 2008; Yang and Klionsky 2010). Notably, emerging evidence supports a critical role for autophagy in the survival of cancer cells (Mathew and White 2011; White 2012; Wu, Coffelt et al. 2012). The same mechanism used by healthy cells to produce internal nutrients and energy is exploited by cancer cells to survive in times of metabolic, hypoxic, and therapeutic stress (Kondo, Kanzawa et al. 2005; Mathew, Karantza-Wadsworth et al. 2007; Wu, Coffelt et al. 2012). Autophagy is particularly important in certain tumor types and in response to specific oncogenic stresses (Shingu, Fujiwara et al. 2009). For example, cancer cells with high metabolic phenotypes can become 'addicted' to autophagy, as it provides necessary building blocks to

maintain growth rates and support cell survival (Mathew, Karantza-Wadsworth et al. 2007; Mathew and White 2011; White 2012). Data suggests that in cancers characterized by oncogenic RAS activation, autophagy is often upregulated and critical for survival (Guo, Chen et al. 2011; Mathew and White 2011). Further evidence shows that autophagy is not only beneficial, but is required, for growth of pancreatic cancers, an estimated 90% of which are driven by oncogenic KRAS (Yang, Wang et al. 2011). Similarly, activation of the oncogene, BRAF, has been shown to upregulate autophagy. Expression of BRAF and the autophagy protein light chain 3 (LC3) were shown to positively correlate in tumors and overexpression of BRAF in cultured cells increased LC3 levels (Maddodi, Huang et al. 2010). This study also demonstrated that treatment with an autophagy inhibitor, 3-methyladenine (3-MA), increased cell death in cells overexpressing BRAF, suggesting that autophagy supports cell survival in this context (Maddodi, Huang et al. 2010). Taken together, autophagy inhibition represents a promising therapeutic target in tumor types where this process is upregulated and required for cell survival.

In addition to increased utilization of basal autophagy in certain tumor types, many anti-cancer therapies have been shown to induce autophagy (Kondo, Kanzawa et al. 2005; Wu, Coffelt et al. 2012). For example, increased autophagy was uncovered in glioma cells resistant to standard of care chemotherapy and radiotherapy. Importantly, treatment with an autophagy inhibitor sensitized these resistant glioma cells to therapy, supporting the role of autophagy in cell survival (Fan, Cheng et al. 2010). In many cases, autophagy contributes to survival as an unintended and counterproductive consequence of treatment. Thus, cancers targeted with a diverse set of therapeutics may be particularly vulnerable to autophagy inhibition, creating a combination therapy opportunity. Studies have demonstrated that both genetic and chemical inhibition of the autophagic pathway can augment the cytotoxic effects of chemotherapy (Kondo,

Kanzawa et al. 2005). Loss of key autophagic machinery proteins including BECN1, ATG5, ATG10, and ATG12, has been shown to confer sensitization to cell death (Boya, Gonzalez-Polo et al. 2005; Morselli, Galluzzi et al. 2009; Liu, Cheng et al. 2010; Wu, Coffelt et al. 2012). Similar results have been obtained with pharmacological inhibitors that target similar points in the autophagy pathway, such as 3-MA, a class III PI3K inhibitor; and bafilomycin A1 and chloroquine, which both disrupt lysosomal activity (Apel, Herr et al. 2008).

The accumulating evidence supporting autophagy-mediated cancer cell survival and therapeutic potential for targeting autophagy in cancer underscores the critical need to develop effective autophagy inhibitors. Of particular interest are inhibitors that can be applied both as single agents for highly autophagic cancers, such as RAS-driven tumors, and also as adjuvants to standard chemotherapeutic regimens. Currently, the most widely used autophagy inhibitor is chloroquine (CQ), a well-known anti-malarial drug that has been in clinical use for over 70 years (Loeb 1946; Foley and Tilley 1998). CQ functions as a freely diffusing lysosomotropic agent that enters the lysosome, is diprotonated, and becomes trapped inside as a diacidic base (Foley and Tilley 1998; Solomon and Lee 2009). By sequestering the free hydrogen ions required to maintain an acidic pH, CQ increases the basicity of the lysosome. This renders lysosomal hydrolases and proteases non-functional, blocks lysosomal turnover, and inhibits the final completion stage of autophagy. With autophagy-mediated cell survival impaired, tumor cells treated with CQ are less able to withstand therapeutic treatments and therefore sensitized to therapy (Amaravadi, Yu et al. 2007; Ma, Piao et al. 2011; Yang, Wang et al. 2011). The safety profile of CQ and its ability to inhibit autophagy make this antimalarial drug an ideal starting point for adjuvant therapeutic strategies.

CQ has proven effective as an adjuvant to cancer therapeutics in several studies. In a myeloid leukemia cell line, treatment with the DNA-damaging anti-tumor agent, anthracycline daunorubicin (DNR), induced cytoprotective autophagy that preceded cell death. CQ increased apoptotic cell death induced by DNR, allowing for a lower, less toxic concentration of DNR to be used (Han, Sun et al. 2011). In a xenograft model of triple negative breast cancer, treatment with CQ and a histone deacetylase (HDAC) inhibitor decreased tumor burden and increased animal survival, compared to the HDAC inhibitor alone (Rao, Balusu et al. 2012). Furthermore, in colon cancer, CQ enhanced cell death induced by topotecan, a DNA damage inducer (Li, Sun et al. 2012). These examples, and a host of others, have contributed to evidence supporting the use of autophagy inhibitors to increase cancer cell death in conjunction with therapeutics. Accordingly, there are currently over 40 clinical trials in progress investigating the use of CQ or hydroxychloroquine (HCQ) in cancer treatment (National Library of Medicine 2013; National Library of Medicine 2013). One particularly promising clinical trial in glioblastoma multiforme found that when combined with conventional treatment of chemotherapy and radiotherapy, CQ prolonged the median survival of patients (Sotelo, Briceno et al. 2006). The sample size in this study was small, thereby preventing statistical significance; however, it supports the potential use of CQ as an adjuvant therapy.

Although CQ has provided proof of principle for combining autophagy inhibitors with existing anti-cancer therapies, CQ is a relatively inadequate inhibitor and requires a large effective concentration (mid-micromolar range) to disrupt autophagy both *in vivo* and *in vitro*. Therefore, small molecules that more potently inhibit autophagy are needed to improve efficacy, and ultimately enhance tumor cell sensitization to therapeutics. In this study, we developed a series of novel acridine and tetrahydroacridine derivatives based on QN and characterized two

117

that yielded up to 150-fold greater autophagy inhibition than CQ. We previously demonstrated that these novel compounds function by deacidifying lysosomes and impairing turnover of incoming vesicles, including autophagosomes (Goodall, Wang et al. 2013). Intriguingly, despite similar effects on autophagy, these molecules displayed diverse cytotoxic profiles ranging from largely cytostatic (VATG032) to more cytotoxic (VATG014). To explore the therapeutic potential of these two lead molecules, we evaluated their activity in a panel of patient-derived metastatic melanoma cell lines. We discovered that both compounds reduced cell viability and anchorage independent colony growth as single agents. Furthermore, combining these molecules with PLX-4032 (vemurafenib), a BRAF inhibitor selective for V600E, or the catalytic mTOR inhibitor, AZD8055, significantly reduced colony formation in a manner that exceeds additivity. Taken together, our data supports the critical role of autophagy in BRAF mutant melanoma. Moreover, the novel compounds developed here may provide utility as both single agents and adjuvant therapeutics in anti-cancer strategies.

RESULTS

Determination of Autophagic Flux in BRAF Mutant Melanoma Lines

Oncogenic mutation of BRAF V600E, a genetic driver in greater than 50% of melanomas, has been shown to increase autophagy, potentially as a cell survival mechanism (Davies, Bignell et al. 2002; Ma, Piao et al. 2011; Chen, Tardell et al. 2012). Accordingly, we chose to evaluate the potential therapeutic utility of autophagy inhibition in the A375 melanoma cell line, as well as eight metastatic patient-derived lines (UACC-91, UACC-257, UACC-502, UACC-903, UACC-1308, UACC-1940, UACC-2534, and UACC-3291), seven of which contain the BRAF V600E mutation (determined by Sanger sequencing). First, basal autophagic flux was determined in each cell line. To do this, we evaluated LC3, an ubiquitin-like molecule that translocates from the cytosol (LC3-I) to autophagic membranes (LC3-II) during autophagy. LC3-II is turned over in the lysosome along with autophagic cargo, therefore, autophagic flux can be determined by measuring the accumulation of (LC3-II) in response to lysosome inhibition over a short period of time (Klionsky 2012). Each cell line was treated with CQ (to inhibit lysosomes) for 0, 1, or 3 hours and quantitative immunoblotting used to measure the fold-change in LC3-II levels with CQ treatment. Importantly, we found that cell lines expressing BRAF V600E had a high level of autophagic flux, with greater than 2-fold accumulation of LC3-II by three hours (Figure 4.1A). In addition, while one cell line expressing wild-type BRAF (UACC-1940) exhibited high autophagic flux, another wild-type BRAF cell line (UACC-2534) did not. Upon further investigation into the mutational status of the two cell lines, we found that UACC-1940 cells contain a mutation in HRAS (G13V), which activates the MAPK pathway similar to BRAF (Figure 4.1B). Taken together, all melanoma lines showed measurable levels of basal autophagic

flux; however, the cell line that was not driven by either oncogenic BRAF or RAS showed the lowest level of autophagic flux.

Next, we determined the sensitivity of each melanoma cell line to CQ, QN, VATG-014, and VATG-032. CQ reduced cell viability with LD_{50} values ranging from 13 μM to 40 μM (Table 4.1). VATG-032 affected cell viability in a similar manner, yielding LD_{50} values between 15 μM and 42 μM. Consistent with observations from U2OS cells in Chapter 2, QN was considerably more cytotoxic than CQ, with LD_{50} values between 1.9 μM and 3.9 μM. VATG-014 treatment produced LD_{50} values that closely matched those of QN, between 0.4 μM to 2.7 μM. Overall, the four inhibitors affected viability of the nine melanoma cell lines comparable to that observed in U2OS cells (Table 4.1; Figure 4.2A).

Combination Treatment of PLX-4032 and Autophagy Inhibitors is More than Additive

Since autophagy is active in melanoma cell lines and they are sensitive to autophagy inhibition, we questioned whether autophagy inhibitors could improve the efficacy of the latest approved drug for advanced metastatic melanoma (Flaherty, Puzanov et al. 2010). This drug, PLX-4032 (vemurafenib), selectively targets V600E mutant BRAF and it is unknown how this drug may affect autophagic flux. To address this, we first determined whether PLX-4032 induces autophagy, as has been observed with other targeted agents (Kondo, Kanzawa et al. 2005). To do this, we measured the accumulation of LC3-II in response to lysosome inhibition by quantitative immunoblotting, as described above. A375 cells were treated with PLX-4032 (10 nM, 100 nM, and 1 μM) for 3 hours in the presence or absence of CQ. While PLX-4032 effectively blocked oncogenic BRAF signaling (as measured by reduced phosphorylation of the

downstream effector, ERK1/2), autophagy was not substantially altered (Figure 4.2B). Next, A375 cells were treated with PLX-4032 in combination with CQ, QN, VATG014, or VATG032. Again, autophagic flux was not substantially altered by PLX-4032, with VATG014 and VATG032 showing greater increases in LC3-II accumulation than observed previously with CQ (Figure 4.2C). This data suggests that while mutant BRAF V600E-expressing cell lines undergo basal autophagy, chemical inhibition of oncogenic MAPK signaling does not considerably alter autophagic flux.

Despite the lack of autophagy induction by PLX-4032, the autophagic capacity retained in cells during treatment suggests that autophagy may potentially mediate cell survival. Inhibition of autophagy is shown be difficult in interpreting the reduction in viability if done only in an acute setting and must also be done in a chronic situation (Kroemer and Levine 2008; Thorburn 2011). Therefore, we hypothesized that autophagy inhibitors may be effective in combinatorial treatment regimens with PLX-4032 with chronic treatment. To evaluate this, we performed soft agar colony formation assays over the course of three weeks to assess anchorage independent growth, one hallmark of cellular transformation and tumor growth. First, A375 cells were plated in soft agar for 3 weeks and treated every other day with a range of concentrations of PLX-4032, CQ, QN, VATG014, or VATG032. In addition, we evaluated how autophagy inhibitors affect efficacy of a known autophagy stimulus, the catalytic mTOR inhibitor, AZD8055. The concentration of each single agent that yielded a minimal effect on colony formation (~10%; LD_{10}) was determined in order to see additivity differences in viability (Figure 4.3). Following, we treated cells plated in soft agar with the LD_{10} of PLX-4032 or AZD8055 alone or in combination with the LD_{10} of CQ, QN, VATG014, or VATG032. To

determine if the effects of each combination were more than, less than, or equal to additive, we made predictions for additivity using the Bliss Independence model (See *Materials and Methods* and Table 4.2) (Hiss, Gabriels et al. 2007; Chou 2010; Yan, Zhang et al. 2010). We found that CQ and PLX-4032 reduced colony formation by 38%, slightly greater than the effect predicted if these agents interact additively (33%) (Figure 4.4 and Table 4.2). Similarly, combinatorial treatment of QN and PLX-4032 reduced colony formation by 59%, just greater than the expected value of 50% (Figure 4.4 and Table 4.2). Both VATG014 and VATG032 were more significant than QN at increasing the efficacy of PLX-4032, reducing colony formation by 64% and 62%, compared to expected values of 49%, respectively (Figure 4.4 and Table 4.2). Similar results were obtained with combinatorial treatments of AZD-8055 and each autophagy inhibitor (Figure 4.5 and Table 4.2). We confirmed that combination treatments of PLX-4032 and QN or VATG032 exceeded additive effects in a second BRAF V600E mutant melanoma cell line, UACC 91 (Figure 4.6). In contrast, while treatment with all compounds as single agents reduced colony formation in the wild-type BRAF cell line, UACC 1940 (which contains a HRAS G13V mutation), their combined effect did not exceed additivity (Figure 4.6 and Table 4.3). This suggests that the observed effectiveness (exceeding drug additivity) of combined PLX4032 and autophagy inhibitors may be selective for cells expressing mutant BRAF V600E, the primary target of PLX-4032. Finally, to provide consistency with prior cell-based experiments, we evaluated PLX-4032 combinations using autophagy inhibitors at 3 µM (except VATG014, which was used at 1 µM owing to its substantial activity as a single agent) and confirmed that combinatorial effects exceeded additivity (Figure 4.7). Taken together, these results suggest that autophagy inhibitors may have utility in melanoma treatment, both as single agents and in combination with PLX-4032.

DISCUSSION

In this study, we utilized melanoma cell models to evaluate the therapeutic potential of autophagy inhibitors. Melanoma is an aggressive cancer that has several well identified oncogenes and tumor suppressors and mutations in these genes have been shown to upregulate autophagy and survival in melanoma in several reports (Ma, Piao et al. 2011; Chen, Tardell et al. 2012; Flaherty, Hodi et al. 2012). Three common genes that are recurrently mutated in melanoma, as well as many other cancers, are those in RAS, BRAF, and PTEN, which in turn activate PI3K/AKT/mTOR and RAS/RAF/MEK/MAPK pathways and have been shown to deregulate autophagy (Janku, McConkey et al. 2011; Corazzari 2013). In a recent report, it was shown that inhibition of both the mTOR pathway (using the mTOR inhibitor, temsirolimus) and autophagy (using HCQ) produced synergistic effects in melanoma cell death (Xie, White et al. 2013). Additional reports have shown that hyperactivated MAPK signaling prevents mTOR-mediated nutrient sensing, specifically its inhibition due to the lack of leucine (Sheen, Zoncu et al. 2011). The role of autophagy and nutrient sensing was further assessed *in vivo* using human melanoma xenografts, and the combination of a leucine-free diet and an autophagy inhibitor dramatically reduced tumor volume (Sheen, Zoncu et al. 2011). Taken together, there is mounting evidence for the role of autophagy inhibition in melanoma tumorigenesis.

Consistent with these findings, we confirmed active basal autophagy in a panel of nine melanoma cell lines and found that all were sensitive to autophagy inhibition. Importantly, we demonstrated that autophagy inhibitors decrease cell viability, both as single agents and in combination with therapeutics, supporting the hypothesis that autophagy promotes cell survival. In addition to activity as single agents, we found that autophagy inhibitors sensitized cells to the

BRAF V600E-specific inhibitor, PLX-4032. This is consistent with evidence that many therapeutics, including targeted agents, can benefit from the addition of an autophagy inhibitor as an adjuvant.

Several studies have found that autophagy inhibition may sensitize cancers to therapeutic treatments that were otherwise ineffective. In colon cancer cells containing a RAS mutation, it was shown the combination of the chemotherapeutic 5-fluorouracil (5FU) with CQ lead to a further increase in cell death than when used alone (Wu, Wu et al. 2009; Sasaki, Tsuno et al. 2010). The effectiveness of autophagy inhibition in colon cancer is particularly exciting as 18% of colon cancers share the BRAF V600E mutation common in melanoma, suggesting the work presented here could be applicable to additional cancer types (Davies, Bignell et al. 2002). Similarly, inhibition of autophagy using both CQ and mefloquine, (also an anti-malarial agent) was able to induce cell death in breast cancer lines expressing RAS and BRAF mutations (Sharma, Thomas et al. 2012).

Many chemotherapeutic treatment strategies have been shown to upregulate autophagy, a counterproductive effect as upregulated autophagy can promote aberrant cell survival. This was demonstrated in a study of lung cancer with the epidermal growth factor receptor (EGFR) tyrosine kinase inhibitors (TKIs), gefitinib and erlotinib. Treatment with these TKIs conferred a marked increase in autophagy activation and cytotoxicity was significantly enhanced upon the addition of CQ (Han, Pan et al. 2011). Similarly, in a model of cervical cancer, it was found that cisplatin treatment induced autophagy, and CQ enhanced the cytotoxicity of cisplatin (Xu, Yu et al. 2012). Increased effectiveness of therapies by cotreatment with autophagy inhibitors demonstrates the value of targeting autophagy in future treatment strategies.

The role of autophagy in cancer is complex and context dependent; this is especially true in models with BRAF mutations. As indicated earlier, a correlation between increased autophagy and mutant BRAF in cell lines has been reported, suggesting autophagy inhibition may be effective in mutant BRAF tumor types (Maddodi, Huang et al. 2010). Despite this, others have suggested that while supporting high basal autophagy, mutant BRAF confers resistance to autophagy activation by mTORC1 inhibition (Armstrong, Corazzari et al. 2011). This discrepancy underscores that not only the tumor stage, but the subtype and collective mutations of a tumor, may contribute to the role of autophagy on cell viability (Corazzari 2013). Our data highlights the importance of measuring cellular autophagic flux and the need for more potent autophagy inhibitors in aggressive cancers and therapeutic treatments. This is an even more important consideration with recent findings that wild-type BRAF tumors where a targeted RAF inhibitor was used could actually increase tumor xenograft growth (Hatzivassiliou, Song et al. 2010). We demonstrated here that use of an autophagy inhibitor in BRAF wild-type cells was effective as a single agent, suggesting that their use may be beneficial in BRAF wild-type scenarios where RAF inhibitors are not an option. Furthermore, the fact that we observed combination treatment effects (i.e., PLX-4032 and autophagy inhibitors) that exceeded additivity using soft colony formation assays suggest that this approach which may be better for observing anti-tumor effects, as opposed to acute drug toxicity in standard 2D cultures.

Prior studies that have investigated the use of CQ analogs in cancer treatment have primarily focused on their ability to induce cell death as single agents (Solomon, Hu et al. 2010). Even though cytotoxic compounds are valuable, potent autophagy inhibition alone does not necessarily elicit cytotoxic effects. Here, we have demonstrated that inhibition of autophagy can be accomplished with compounds that are relatively well-tolerated by cells (i.e., VATG032).

The development of such potent autophagy inhibitors provides an opportunity for use as adjuvants in treatment strategies, effectively blocking autophagy-mediated cancer cell survival without significantly increasing toxicity as a single agent. This type of compound provides an exciting outlet for sensitization of cancer cells to the latest anti-cancer therapeutics.

MATERIALS AND METHODS

Cell Viability (LD$_{50}$) Screen

All melanoma cell lines (A375, UACC-91, UACC-257, UACC-502, UACC-903, UACC-1308, UACC-1940, UACC-2534, and UACC-3291) were seeded at 5,000 cells per well in RPMI 1640 with 10% FBS in 96-well clear bottom, black-walled tissue culture plates. After 24 hour incubation, cells were treated with CQ, QN, and VATG compounds in triplicate with a 10-point half log dose response from 0.001 μM to 1000 μM for 24 and 48 hours. Medium was removed and 2x CellTiter Glo (Promega, G7571) reagent mixed 1:1 with Opti-MEM (Invitrogen, 31985062) was added at 100 μL per well and incubated at room temperature for 15 minutes while rocking. 75 μL per well was moved to a white-walled 96-well plate and luminescence quantified using the 96 LUM program on an EnVision plate reader (PerkinElmer) and exported for analysis. All triplicate data points were averaged and luminescent readings for each treatment were normalized to vehicle control for change in viability. Dose response curves were analyzed in SigmaPlot and LD$_{50}$ values determined (Systat Software Inc).

Immunoblot Analyses

For immunoblotting, all melanoma lines were seeded in 10cm plates in RPMI 1640 with 10% FBS at 1 x10^{6} cells per plate. After 24 hours, cells were treated with CQ, QN, VATG014, or VATG032 in a dose response of 3 μM and 30 μM for three hours. A375 were treated with PLX-4032 (Selleck Chemicals, S1267) at 10 nM, 100 nM, and 1 μM for three hours with and without CQ, QN, VATG014, and VATG032 at 3 μM and 30 μM. After treatment, cells were

lysed [10mM KPO4, 1mM EDTA, 10mM $MgCl_2$, 5mM EGTA, 50mM bis-glycerophosphate, 0.5% NP_40, 0.1% Brij35, 0.1% sodium deoxycholate, 1mM $NaVO_4$, 5mM NaF, 2mM DTT, and complete protease inhibitors (Sigma, P8340)] and 50 μg of protein was resolved by SDS-PAGE. Proteins were transferred to PVDF membranes and probed with primary antibodies [LC3 (Sigma, L7543), anti-α-tubulin (Sigma, T6199), cathepsin B (Santa Cruz, sc-13985)] for 16 hours at $4^{o}C$ followed by a secondary antibody [HRP-linked rabbit or mouse IgG (GE Healthcare, NA934 or NA931) or Odyssey IRDye 680CW Goat anti-rabbit IgG (LI-COR, 926-32221) or IRDye 800CW Goat anti-mouse IgG (LI-COR, 926-32210)] for 1 hour at room temperature. Proteins were detected with enhanced chemiluminescence or using the Odyssey Imaging System (Li-Cor Biosciences) and quantified.

Soft Agar Colony Formation Assay

In a 6-well plate, a solidified base was created using a 1:1 solution of RPMI 1640 (with 20% FBS) and 1% agarose solution. This was overlaid with A375, UACC 1940, or UACC 91 cells at 40,000 cells per well in RPMI 1640 (with 10% FBS) mixed 1:1 with 0.7% agarose. The soft agarose containing cells was then overlaid with 0.75 mL RPMI 1640 (with 10% FBS) and incubated at $37^{o}C$ in 5% CO_2. After 24 hours, cells were treated in a dose response or at the determined LD10 with PLX-4032, CQ, QN, VATG014, or VATG032 every other day for three weeks. After three weeks of treatment, cells were fixed and stained in 1% paraformaldehyde in 1xPBS containing 0.005% crystal violet overnight. Cells were destained with multiple washes of 1xPBS to remove background staining. Plates were scanned and images quantified using NIS Elements software (Nikon). To quantify, each image was sharpened and a region of interest

(ROI) of equal size drawn around each well. Intensity thresholds were set to include all pixels greater than the intensity of the mean background fluorescence. Object counts within the threshold of each ROI were quantified using an automated object count function to denote total colony formation. Additivity was determined using the fractional product concept or Bliss Independence model: $E_{xy} = E_x + E_y - (E_x E_y)$ where E_{xy} is the additive effect of the two compounds x and y as calculated by the product of the individual effect of the two compounds, E_x and E_y (Hiss, Gabriels et al. 2007; Yan, Zhang et al. 2010). In other words, the expected amount of additivity is the combined effect of the ability of each compound to reduce viability, independent of each other, added together. If the calculated number is equal to the actual number, then the compounds are determined to be additive. If the actual number is lower than the calculated number then compounds are considered antagonistic and if higher, then synergistic. Additivity, synergism, or antagonism was established when the expected viability determined by the Bliss independence model was equal to the actual viability. This model was chosen since the effects of both compounds are mutually non-exclusive and follow first order Michaelis-Menten kinetics (Chou 2010).

Table 4.1. IC_{50} (µM) of CQ, QN, VATG014, VATG032, and PLX-4032.

	Chloroquine	**Quinacrine**	**VATG014**	**VATG032**	**PLX-4032**
A375	24.6 µM	2.3 µM	0.4 µM	24.3 µM	1 µM
UACC-91	13.4 µM	2.9 µM	0.5 µM	22.2 µM	0.6 µM
UACC-257	14 µM	3 µM	2 µM	25.3 µM	4 µM
UACC-502	24.3 µM	2.2 µM	1.8 µM	42.3 µM	4.2 µM
UACC-903	34.1 µM	2.7 µM	1.5 µM	27.2 µM	69 µM
UACC-1308	39.6 µM	3.9 µM	2.1 µM	14.9 µM	0.6 µM
UACC-1940	19.6 µM	1.9 µM	4 µM	21.6 µM	3.3 µM
UACC-2534	18 µM	2.2 µM	2.7 µM	26.6 µM	19.3 µM
UACC-3291	28.1 µM	2 µM	0.8 µM	25.3 µM	1.5 µM
U20S	75 µM	2.5 µM	0.7 µM	27µM	-------

All cell lines (A375, UACC91, UACC257, UACC502, UACC903, UACC1308, UACC1940, UACC2534, UACC3291, and U2OS) were treated in a 10-point dose-response curve with CQ, QN, VATG014, VATG032, or PLX-4032 for 48 hours and IC_{50} values were determined.

Table 4.2. A375 cells using the Bliss independence model calculations of additivity for autophagy inhibitors with PLX-4032 and AZD-8055.

Compound A	Compound B	Single Compound		Autophagy Inhibitor + PLX-4032	
		Relative Growth Inhibition Compound A	Relative Growth Inhibition Compound B	Expected Bliss Additive Inhibition Value	Actual Growth Inhibition
Chloroquine	PLX-4032	0.16	0.19	0.33	0.38
Quinacrine	PLX-4032	0.38	0.19	0.50	0.59
VATG014	PLX-4032	0.37	0.19	0.49	0.64
VATG032	PLX-4032	0.37	0.19	0.49	0.62
Chloroquine	AZD-8055	0.16	0.12	0.26	0.29
Quinacrine	AZD-8055	0.38	0.12	0.45	0.54
VATG014	AZD-8055	0.37	0.12	0.44	0.57
VATG032	AZD-8055	0.37	0.12	0.44	0.50

$E_{AB}= E_A+E_B-(E_A*E_B)$, **where E_A is the effect of compound A alone and E_B is the effect of compound B alone.**

Soft agar assays were treated with the LD_{10} of CQ, QN, VATG014, VATG032 independently and in combination with the LD_{10} of PLX-4032 and AZD-8055. Relative colony formation was calculated in relation to the control and additivity was determined using the Bliss independence model calculation: $E_{xy}= E_x + E_y - (E_x*E_y)$, where E_x is the effect of compound A alone and E_y is the effect of compound B alone, making the equation $E_{AB}= E_A+E_B-(E_A*E_B)$.

Table 4.3. UACC 1940 cells using the Bliss independence model calculations of additivity for autophagy inhibitors with PLX-4032.

| Compound A | Compound B | Single Compound | | Autophagy Inhibitor + PLX-4032 | |
		Relative Growth Inhibition Compound A	Relative Growth Inhibition Compound B	Expected Bliss Additive Inhibition Value	Actual Growth Inhibition
Chloroquine	PLX-4032	0.51	0.62	0.82	0.80
Quinacrine	PLX-4032	0.62	0.62	0.86	0.81
VATG014	PLX-4032	0.72	0.62	0.90	0.87
VATG032	PLX-4032	0.70	0.62	0.89	0.83

$E_{AB}= E_A+E_B-(E_A*E_B)$, **where E_A is the effect of compound A alone and E_B is the effect of compound B alone.**

Soft agar assays were treated with the LD_{10} of CQ, QN, VATG014, and VATG032 independently and in combination with the LD_{10} of PLX-4032. Relative colony formation was calculated in relation to the control and additivity was determined using the Bliss independence model calculation: $E_{xy}= E_x + E_y - (E_x*E_y)$, where E_x is the effect of compound A alone and E_y is the effect of compound B alone, making the equation $E_{AB}= E_A+E_B-(E_A*E_B)$.

Figure 4.1. Melanoma cell lines have active basal autophagy.
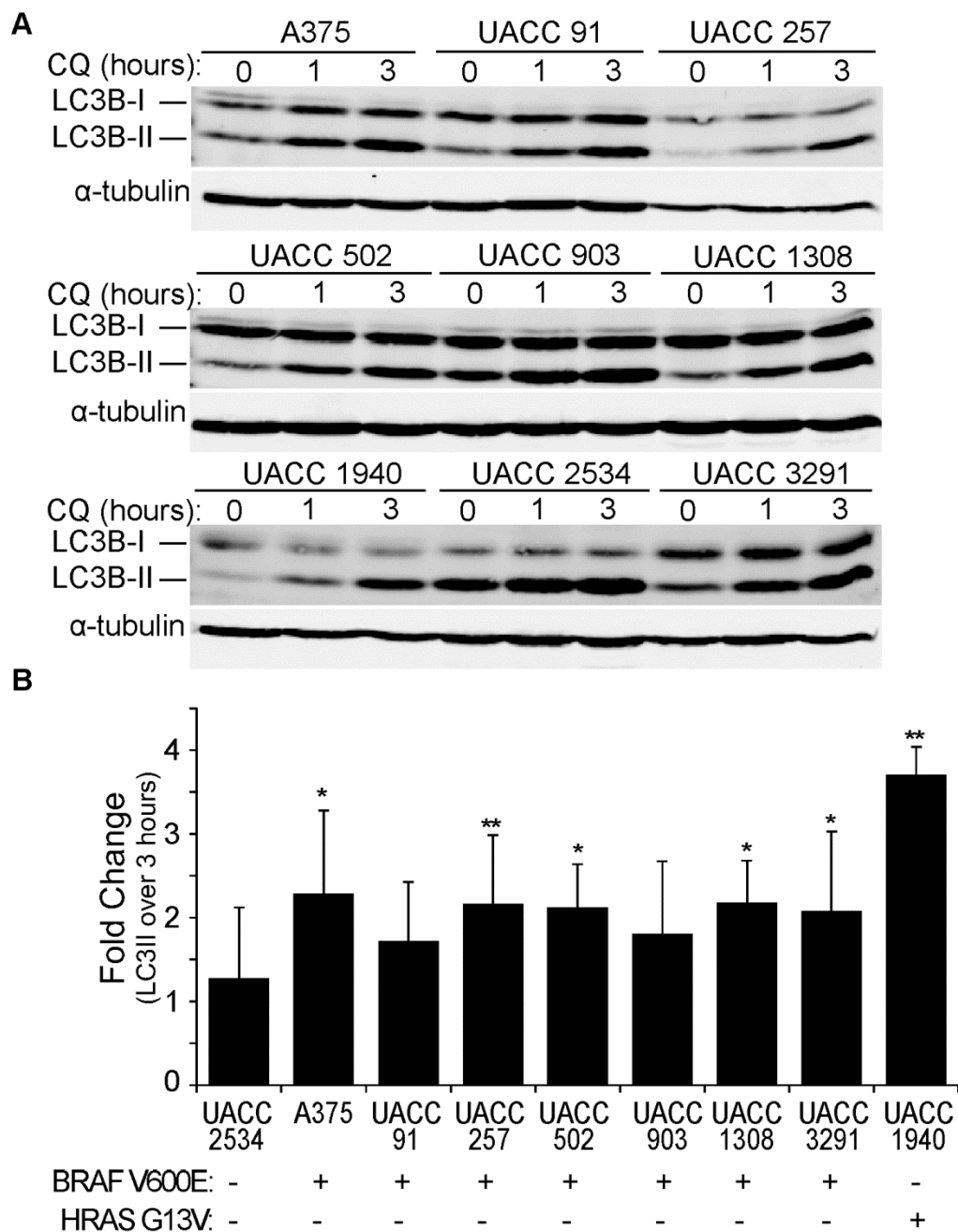
Figure 4.1 (cont'd)

(A) Nine patient-derived melanoma cell lines were treated with 50 μM CQ for 0, 1, or 3 hours. Cell lysates were probed by immunoblotting for endogenous LC3B (LC3B-I: cytosolic; LC3B-II: membrane-bound. (**B**) The levels of LC3B-II and α-tubulin were measured using a digital imaging system (Odyssey) and quantitative immunoblotting. The fold change was determined by the change in LC3B-II normalized to α-tubulin (LC3-II/α-tubulin) from 0 to 3 hours (Y-axis). Error bars indicate standard deviation. Student 2-tailed t-test p-value < 0.05 (*) and 0.01 (**) compared to UACC2534 cells. Mutational status of BRAF and HRAS is indicated as mutant by (+) and wild-type by (-).

Figure 4.2. The BRAF-V600E inhibitor, PLX-4032, does not alter autophagic flux.
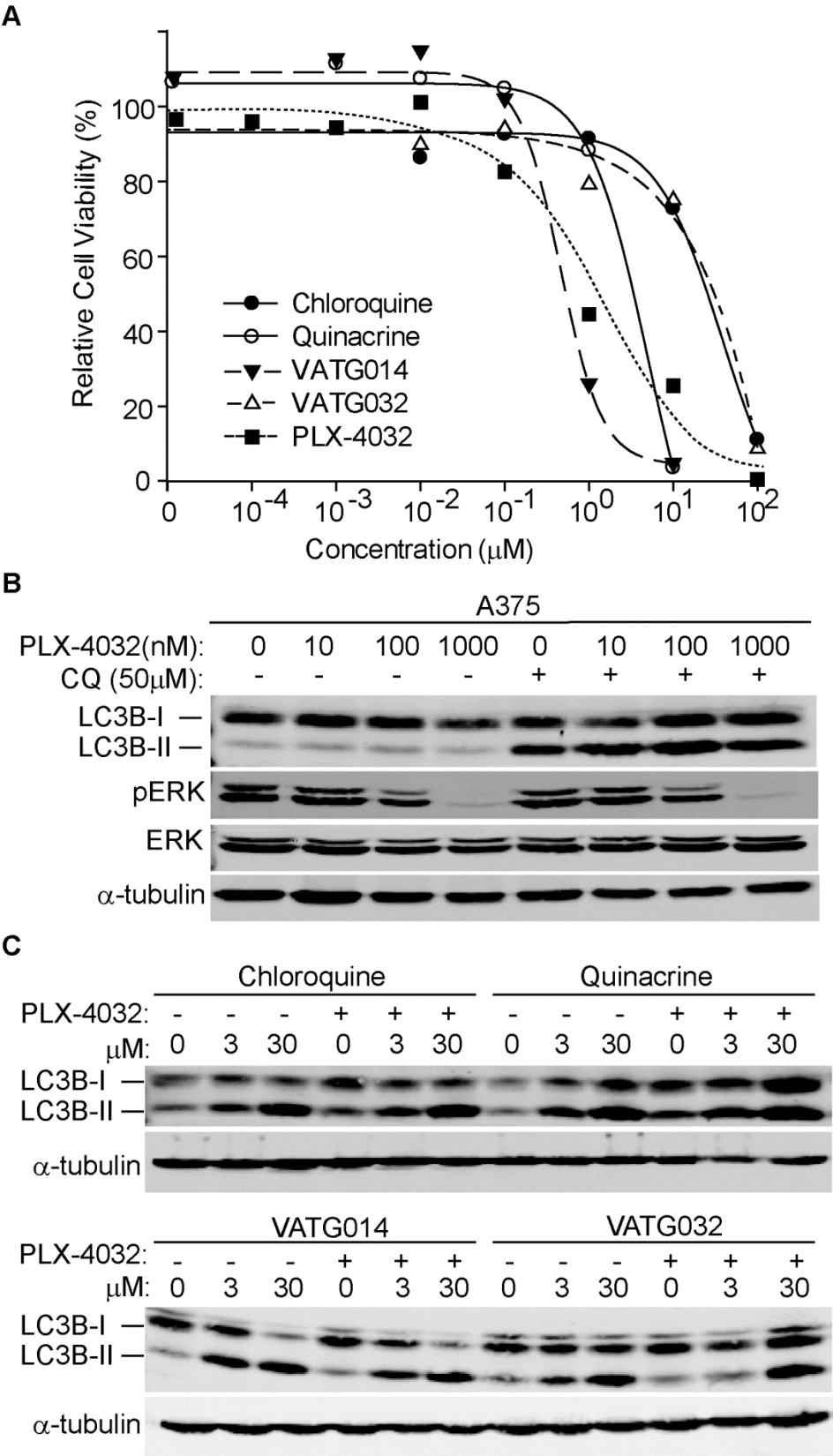
Figure 4.2 (cont'd)

(**A**) A375 cell viability was determined using the CellTiter-Glo luminescent assay after cells were treated for 48 hours with CQ (filled circles), QN (open circles), VATG014 (filled triangles), VATG032 (open triangles), or PLX-4032 (filled squares). Relative cell viability (as a percent of vehicle treatment) is plotted at each compound concentration (log scale). (**B**) Immunoblot of A375 cells treated with 0 μM, 10 nM, 100 nM, and 1 μM of PLX-4032 in the presence (+) or absence (-) of CQ (50 μM). Cell lysates and probed for total ERK1/2, phospho-ERK1/2, and LC3B (LC3B-I: cytosolic; LC3B-II: membrane-bound). Alpha-tubulin was included as a loading control. (**C**) U2OS cells were treated with 0 μM, 3 μM, and 30 μM CQ, QN, VATG014, or VATG032 for 3 hours with (+) or without (-) PLX-4032 (400 nM). Cell lysates were probed by immunoblotting for endogenous LC3B (LC3B-I: cytosolic; LC3B-II: membrane-bound). Alpha-tubulin was included as a loading control.

Figure 4.3. A375 soft agar colony formation dose responses.

A
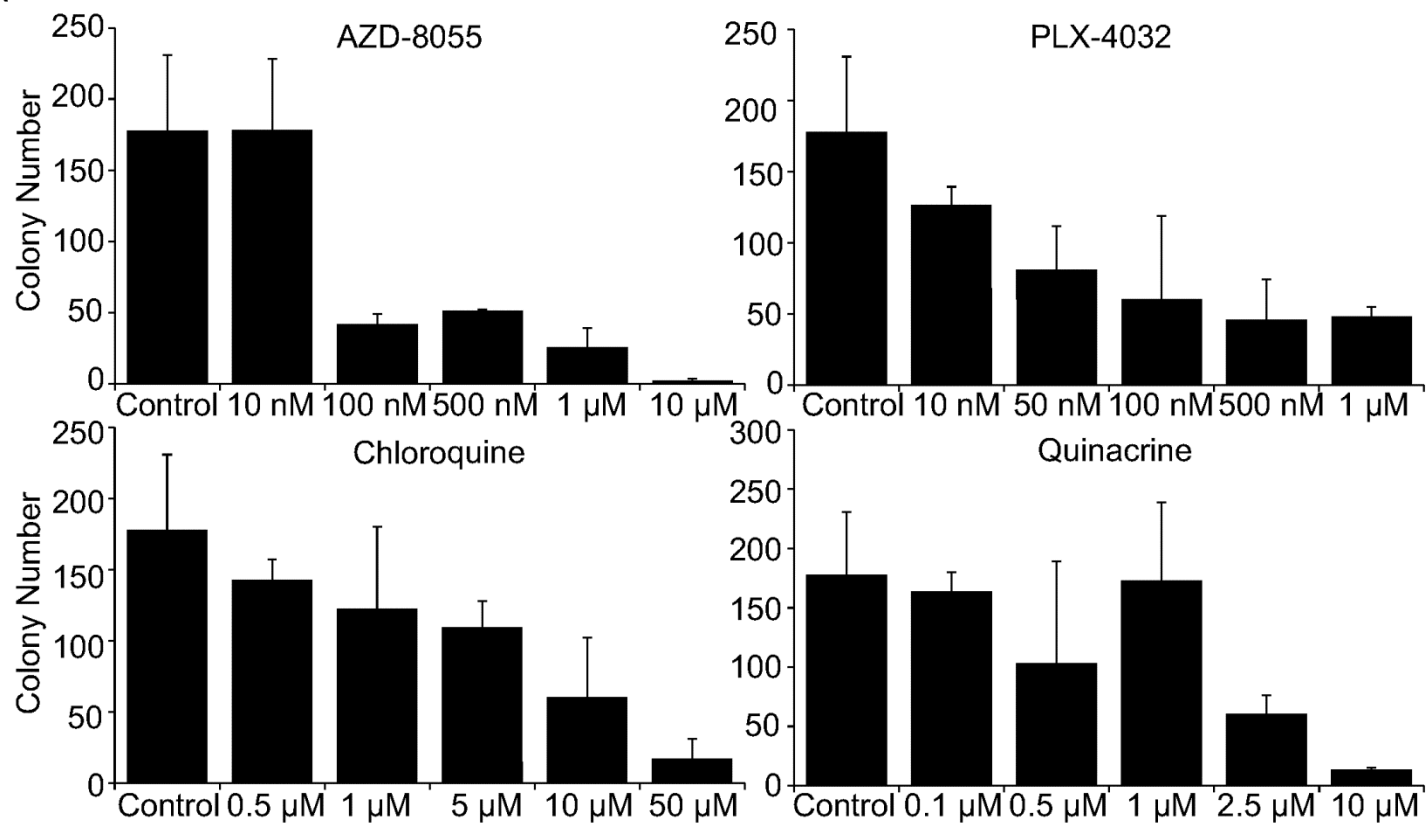
Figure 4.3 (cont'd)
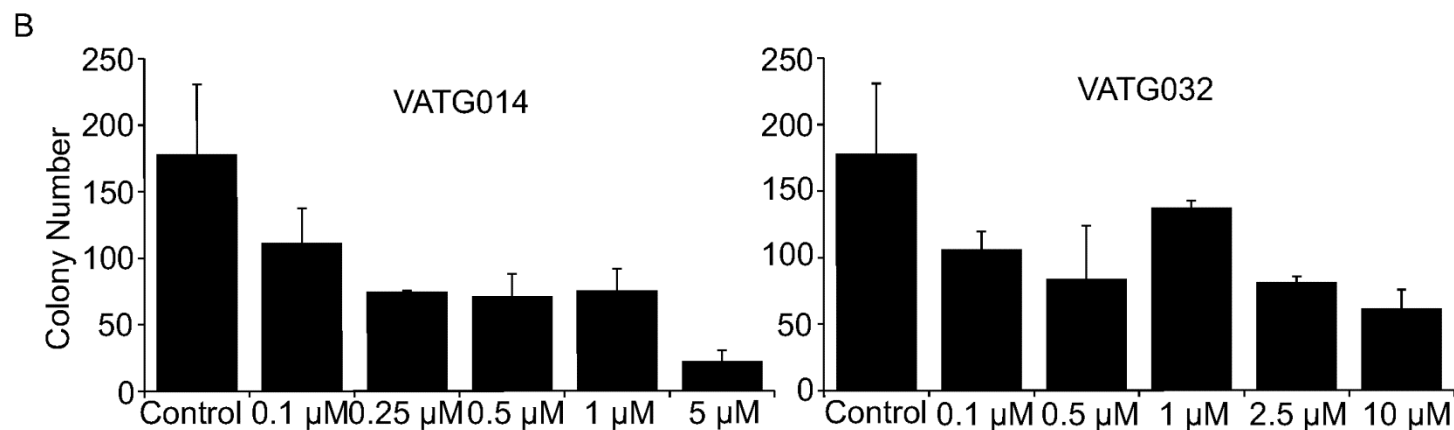
B

(**A**) Soft agar assays were performed using A375 cells treated every other day for 3 weeks with the indicated concentrations of CQ,

QN, PLX-4032, or AZD-8055. Colonies were stained with crystal violet and quantified using image analysis software. Colony

numbers (per well of a 6-well dish) from 3 independent experiments were averaged and error bars indicate standard deviation. (**B**)

Soft agar assays were performed using A375 cells treated every other day for 3 weeks with the indicated concentrations of VATG014

and VATG032. Colonies were stained with crystal violet and quantified using image analysis software. Colony numbers (per well of

a 6-well dish) from 3 independent experiments were averaged and error bars indicate standard deviation.

Figure 4.4. Autophagy inhibitors reduce A375 colony formation alone and in combination with PLX-4032.

Figure 4.4 (cont'd)

B
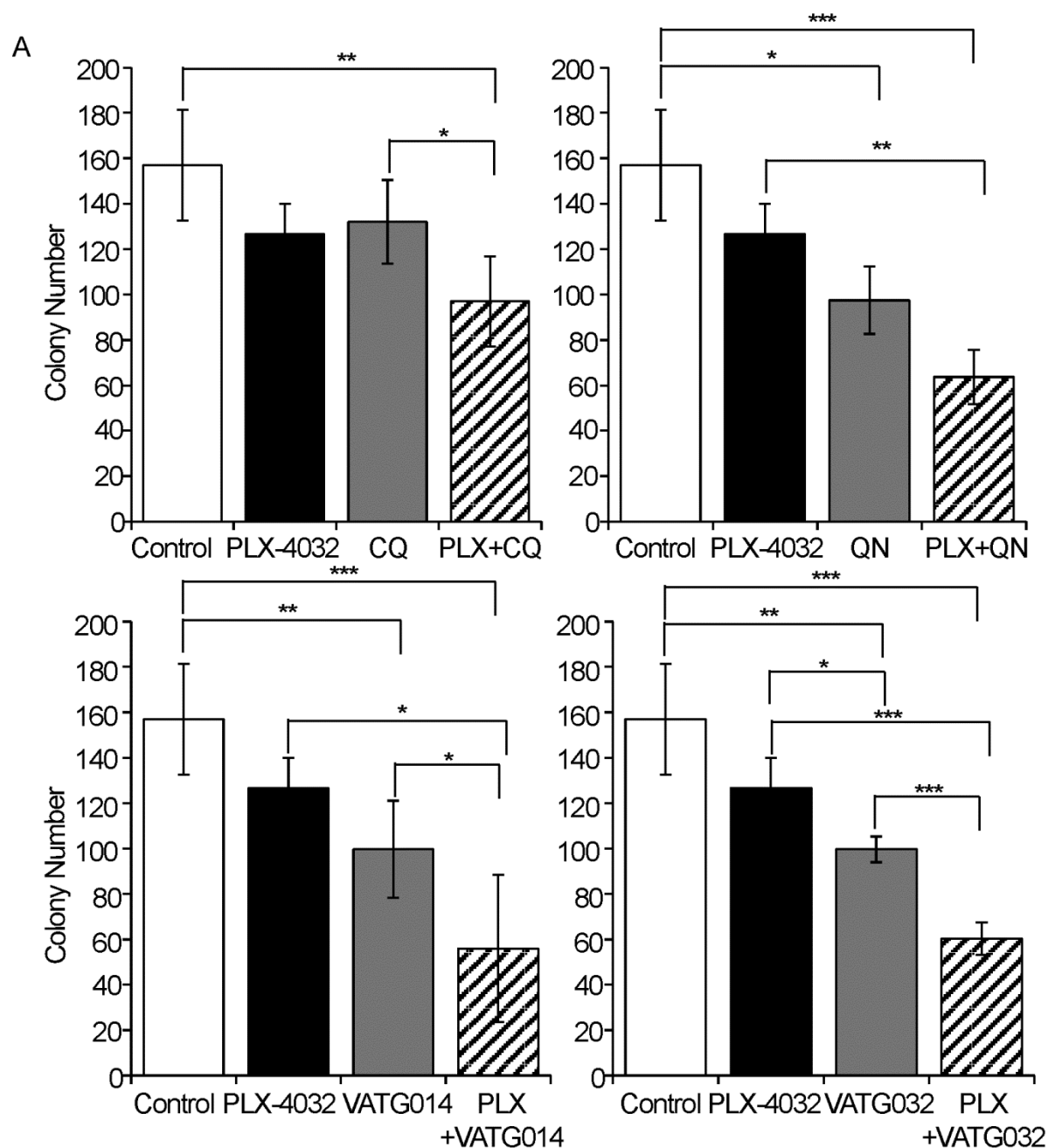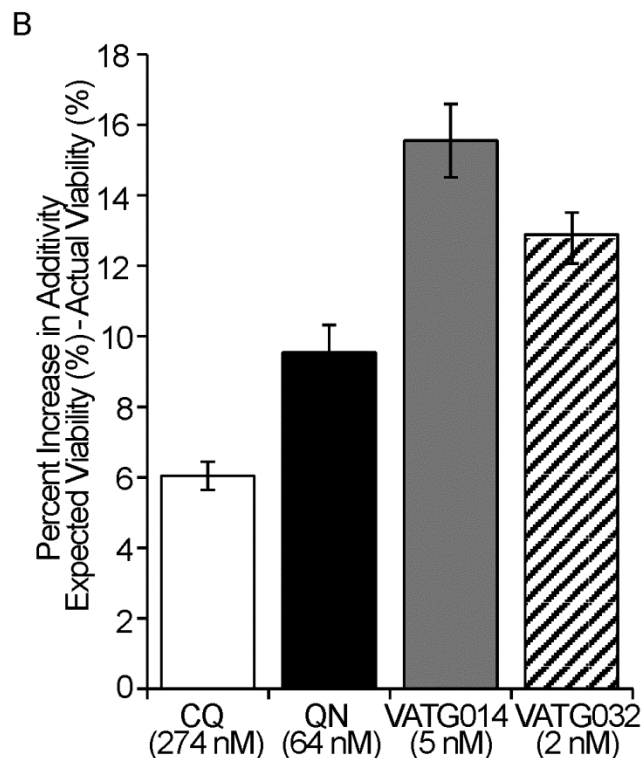
(**A**) Soft agar assays were performed using A375 cells that were treated every other day for 3 weeks at the LD_{10} concentration of PLX-4032 (1.3 nM) in the presence or absence of the IC_{10} concentration for chloroquine (CQ; 274 nM), quinacrine (QN; 64 nM), VATG014 (5 nM), or VATG032 (2 nM). Colonies were stained with crystal violet and quantified using image analysis software. Colony numbers (per well of a 6-well dish) from three independent experiments were averaged and standard deviation is shown by error bars. Student 2-tailed t-test p-values < 0.05 (*), 0.01 (**), and 0.001 (***). (**B**) The total percent change in additivity above that of the expected additive effect (as determined by the Bliss Independence model) was determined for each autophagy inhibitor in combination with PLX-4032.

Figure 4.5. Autophagy inhibitors reduce A375 colony formation alone and in combination with AZD-8055.

A

Figure 4.5 (cont'd)

B
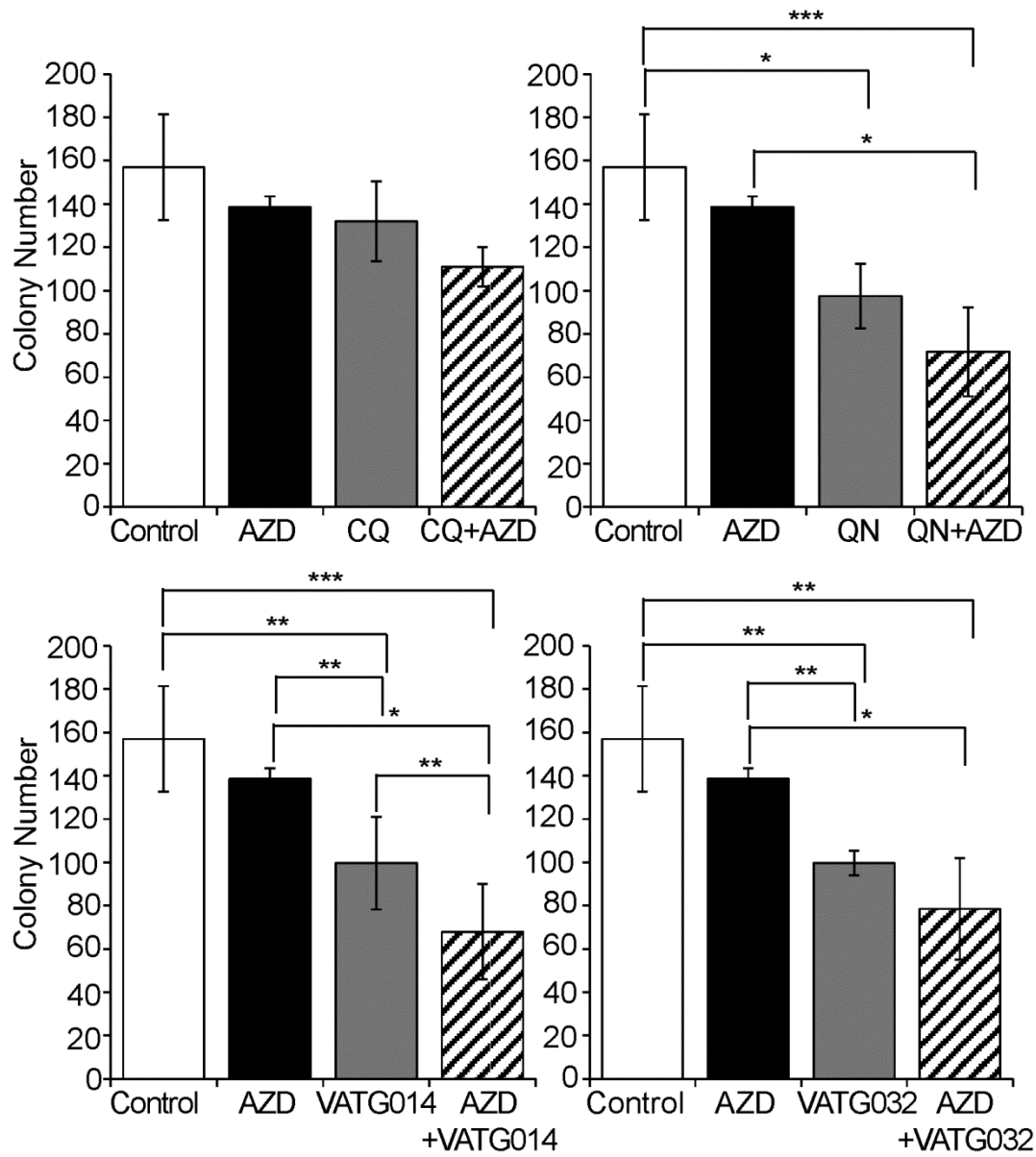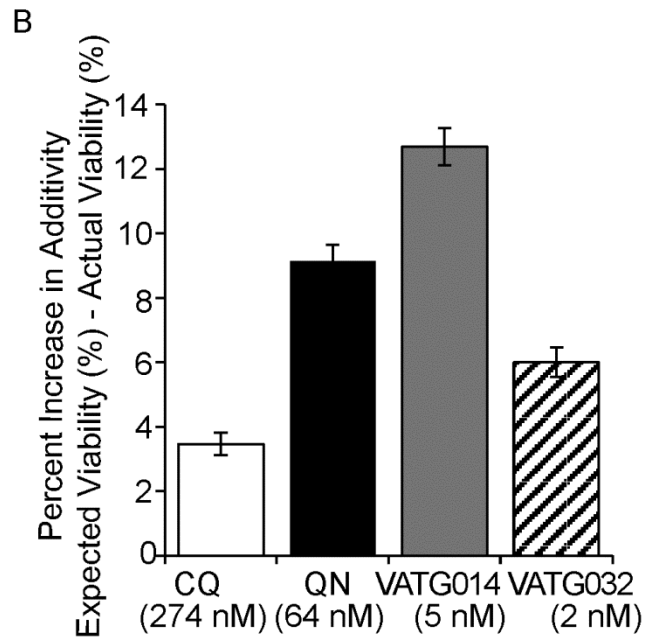
(**A**) A347 cells were cultured in soft agar and treated every other day for 3 weeks with the LD_{10}

of AZD-8055 (AZD) with or without co-treatment of the LD_{10} of chloroquine (CQ), quinacrine

(QN), VATG014, or VATG032. Colonies were stained with crystal violet and quantified using

image analysis software. Colony numbers (per well of a 6-well dish) from 3 independent

experiments were averaged. Error bars indicate standard deviation. Student 2-tailed t-test p-

values < 0.05 (*), 0.01 (**), and 0.001 (***). (**B**) The percent change in total additivity of

colony formation compared to the expected additive effect determined by the Bliss Independence

model for each autophagy inhibitor in combination with AZD-8055. Error bars represent the

standard deviation.

Figure 4.6. UACC 1940 and UACC 91 soft agar colony formation assays.

Figure 4.6 (cont'd)

B
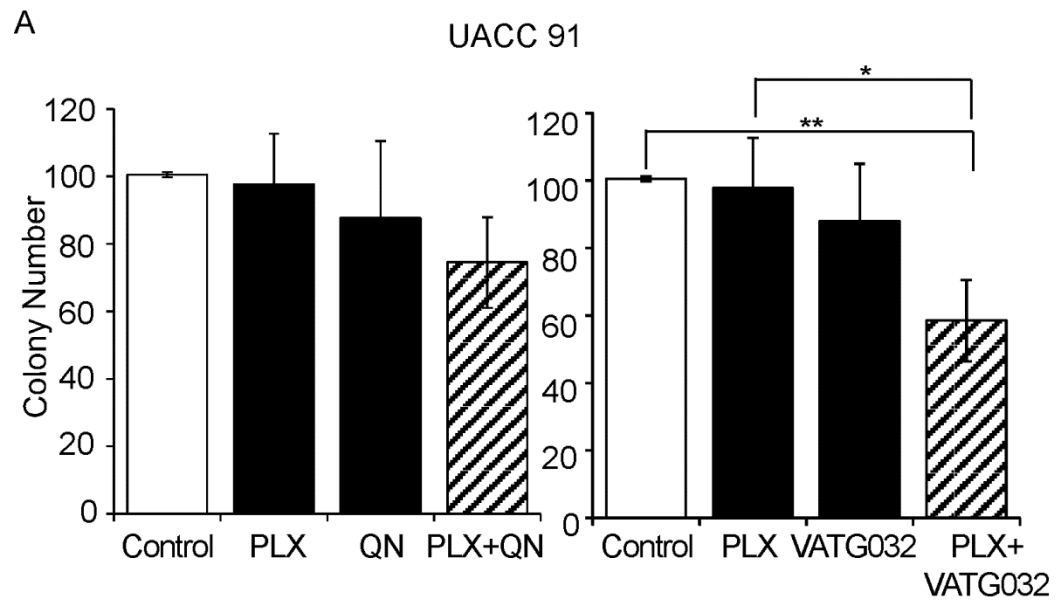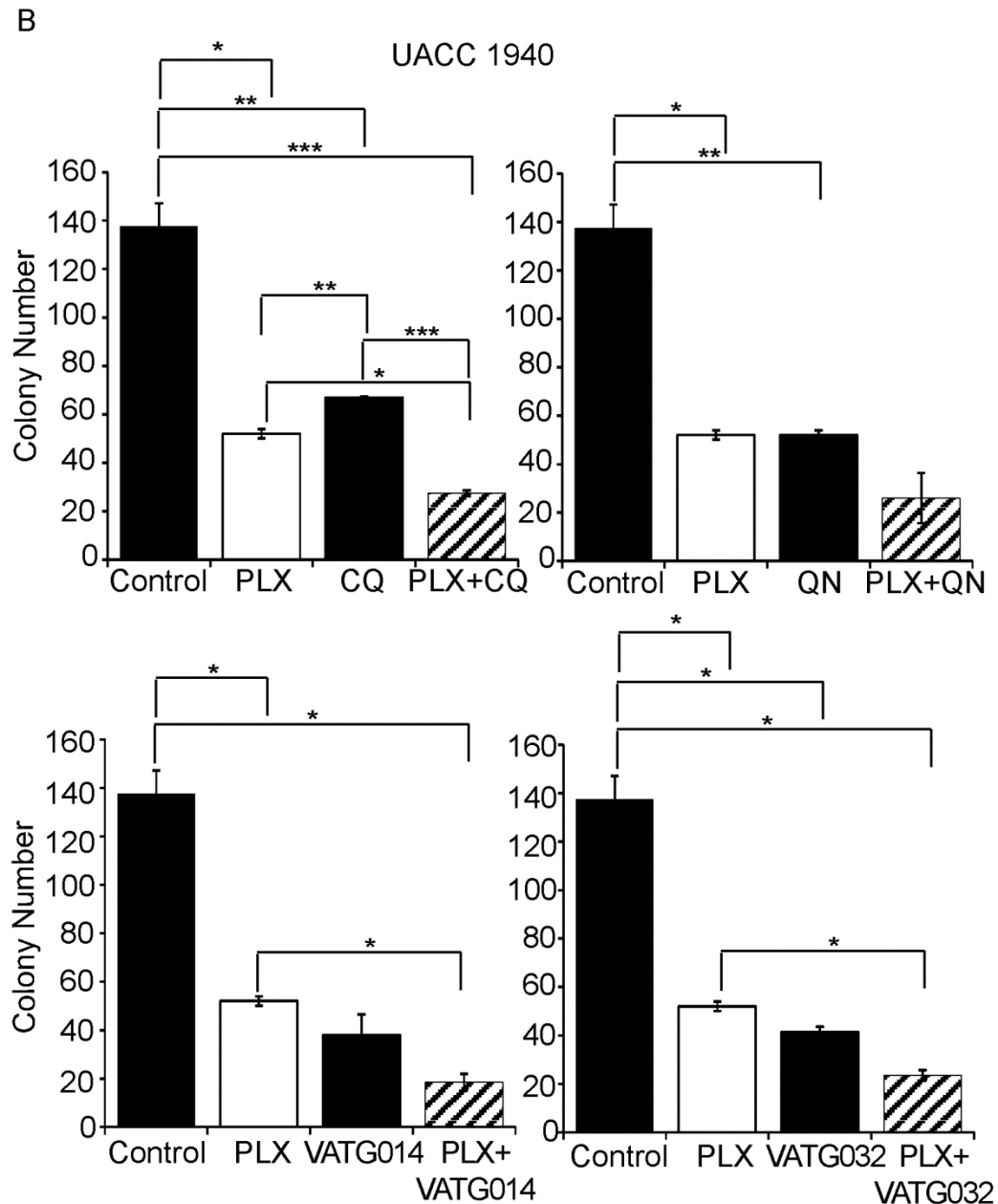
(A) Soft agar colony formation assays were performed using UACC 1940 cells that were treated

every other day for 3 weeks at the LD_{10} of PLX-4032 with or without co-treatment with the LD_{10}

of chloroquine (CQ), quinacrine (QN), VATG014, or VATG032. Colonies were stained with

crystal violet and quantified using image analysis software. Colony numbers (per well of a 6-well

Figure 4.6 (cont'd)

dish) from 3 independent experiments were averaged. Error bars indicate standard deviation. Student 2-tailed t-test p-values < 0.05 (*), 0.01 (**), and 0.001 (***). (**B**) Soft agar colony formation assays were performed using UACC 91 cells that were treated every other day for 3 weeks at the LD_{10} of PLX-4032 with and without co-treatment at the LD_{10} of QN or VATG032. Colonies were stained with crystal violet and quantified using image analysis software. Colony numbers (per well of a 6-well dish) from 3 independent experiments were averaged. Error bars indicate standard deviation. Student 2-tailed t-test p-values < 0.05 (*) and 0.01 (**).

Figure 4.7. Autophagy inhibitors reduce A375 colony formation alone and in combination with PLX-4032 at fixed concentrations.
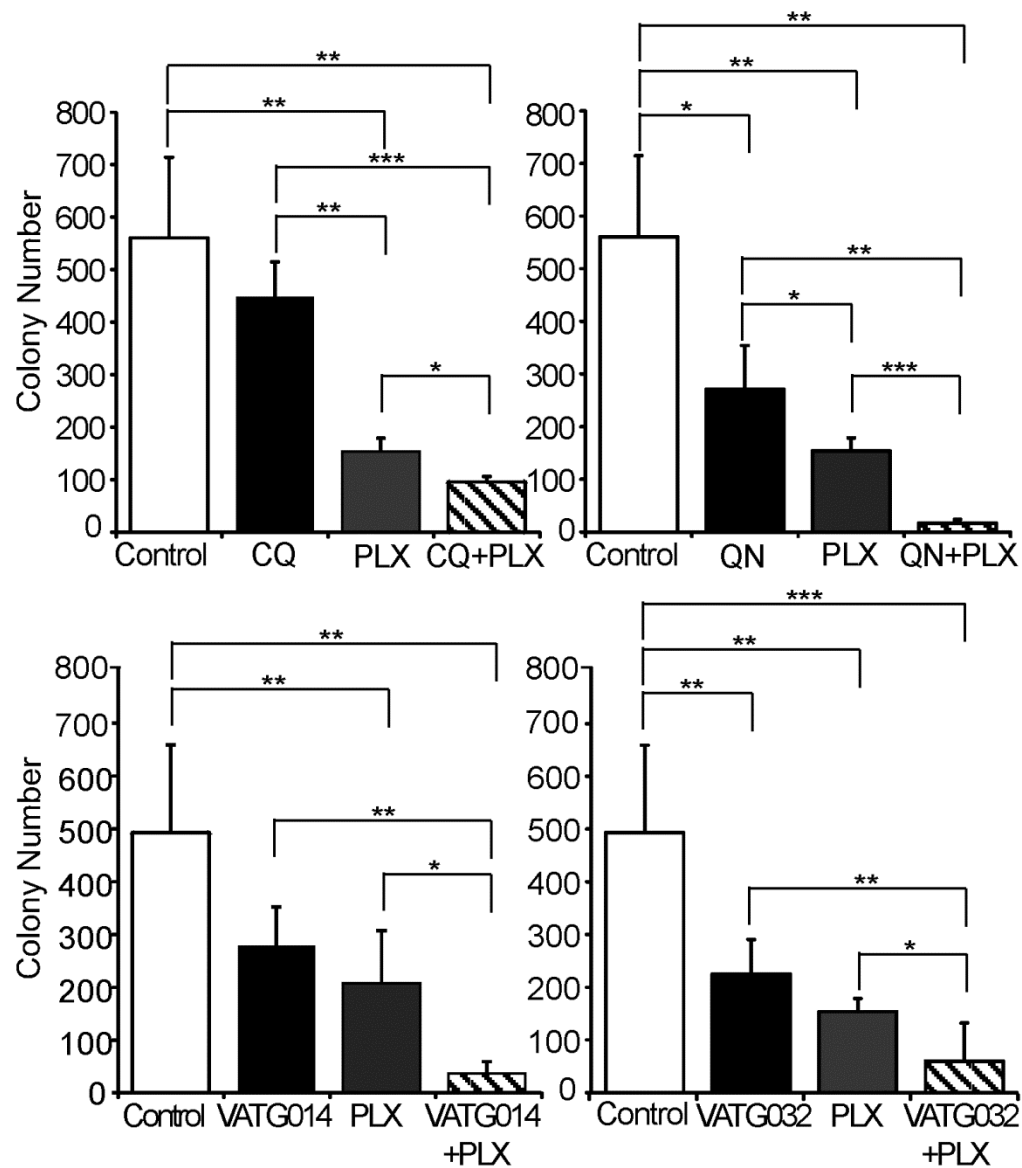
A375 cells were grown in soft agar and treated every other day for 3 weeks with 3 μM of chloroquine (CQ), quinacrine (QN), VATG032, or 1 μM VATG014 in the presence or absence of PLX-4032 (400 nM). Colonies were stained with crystal violet and quantified using image analysis software. Colony numbers (per well of a 6-well dish) from 3 replicates were averaged

Figure 4.7 (cont'd)

and standard deviation is shown by error bars. Student 2-tailed t-test p-values < 0.05 (*), 0.01 (**), and 0.001 (***).

CHAPTER 5

IDENTIFICATION AND BIOCHEMICAL CHARACTERIZATION OF A REVERTANT MUTATION IN ONCOGENIC BRAF THAT CONFERS VEMURAFENIB RESISTANCE

Megan L. Goodall, Jeffrey P. MacKeigan, Aleksander Sekulic, Ashani Weeraratna, and Jeff

Trent

ABSTRACT

Malignant melanoma has very poor prognosis and the development of targeted therapies, such as vemurafenib to BRAF V600E mutations, has brought about the promise of new treatment options. However, as with most targeted agents, therapeutic resistance to vemurafenib remains a major clinical problem and resistance mutations have yet to be identified. Vemurafenib is a small molecule known to function by preferentially binding to the active form of the BRAF kinase. The BRAF V600E mutation converts BRAF to a constitutively active kinase, and thus makes vemurafenib a BRAF V600E selective inhibitor. Here, we present an extraordinary case study of vemurafenib resistance in metastatic melanoma. The vemurafenib resistance mutation was identified in both the mother and infant after transplacental melanoma transfer. Through genome sequencing, we discovered a second kinase domain mutation L567V. We establish that dual V600E/L567V mutation diminishes BRAF kinase activity compared to the V600E mutation alone. Moreover, the BRAF double mutant activity is less sensitive to vemurafenib *in vitro* than the single BRAF V600E mutant. Further, we show that cells expressing the single (L567V) or double (V600E/L567V) mutant are less sensitive to vemurafenib than both wild-type and BRAF V600E expressing cells. Taken together, we hypothesize that the second BRAF L567V mutation, which restores V600E kinase activity to wild-type levels, disrupts the preferential binding of vemurafenib. Therefore, the L567V mutation may represent a classical revertant mutation and possibly the first clinical report of vemurafenib resistance caused by a second-site mutation in BRAF V600E.

INTRODUCTION

Skin cancer is the third most common cancer (excluding sex specific cancers) in the world, with melanoma accounting for the most skin cancer related deaths (Gray-Schopfer, Wellbrock et al. 2007). Majority of melanoma cases are influenced by geographical location and the pigmentation of the population, demonstrating that ultraviolet (UV) light plays a major contributing role in its development (Chin 2003). In recent years there has been a rise in melanoma incidence, most likely due to the popularity of sun-tanning (Gilchrest, Eller et al. 1999; Chin 2003). Prevention (i.e. sunscreen) and early detection are the only successful means to reduce melanoma risk. In cases where melanoma is detected early, it is typically curable by surgical resection. However, if found undetected, malignant melanoma has a very poor prognosis and tends to be refractory to most therapies (Gray-Schopfer, Wellbrock et al. 2007).

The RAS/RAF/MEK/ERK pathway has become known as a crucial regulator of melanoma proliferation. ERK is hyperactivated in 90% of cases through one of its upstream regulators NRAS (mutated in 15-30% of cases) or BRAF (mutated in 50-70% of cases). Equally informative these mutations are mutually exclusive (Davies, Bignell et al. 2002; Gray-Schopfer, Wellbrock et al. 2007). In cases of BRAF mutant melanoma, 60% occur at the V600E site within the kinase domain (Figure 5.1) (Chin 2003). This same amino acid position has also been shown to be mutated in multiple other cancers, including colorectal, thyroid, non-small cell lung, and multiple others (Davies, Bignell et al. 2002). The BRAF V600E mutation constitutively increases BRAF kinase activity and hyperactivates downstream MAPK signaling, making it a compelling drug discovery target in oncology (Bollag, Tsai et al. 2012).

In early 2008, the discovery of vemurafenib (PLX-4032) was first published by Plexxikon (Tsai, Lee et al. 2008). Vemurafenib preferentially binds to the active form of the

kinase, making it a selective inhibitor of the V600E form of BRAF over the wild-type enzyme (Tsai, Lee et al. 2008; Bollag, Hirth et al. 2010; Bollag, Tsai et al. 2012). Due to the remarkable results observed both *in vitro* and *in vivo*, vemurafenib was moved into clinical trials as a targeted agent for the treatment of metastatic melanoma (Flaherty, Puzanov et al. 2010). In phase II clinical trials, an overall response rate of 53% was observed, with 6% having complete responses, and progression-free survival lasting up to 7 months (Sosman, Kim et al. 2012). Until vemurafenib, the typical response rate to the current standard of care, dacarbazine, was only 10% with progression-free survival lasting up to 2 months (Bollag, Hirth et al. 2010).

Despite the promising results observed in metastatic melanoma, recurrence of tumors and vemurafenib resistance frequently appears in 8 to 12 months after treatment (Solit and Sawyers 2010). There are many potential suggested mechanisms of resistance to vemurafenib; however, as vemurafenib is still fairly new to treatment regimens, only a few resistance mechanisms have been explored. One proposed mechanism involves activation of parallel pathways by RAS, epidermal growth factor receptor (EGFR), and platelet-derived growth factor 1 receptor (PDGFR) (Solit and Sawyers 2010; Solit and Rosen 2011; Prahallad, Sun et al. 2012). While there are many other single case studies of potential mechanisms for vemurafenib resistance, a commonly expected resistance mechanism, a second-site mutation, has not been found (Solit and Rosen 2011; Bollag, Tsai et al. 2012). Here, we present a case study of what is, to our knowledge, the first second-site mutation that causes resistance to vemurafenib.

Case study identification of potential vemurafenib resistance mutation

An extraordinary case study involving a potential BRAF resistance mutation to vemurafenib was brought to us by a long standing collaboration between Drs. Aleksander Sekulic (Mayo Clinic Arizona), Ashani Weeraratna (The Wistar Institute), and Jeffrey Trent (Translational Genomics Research Institute). This case study was of pregnant woman with malignant melanoma driven by a BRAF V600E mutation, which refused chemotherapeutic treatment to spare her unborn child. However, in an unfortunate and an extremely rare occurrence, the melanoma crossed the placenta and spread to the unborn child (Alexander, Samlowski et al. 2003). This child was then born with metastatic melanoma containing the BRAF V600E mutation. In late 2011, both the mother and infant were treated with vemurafenib; however, the metastatic melanoma was not responding to treatment, leading to the question as to whether a possible vemurafenib resistance mechanism had emerged. Next generation sequencing was performed on the melanoma and uncovered a second-site mutation, L567V, in the kinase domain of BRAF. To determine whether this second-site mutation conferred vemurafenib resistance, a series of BRAF constructs were generated, which we evaluated using *in vitro* kinase assays.

Kinase assays indicate BRAF L567V is a putative revertant mutant

To determine how L567V mutation affects BRAF kinase activity, we performed radioactive kinase assays using BRAF mutants (wild-type, V600E, L567V, or the double mutant V600E/L567V) immunoprecipitated from 293FT cells (Figure 5.2A). Consistent with prior reports, we found that BRAF V600E had substantially higher activity (2.5 fold) than wild-type

BRAF, while L567V had slightly lower kinase activity (Davies, Bignell et al. 2002). Intriguingly, the dual V600E/L567V mutation had much lower activity than V600E alone, and returned BRAF kinase activity to near wild-type kinase activity levels.

Next, we sought to determine if the dual BRAF mutation conferred resistance to PLX-4032 *in vitro.* To do this, we repeated immunoprecipitations and supplemented kinase reactions with 50 nM PLX-4032 (Figure 5.2B). We found that while PLX-4032 significantly reduced V600E kinase activity, wild-type kinase activity was unchanged, as expected. PLX-4032 slightly reduced L567V kinase activity, and V600E/L567V kinase activity was only slightly reduced, but not to the full extent of BRAF V600E kinase activity. To further explore this result, kinase activity was measured after treatment with 10, 25, or 50 nM PLX-4032. At 50 nM PLX-4032, wild-type BRAF kinase activity was not inhibited, in contrast V600E BRAF kinase activity was abolished (Figure 5.2C). Although BRAF V600E/L567V kinase activity was reduced in response to 50 nM PLX-4032, it was not ablated as in the BRAF V600E mutant context and partially retained 20 to 30% kinase activity (Figure 5.2). This finding suggests that L567V is not a full resistance mutation, but a putative second-site revertant mutation.

Cell viability measurements support BRAF L567V as a BRAF V600E revertant mutant

To assess if the revertant kinase activity observed by L567V was responsible for resistance to PLX-4032, a half-log PLX-4032 dose-response curve was performed in cells exogenously expressing BRAF constructs. Cells were transfected with constructs containing wild-type BRAF, BRAF V600E, BRAF L567V, and BRAF V600E/L567V for 24 hours prior to treatment with PLX-4032. After 48 hour PLX-4032 treatment, cell viability was measured and LD_{50} values were determined. Cells expressing wild-type BRAF had an LD_{50} equal to 41 μM

while those with the V600E mutation had an LD_{50} of 28 μM, less than wild-type as expected.

However, cells expressing either L567V or the double mutant V600E/L567V both had an LD_{50}

equal to 51 μM. At concentrations of PLX-4032 shown to inhibit ERK phosphorylation in the

V600E mutant A375 melanoma cells (see Chapter 4), viability was reduced by 20% in the 293FT

cells overexpressing V600E, while viability remained unchanged to wild-type in BRAF L567V

or BRAF V600E/L567V mutant cells (Figure 5.2D). This further supports that the BRAF

L567V mutation may promote acquired resistance to PLX-4032, even in the presence of an

oncogenic BRAF V600E mutation.

DISCUSSION

The development of targeted therapies for metastatic melanoma, such as vemurafenib for BRAF V600E mutant tumors, has brought about the promise of treatment options to those who originally had none. Unfortunately, the early promise of vemurafenib as an effective therapeutic is not as encouraging as originally hoped. The development of resistance has already been publicized; however, since vemurafenib is still a relatively new therapeutic, the molecular mechanisms detailing how drug resistance occurs is not fully understood. This is partially due to the fact that the activation of BRAF itself, and the other RAFs (A and C), is still not completely resolved (Lito, Rosen et al. 2013). Understanding the differences in the isoforms of RAF also explain why BRAF is the leading mutation in human cancers; as it has higher basal activity than its counterparts allowing a single mutation to result in constitutive activity (Lito, Rosen et al. 2013).

It has been shown that there are multiple ways that resistance has occurred in vemurafenib resistance (Holohan, Van Schaeybroeck et al. 2013). However, most if not all of the resistance mechanisms are through bypassing BRAF. Early work indicated that some mechanisms for vemurafenib resistance are by upregulating alternative pathways, such as RAS or other RTKs, or mutations in downstream proteins, such as MEK1 or MAPK (Johannessen, Boehm et al. 2010; Nazarian, Shi et al. 2010; Wagle, Emery et al. 2011). More recently, it has been shown that loss of exons 4-8 in the RAS binding domain of BRAF V600E allows for RAF dimerization, which does occur in BRAF V600E mutants normally, and prevents vemurafenib from binding (Poulikakos, Persaud et al. 2011; Lito, Rosen et al. 2013). This is the first reported structural change in BRAF that confers vermurafenib resistance (Poulikakos, Persaud et al. 2011).

155

There are many other cases of developed resistance to targeted therapies known, some of which have identified second site mutations; examples include BCR-ABL with imatinib, dasatinib, and nilotinib, as well as EGFR with gefitinib and cetuximab (Holohan, Van Schaeybroeck et al. 2013). However, there are still several targeted therapies that have developed resistance with no second site mutations yet identified, such as vermurafenib to BRAF V600E (Solit and Rosen 2011; Bollag, Tsai et al. 2012; Holohan, Van Schaeybroeck et al. 2013). Lack of a second site mutation in BRAF V600E conferring resistance is surprising due to a mutational hot spot overlapping in the kinase domain (Greaves, Verma et al. 2013). The surprise is further underlined due to the fact that in the case of BCR-ABL, the most common form of resistance is by a point mutation in the kinase domain, occurring up to 90% of cases (Jabbour, Kantarjian et al. 2006).

Here, we illustrate a case study of vemurafenib resistance where a second-site mutation in BRAF was identified after sequencing in a mother and child that did not respond to vemurafenib, despite having the BRAF V600E mutations. This BRAF mutation, L567V, was shown to be located in the kinase domain, similarly to V600E. To determine if this dual mutation conferred resistance to vemurafenib, we tested BRAF V600E/L567V kinase activity and report revertant kinase activity back to wild-type when compared to the constitutively active V600E mutation alone. In addition, the V600E/L567V mutation did not respond as strongly to BRAF kinase inhibition by vemurafenib in *in vitro* kinase assays. We further showed that both the L567V and V600E/L567V mutations had a higher LD_{50s} compared to both wild-type and V600E in dose-response curves in response to vemurafenib.

We believe that since the BRAF L567V mutation lies within the kinase domain, it interferes with the kinase activity and more specifically the constitutive activity of the V600E

mutation. The decreased kinase activity back to wild-type levels in the L567V mutations prevents vemurafenib from preferentially binding, as vemurafenib is known to function by preferentially binding to the active form of the BRAF kinase. It is also possible that this mutation could potentiate a similar effect observed in the BRAF mutant lacking the RAS binding domain and allowing increased dimerization not typically observed with the BRAF V600E mutant, preventing vemurafenib binding. This observation makes the L567V mutation a putative revertant mutant and the first case of resistance in a patient by a second-site mutation in BRAF (Solit and Sawyers 2010; Solit and Rosen 2011; Bollag, Tsai et al. 2012). Further, resistance in cancer through reversions are an incredibly rare event, mainly due to the inefficiency in returning to a wild-type state, making this an even more interesting finding (Telerman and Amson 2009).

MATERIALS AND METHODS

Transfection of BRAF Constructs

293FT cells were seeded in 10 cm plates in DMEM with 10% FBS at 1×10^6 cells per plate. After 24 hours, cells were transfected with a final concentration of 2 µg of BRAF DNA constructs (wild-type, V600E, L567V, and V600E/L567V) using 6 µL of FuGene HD (Promega, E2311) in 200 µL of Opti-MEM (Invitrogen, 31985-062) and 4 mL of DMEM with 10% FBS. DNA constructs are pLU vector backbones which were developed at the Wistar Institute. These vectors contain a CMV driven promoter, viral packaging proteins, and a puromycin selectable marker.

Immunoblotting

For immunoblotting, 293FT cells were transfected with BRAF expressing constructs (wild-type, V600E, L567V, and V600E/L567V) as described above. After 24 hours, cells were lysed [10mM KPO4, 1mM EDTA, 10mM $MgCl_2$, 5mM EGTA, 50mM bis-glycerophosphate, 0.5% NP40, 0.1% Brij35, 0.1% sodium deoxycholate, 1mM NaVO4, 5mM NaF, 2mM DTT, and complete protease inhibitors (Sigma, P8340)] and 25 µg of protein was resolved by SDS-PAGE. Proteins were transferred to nitrocellulose membranes and probed with primary antibodies [BRAF (Millipore, 07-453), anti-α-tubulin (Sigma, T6199), pERK (Cell Signaling Technology, 9101), ERK (Cell Signaling Technology, 4695) pMEK (Cell Signaling Technology, 9154), MEK (Cell Signaling Technology, 9126)] for 16 hours at 4^oC followed by a secondary antibody [Odyssey IRDye 680CW Goat anti-rabbit IgG (LI-COR, 926-32221) or IRDye 800CW Goat

anti-mouse IgG (LI-COR, 926-32210)] for 1 hour at room temperature. Proteins were detected with Odyssey Imaging System (Li-Cor Biosciences) and quantified.

BRAF Kinase Assays

293FT cells were seeded in 10 cm plates in DMEM with 10% FBS and transfected with BRAF constructs (WT, V600E, L567V, and V600E/L567V) for 24 hours. Cells were lysed [10mM KPO4, 1mM EDTA, 10mM $MgCl_2$, 5mM EGTA, 50mM bis-glycerophosphate, 0.5% NP40, 0.1% Brij35, 0.1% sodium deoxycholate, 1mM $NaVO_4$, 5mM NaF, 2mM DTT, and complete protease inhibitors (Sigma, P8340)] and clarified by centrifugation. Lysates were immunoprecipitated with anti-BRAF antibody (Millipore, 07-453) for 2 hours at 4°C, complexed with IgG agarose beads for 1 hour, washed twice in lysis buffer, and twice in kinase assay buffer [50mM Tris-HCl pH 7.5, 1mM Na_3VO_4, 2mM DTT, 1mM EGTA, 10mM glycerophosphate, 20mM $MgCl_2$]. To normalize the amount of BRAF protein immunoprecipitated, a bovine serum albumin (BSA) protein loading control and the protein from immunoprecipitated BRAF constructs were resolved by SDS-PAGE and BRAF protein levels were quantified using Coomassie staining. Assays with PLX-4032 were pre-treated 5 minutes prior to the kinase reaction. Radioactive kinase assays contained 1mM ATP, 0.4 μg MEK1 inactive (Millipore, 14-420), 0.2 mCi [γ-^{32}P] ATP (PerkinElmer, NEG002H250UC), kinase buffer, and beads complexed with BRAF protein normalized to wild-type BRAF. Kinase assays were incubated for 20 min at 25°C, stopped with 2x sample buffer, and resolved by SDS-PAGE. Gels were dried, incubated for one hour by phosphorimager, and quantified.

Cell Viability (LD$_{50}$) Screen

293FT cells were seeded at 500 cells per well in DMEM with 10% FBS in 96-well clear bottom, black-walled tissue culture plates. After 24 hour incubation, cells were transfected with BRAF constructs (WT, V600E, L567V, and V600E/L567V) for 24 hours. Cells were then treated with PLX-4032 in triplicate with a 10-point half log dose response from 1 nM to 100 μM for 48 hours. Medium was removed and 2x CellTiter Glo (Promega, G7571) reagent mixed 1:1 with Opti-MEM (Invitrogen, 31985062) was added at 100 μL per well and incubated at room temperature for 15 minutes while rocking. A total of 75 μL per well was moved to a white-walled 96-well plate and luminescence quantified using the 96 LUM program on an EnVision plate reader (PerkinElmer) and exported for analysis. All triplicate data points were averaged and luminescent readings for each treatment were normalized to vehicle control for change in viability. Data from dose response curves were entered in Prism for LD$_{50}$ calculations (GraphPad).

Figure 5.1.BRAF Protein Domain Structure
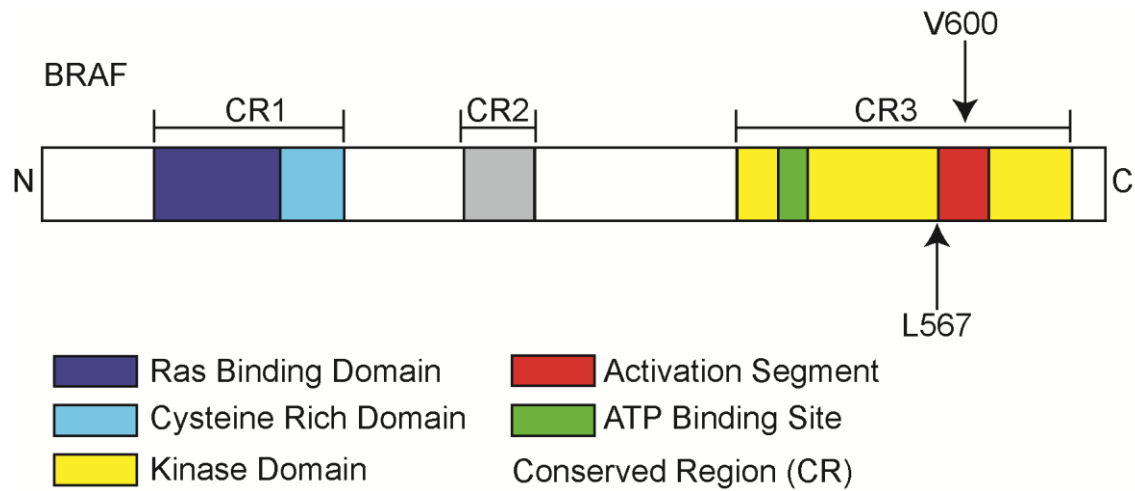
The V600E BRAF mutation lies within the activation segment of the kinase domain, while the

new mutation, L567V, lies at the border of the activation segment.

Figure 5.2 Kinase assays identify L567 is a putative revertant mutant of BRAF V600E.
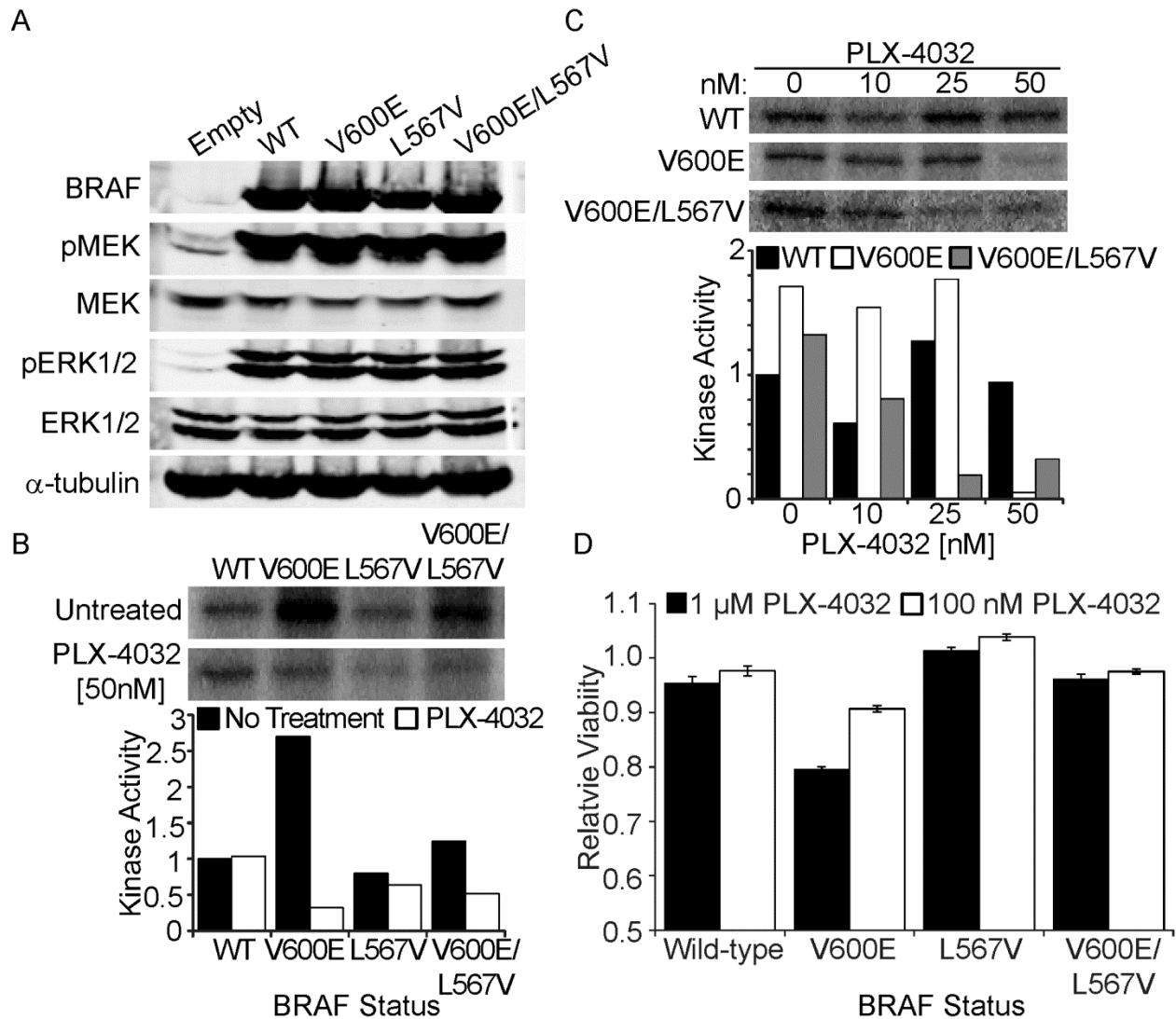
(A) 293FT cells were transfected with BRAF constructs: wild-type, V600E, L567V, or V600E/L567V. Cell lysates were probed by immunoblotting for BRAF and downstream proteins MEK and ERK1/2, both total and their activated phosphorylated forms. Alpha-tubulin was included as a loading control. (B) Radioactive kinase assays of immunoprecipitated BRAF constructs with and without treatment of 50 nM PLX-4032 using MEK as a substrate. Levels of radioactive MEK were measured using phosphorimaging. (C) PLX-4032 treatment (0, 10, 25, 50 nM) using radioactive kinase assays of immunoprecipitated BRAF constructs (wild-type,

162

Figure 5.2 (cont'd)

V600E, and V600E/L567V). (**D**) 293FT cells overexpressing BRAF constructs (wild-type, V600E, L567V, and V600E/L567V) were treated with 1 µM or 100 nM PLX-4032 for 48 hours and viability was determined.

CHAPTER 6:

DEVELOPMENT OF AN INNOVATIVE FLOURESCENT LIVE CELL AUTOPHAGY

ASSAY: mEOS2-LC3

ABSTRACT

Autophagy is responsible for maintaining homeostasis and cell survival during times of stress. To be able to respond to these needs, response to stress requires that autophagy be dynamic and therefore tightly regulated at multiple stages. This makes monitoring autophagic flux a complicated process, as autophagosomes are continuously created and turned over. Many cell based assays are currently used to measure autophagy; however, not all assays are suitable or capable of answering the desired mechanistic questions. To address the need for more precise autophagy assays, we created an innovative autophagy reporter assay incorporating a photoconvertable protein, mEOS2, adjacent to the autophagosome marker, LC3. Here, we demonstrate that this assay can be used to accurately monitor autophagosome populations, single or multiple autophagosomes, as well as cytosolic LC3-I protein localization to autophagosomes upon lipidation to LC3-II. The flexibility of this assay will allow for current questions within the autophagy field to begin to be answered.

INTRODUCTION

Autophagy is a dynamic, multi-step process that is used by cells to recycle nutrients and catabolize damaged proteins and organelles. Due to the dynamic nature of autophagy in maintaining cellular homeostasis and cell survival during stress, there are multiple stages, each of which is tightly regulated through the coordinated activity of a large network of proteins (Yang and Klionsky 2010). Following autophagy initiation, cytosolic contents are sequestered by a double bi-lipid membrane called a phagophore, or isolation membrane. Once the membrane is fully matured into a closed double-membrane vesicle, or autophagosome, it is then destined to fuse with a lysosome, creating an autolysosome. Autolysosomes and lysosomes function to take these sequestered components and recycle the organic material. Autophagic flux is the term used to describe the complete autophagic process from pathway initiation to autophagosome synthesis through to lysosomal turnover (Klionsky 2007; Klionsky 2012).

Multiple assays are available to measure autophagy; including immunoblotting and immunohistochemistry for autophagic proteins, electron microscopy to identify double-membrane autophagic vesicles, and many fluorescent microscopy techniques using both antibodies and fluorescently labeled proteins. Despite the abundance of assays available for observing autophagy, most if not all of these assays are appropriate or able to answer important remaining unanswered questions (Klionsky 2012). The primary issue lies in the fact that autophagic flux is not only time dependent, it is also difficult to monitor or distinguish increases from decreases in autophagy (Figure 6.1).

Currently available assays, such as fluorescent microscopy and western blotting techniques, often use the autophagy protein light chain 3 (LC3) which is found in two forms:

166

LC3-I, which exists in the cytosol, and LC3-II, which is lipidated to the autophagosome membrane during autophagy. A portion of LC3-II is degraded in the autolysosome along with autophagic cargo; therefore, LC3-II accumulation in response to lysosome inhibition, is best monitored by treatment with chloroquine (CQ) or Bafilomycin A1 (Baf A1), is used to approximate autophagic flux. Unfortunately, since these techniques require inhibiting autophagosome turnover, it makes it difficult to interpret if there is an alteration observed in autophagic flux due to a defect in downstream turnover or a lack of upstream activation. Moreover, the use of autophagy inhibitors can further interfere with the lysosomal-dependent activation of mTOR signaling, creating the potential for further misleading results (Zoncu, Bar-Peled et al. 2011; Juhasz 2012; Hegedus, Takats et al. 2013).

To address this issue, we sought to create an autophagy assay that would better evaluate autophagic flux while circumventing the need for lysosome inhibitors. To this end, we developed a photoconvertable protein fused to LC3. We used the photoconvertable protein, monomeric EOS (mEOS2) named after the Greek goddess Eos, goddess of dawn, which is converted from a green to red fluorescent protein following excitation with a 405 nm wavelength laser (McKinney, Murphy et al. 2009). We selected the mEOS2 fluorescent protein given its photostability once photoconverted to its red form, preventing quenching upon fusion with the lysosome, which is a problematic features of pH-sensitive green fluorescent proteins, such as GFP (Alkaabi, Yafea et al. 2005). Autophagosomes can then be monitored by labeling of the mEOS2-LC3 molecules, either in their green (unconverted) or red (converted) forms.

This construct will be able to answer multiple autophagy questions that are currently challenging to address, in addition to questions that we have not thought of yet. Some questions that can be addressed with this assay are: *1)* At what rate are new autophagosomes formed?; *2)*

167

Can autophagosomes fuse with other autophagosomes through homotypic fusion?; *3)* At what rate do autolysosomes turnover?; and *4)* Can the progress and interaction of single autophagosomes with other vesicles or organelles be measured in real time? Here, we describe the development and optimization of this assay, while providing examples of the types of questions that this new assay can be used to answer.

RESULTS

Development of a LC3 tagged photoconvertible fluorescent protein

The photoconvertible fluorescent protein mEOS2 vector was obtained from Loren Looger at the Howard Hughes Medical Institute at the Janelia Farms Research Campus (McKinney, Murphy et al. 2009). We inserted the coding sequence of MAP1LC3B downstream of mEOS2 into the Multiple Cloning Site (MCS) (Figure 6.2). mEOS2-LC3 was transfected into U2OS cells and protein expression was confirmed through immunoblotting with LC3-targeted antibodies (note: mEOS2 is not detected by antibodies, including those to similar fluorescent proteins, i.e. GFP). Finally, mEOS2-LC3 was confirmed to properly localize and photoconvert (Figure 6.2D).

Monitoring cytosolic incorporation of LC3 into autophagosomes

U2OS cells expressing stably expressing mEOS2-LC3 were visualized by live cell confocal microscopy using an adaptation of a technique called Fluorescence Localization After Photobleaching (FLAP). FLAP is traditionally used to monitor the movement of molecules within a cell and at membranes by observing the disappearance (or bleaching) of a signal. However, instead of photobleaching, we use photoconvert in this approach (Figure 6.3). To our knowledge, this microscopy technique - which we call Fluorescent Localization After Conversion (FLAC) - has not yet been reported and represents an innovative and complimentary approach to current microscopy techniques. We found that by repetitively photoconverting the cytosolic portion of the U2OS cells from green to red at each image acquisition step, we can monitor the photoconverted (red) cytosolic mEOS2-LC3-I protein as it is incorporated onto

169

autophagosome membranes as mEOS2-LC3-II (Figure 6.4). Using Elements software, the ratio of the pixels in red channel were taken compared to the pixels in the green channel. This allows for the visualization of photoconverted cytosolic mEOS2-LC3 that is distributed within the cytosol as it incorporates into autophagosomes. Only the three cells (outlined) that lay within the region of interest (ROI) show observable photoconversion. Images contain pseudo colored red pixels (representing unconverted mEOS2-LC3), white pixels (a 1:1 ratio of unconverted and converted mEOS2-LC3), and blue pixels (representing photoconverted mEOS2-LC3). After 46 seconds, the first appearance of photoconverted LC3-II on an autophagosome appears as indicated by a white arrow. As time progresses, the cytosolic LC3-I begins to become fully photoconverted (blue) and more photoconverted LC3-I is incorporated onto autophagic vesicles as photoconverted LC3-II (white) shown by white arrows.

Using mEOS2-LC3 to monitor whole populations or a single autophagosome

U2OS cells expressing the mEOS2-LC3 vector were visualized by live cell confocal microscopy to determine if autophagosomes could be monitored by photoconverting. We found that photoconverting of single autophagosomes was feasible by quickly drawing an ROI around the autophagosome(s) of interest after quick image acquisition within the target Z-plane and immediate exposure to a 405 nm laser at 0.3 percent power for 4 passes of 1 frame/second (Figure 6.5). It was shown that a longer dwell time (rate at which the laser scanned a field of view) and lower laser power was more effective at photoconverting. After photoconverting occurred, autophagosome(s) were able to be monitored accurately over time and in the Z-dimension with appropriate laser settings.

Photoconverting a whole cell population was also shown to be possible (Figure 6.6A). However, as the field of photoconverting is considerably larger; the frame rate needed to be adjusted in order to compensate for the larger scanning area in order to achieve an equal amount of laser dwell time, per area being photoconverted, as previously achieved. Again, once photoconversion had occurred, the whole population of red autophagosomes was able to be monitored to completion and the appearance of new green autophagosomes was able to be witnessed over four hours. Quantification was performed for both the red and green autophagosome populations at time zero and after four hours (Figure 6.6B). The photoconverted red population was shown to decrease from 900 punctae to 250 punctae per field of view over four hours, while the appearance of unconverted green autophagosomes increased from 150 to 450 punctae per field of view. This demonstrates that the assay is capable of measuring autophagic flux without the use of an autophagy inhibitor.

DISCUSSION

Monitoring autophagic flux is a technical challenge, as autophagosomes are continuously created and turned over. In addition, the rate of autophagic flux can be altered by multiple stimuli that can up or downregulate the pathway. There are many techniques available for measuring autophagy; however, their interpretation is not always straightforward and they are not always able to answer the needed questions, making the need for new assays ever present. Here, we developed an innovative fluorescent construct used to measure autophagic flux, mEOS2-LC3, which will allow diverse questions to be addressed in the autophagy field.

A major strength of this assay is the ability to track one or more autophagosomes within a larger population of autophagosomes. The advantage to being able to track individual autophagosomes is that it allows one to determine the discreet interactions that autophagosomes undergo. For instance, it is currently known that autophagosomes can fuse with lysosomes and endosomes (Hegedus, Takats et al. 2013). However, it is unclear whether autophagosomes fuse to one another through homotypic fusion. While there is some knowledge that homotypic fusion of certain autophagy proteins (ATG16L) is required for autophagosome maturation, it has not been shown if this can occur after maturation in a cellular system (Moreau, Ravikumar et al. 2011). Using this assay, it is possible to monitor a population of autophagosomes in real time and determine whether they eventually fuse with one another or exclusively fuse with endosomes and lysosomes. Understanding the vesicle dynamics that underlie autophagy is an important issue to resolve. Moreover, this type of question could be further examined by conjugating other autophagy proteins to the mEOS2 reporter.

A second important capability of this assay is the ability to track a complete population of autophagosomes, including the formation of new autophagic vesicles through delivery to the lysosome. We have demonstrated the feasibility of photoconverting an entire field of view or a single cell. Once converted, all red autophagic vesicles can be monitored for turnover or disappearance. In addition, the formation of any new autophagosomes, which appear green (unconverted), can also be observed, allowing for the observations of upstream autophagic regulation (autophagy induction and vesicle nucleation). Taken together this allows for determination of autophagic flux without the use of lysosome inhibitors, avoiding the potential for confounding issues that these chemicals create.

Finally, this assay allows the localization of cytosolic autophagic proteins to be monitored as they traffic to their destined membranes. To demonstrate the feasibility of this approach, we developed the imaging technique, Fluorescent Localization After Conversion (FLAC). This involves continually photoconverting portions of the cytosol from green to red and monitoring as the cytoplasmic red proteins dissipates and become incorporated into membranes, in this case the incorporation of LC3-II onto autophagosomes. This allows determination of the rate of which LC3 is incorporated into new autophagic vesicles, in addition to the rate of growth of these autophagic vesicles.

Using this assay for the experiments done in chapter 2, are expected to produce similar results. However, the ability to monitor two populations would allow for not only measuring inhibition of the existing converted autophagosome population, but could also demonstrate how the new unconverted autophagosome population would be affected. For instance, if the autophagy inhibitor is potent at the lysosomal level and feedback inhibition through mTOR strongly inhibits upstream autophagy activation, then we would not only expect an accumulation

of our converted (red) autophagosomes, but a decrease in new unconverted (green) autophagosome formation compared to a cell that was not inhibited by mTOR. This assay would allow us to not only measure downstream autophagy inhibition, but potentially upstream autophagy inhibition through a feedback loop with mTOR as well. Knowing both downstream and upstream activation (or inhibition) of the pathway yields more accurate information to exactly how the VATG compounds (or any others) are affecting the autophagy pathway.

In conclusion, the mEOS2-LC3 assay described here will allow for detailed investigations into autophagic flux without the additional confounding factors caused by use of autophagy inhibitors. This assay will prove to be useful for measuring vesicle formation, movement, fusion, and degradation.

MATERIALS AND METHODS

Cloning of mEOS2-LC3 Construct

The coding region of MAP1LC3B was PCR amplified from the ptf-LC3 vector (Addgene, 21074) and restriction sites, HindIII and PstI, incorporated to the 5' and 3' ends, respectively. The mEOS2 protein vector was obtained from the Looger lab the Howard Hughes Medical Institute at the Janelia Farms Research Campus. Both the LC3 fragment and mEOS2 vector were digested with HindIII and PstI, gel isolated, and ligated together using ligase enzyme. After ligation, the vector was transformed into TOP 10 competent bacteria (Invitrogen, C4040-10) and colonies were selected for using 50 mg/mL kanamycin. Colonies were confirmed for LC3 insertion into the mEOS vector by digestion analysis.

Transfection of mEOS2-LC3 into U2OS

U2OS cells were seeded onto a 10 cm plate in 5A McCoy's with 10% FBS at 5×10^5 cells per plate. After 24 hours, cells were transfected with a 4 µg of mEOS-LC3 vector using 12 µL of FuGene HD (Promega, E2311) in 100 µL of Opti-MEM (Invitrogen, 31985-062) and 10 mL of 5A McCoy's with 10% FBS. Cells were selected after 48 hours with 500 µg/mL Geneticin (Invitrogen, 11811-023) for one week with media changes.

Immunoblotting

For immunoblotting, mEOS2-LC3 cells were cells were lysed [10mM KPO4, 1mM EDTA, 10mM $MgCl_2$, 5mM EGTA, 50mM bis-glycerophosphate, 0.5% NP40, 0.1% Brij35, 0.1% sodium deoxycholate, 1mM NaVO4, 5mM NaF, 2mM DTT, and complete protease

inhibitors (Sigma, P8340-5mL)] and 50 μg of protein was resolved by SDS-PAGE. Proteins were transferred to PVDF membranes and probed with primary antibodies LC3 (CST, 2775) for 16 hours at 4°C followed by a secondary antibody [HRP-linked rabbit or mouse IgG (GE Healthcare, NA934 or NA931) for 1 hour at room temperature. Proteins were detected with the enhanced chemiluminescence.

Wide-field Fluorescence

U2OS cells stably expressing mEOS2-LC3 were seeded at 50,000 cells per well in 5A McCoy's with 10% FBS on number 1.5 coverglass. Cells were washed with 1x PBS, fixed with 3.7% formaldehyde, and nuclei were stained with Hoechst 33342 (2 μg/mL). Using mounting gel, coverglass was inverted onto microscope slides. Cells were imaged using a 60x oil-immersion objective on a Nikon Eclipse Ti fluorescent microscope. Photoconverting was assessed by taking before and after images of the red and green channels after exposure to the UV light source (~405 nm).

Confocal Analysis

U2OS cells stably expressing mEOS2-LC3 were seeded at 50,000 cells per plate in a 35mm Mattek glass bottom plate (Mattek, P35G-1.5-10-C) with 5A McCoy's with 10% FBS. Cells were imaged by live cell microscopy using a 60x oil-immersion objective on a Nikon A1 confocal microscope using spectrally unmixed mEOS2 before (green) and after (red) settings. Photoconverting was achieved in small localized areas (15 μm $\geq$) by using the 405 nm laser at 0.3 laser power for 4 passes of 1 frame/second dwell time. Larger areas (15 μm $<$) were

photoconverted using the 405 nm laser at 0.3 laser power for 4 passes of 1/12 frame/second

dwell time. Data analysis was performed using NIS Elements (Nikon).

ACKNOWLEDGEMENTS

Figure 6.1. Model of autophagy inhibition
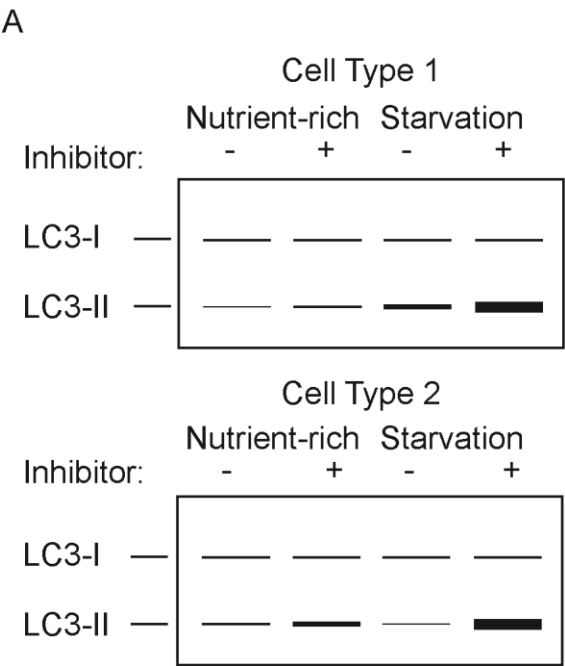
Figure 6.1 (cont'd)
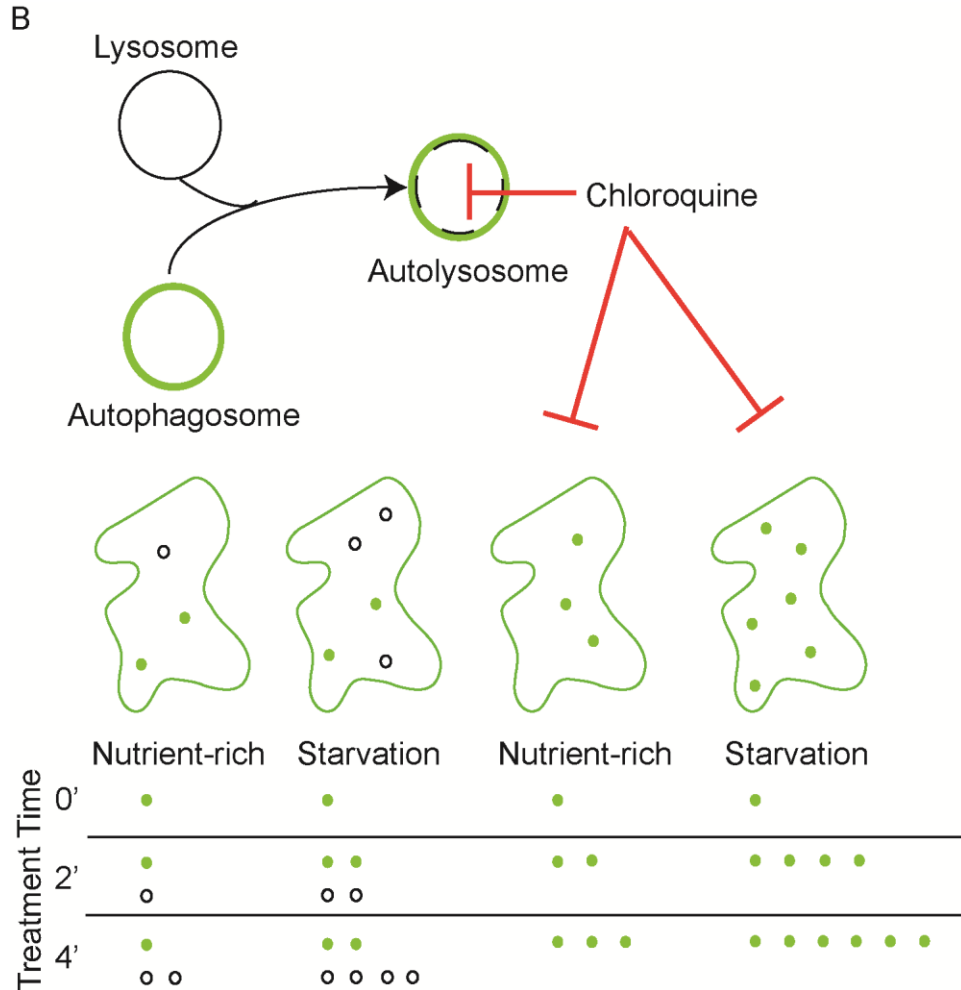
A) Hypothetical example of immunoblot results demonstrating the turnover of LC3 from cytosolic LC3-I to lipidated LC3-II. Turnover of LC3 in starvation conditions is difficult to interpret, as demonstrated between cell types. For instance, starvation can increase the amount of autophagic flux, thereby increasing LC3-II levels (as in cell type 1), however, an increase in autophagic flux can also result in increased turnover (lower levels) of LC3-II (as in cell type 2). Therefore, an autophagy inhibitor is required to determine if autophagic flux has in fact increased or decreased with the lack of LC3-II in cell type 2. Accumulation of LC3-II occurs in the presence of an inhibitor. (**B**) Diagram demonstrating autophagic flux in fluorescently labeled

Figure 6.1 (cont'd)

cells (here, GFP-LC3). Autophagosomes fuse with lysosomes, creating autolysosomes that are then degraded. Over time, the amount of autophagosomes (green circles) remain stable in nutrient rich conditions due to an equivalent turnover of autophagosomes (steady state). However, under starvation conditions, the amount of autophagosomes will increase, from 1 to 2, while the amount turned over (empty circles) also increases, from 0 to 4. With the use of an autophagy inhibitor (chloroquine), autophagosomes will accumulate in both conditions despite a lack of turnover. Yet with increased autophagic flux in starvation conditions, autophagosome number will further increase owing to increased pathway activation.

Figure 6.2. Confirmation of mEOS2-LC3
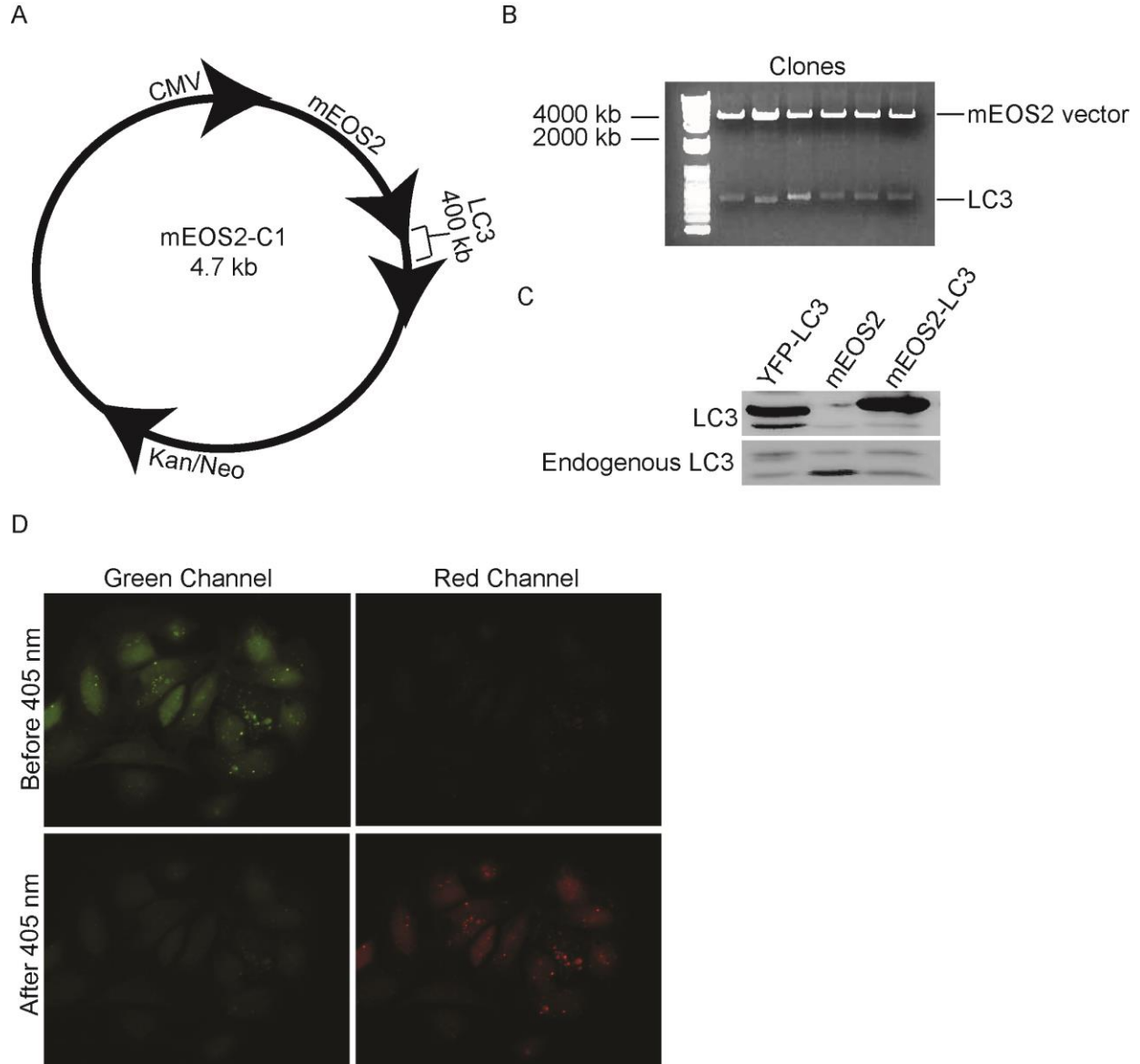
(A) The mEOS2-C1 vector is 4.7 kb is size and contains an upstream CMV promoter. A multiple cloning site (MCS) is located C-terminally for insertion of LC3. The prokaryotic selectable marker is kanamycin and the eukaryotic selectable marker is neomycin. **(B)** Restriction digest of mEOS2-LC3 vector using HindIII and PstI confirmed that the coding region of LC3 was inserted into mEOS2 vector. **(C)** Cell lysates of U2OS cells expressing YFP-LC3, mEOS2 empty vector, and mEOS2-LC3 were probed by immunoblotting for LC3. **(D)** U2OS

Figure 6.2 (cont'd)

cells expressing mEOS2- LC3 were fixed and imaged at 60x magnification. Cells were

photoconverted by exposure to UV laser (~ 405 nm) and imaged pre (top panels) or post (bottom

panels) photoconverting.

Figure 6.3. Diagram of FLAC technique
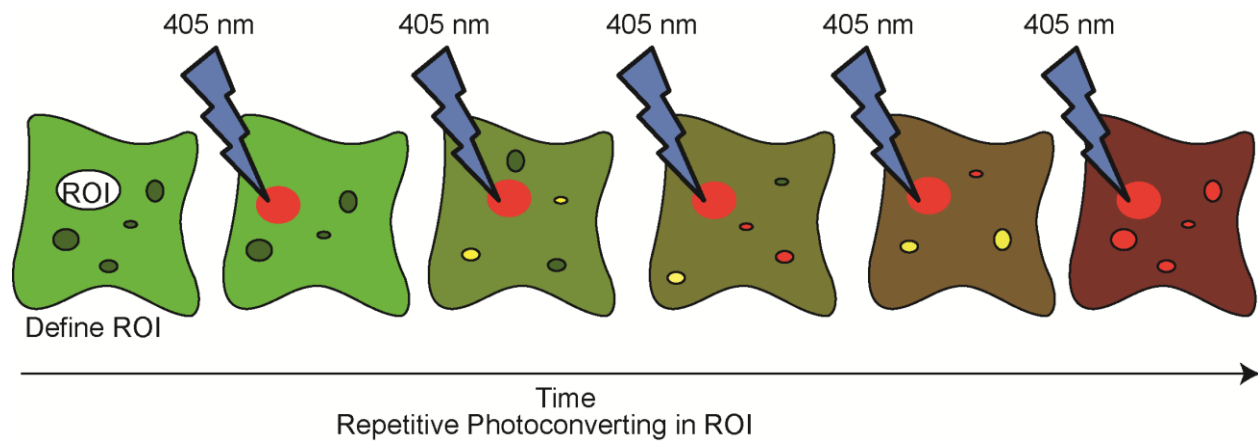
Using a 405 nm laser, a defined region of interest (ROI) within the cytosol is photoconverted from green to red at each image acquisition. Photoconverted cytosolic proteins can then be tracked as they localize to their intended membranes.

Figure 6.4. mEOS2-LC3 FLAC
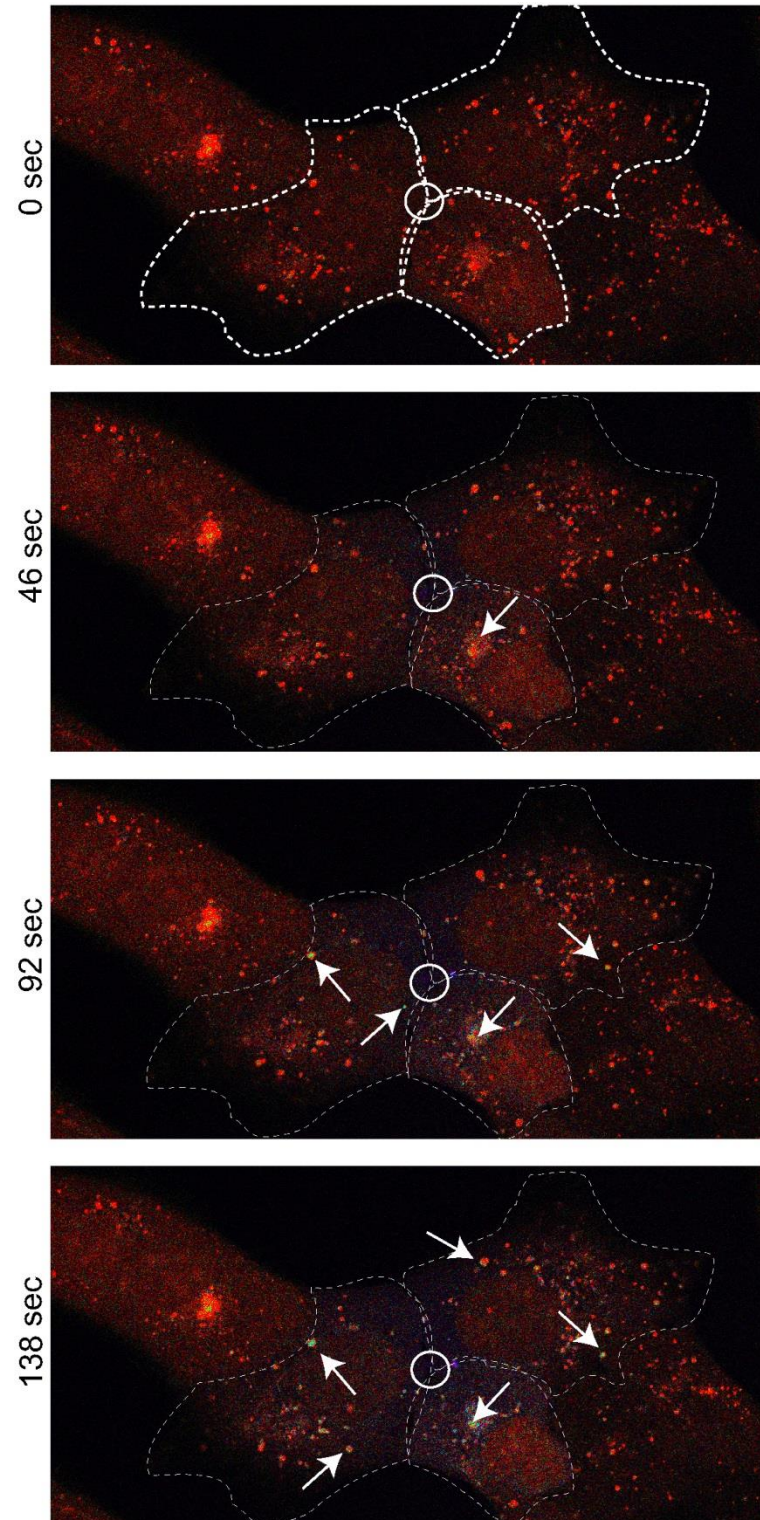
Figure 6.4 (cont'd)

U2OS cells expressing mEOS2-LC3 imaged over a 138 second time course, photoconverting with a 405nm UV laser at 2 second intervals occurs in the defined region of interest (ROI, circle). Cells targeted within the ROI are outlined with a dashed white line. Shown here is the ratio of green to red. Red pseudo coloring represents green-only pixels (unconverted), white represents a 1:1 ratio of green and red pixels (1:1 unconverted and photoconverted), and blue represents red-only pixels (photoconverted). Over time, the amount of photoconverted cytosolic LC3-I (blue) incorporates into the unconverted punctae as LC3-II (red) creating partially converted punctae (white) as indicated by white arrows.

Figure 6.5. Z-stack in time of photoconverted mEOS2-LC3
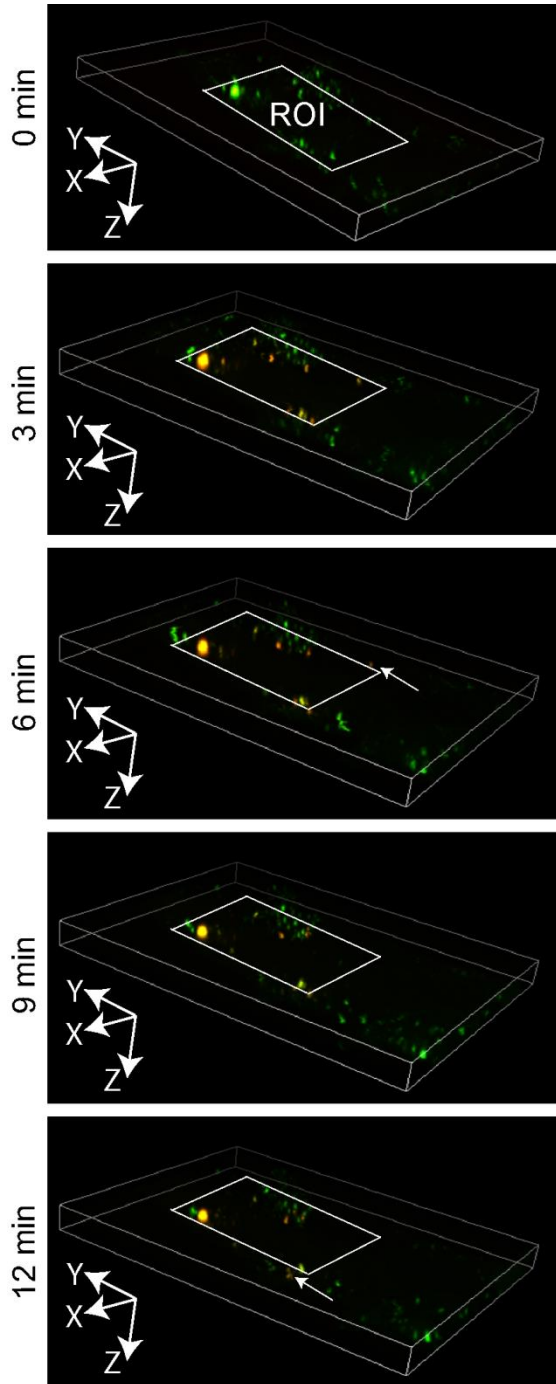
U2OS cells expressing mEOS2-LC3 were imaged over a 12 minute time course in Z-plane with photoconverting within the defined region of interest (ROI, square). Arrows indicate where an autophagosome moves out of the original ROI.

Figure 6.6. Photoconverting mEOS2-LC3 within the whole field of view

A
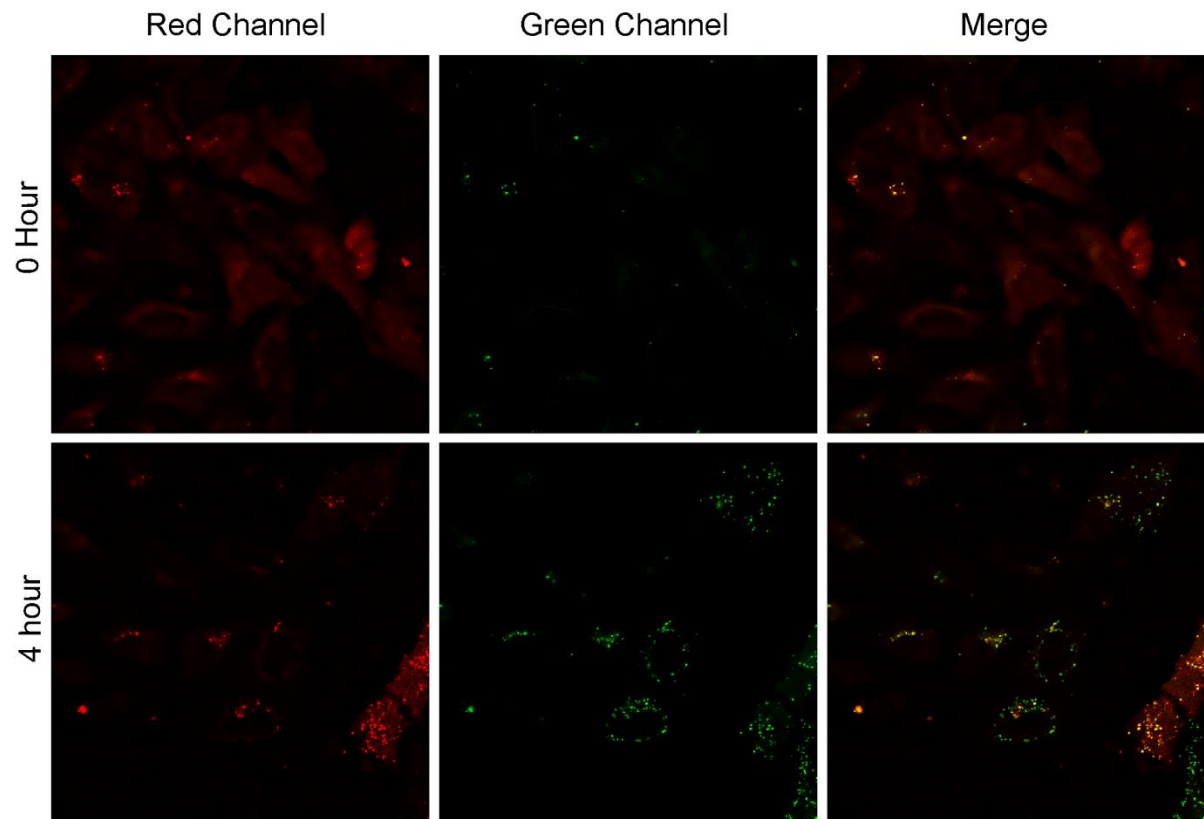
B
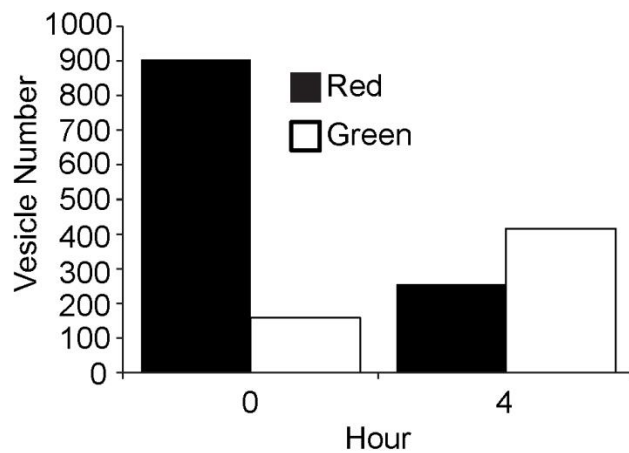
(A) U2OS cells expressing mEOS2-LC3 were imaged over a 4 hour time course with

photoconversion occurring within the entire field of view at time 0. The red channel (converted)

is the left column and the green channel (unconverted) is the middle column with the merged

Figure 6.6 (cont'd)

channels shown in the right column. (**B**) Quantification of the red and green vesicle number of

the whole field of view at times 0 and 4 hours.

CHAPTER 7

SUMMARY AND FUTURE DIRECTIONS

SUMMARY AND FUTURE DIRECTIONS

Chloroquine has proven to be a very versatile drug in its ability to treat a multitude of diseases, including malaria and cancer. However with each of these diseases, chloroquine has begun to fall short. In the case of malaria, the development of *P.falciparum* resistance has become a global issue ((WHO) March 2013). While in the case of cancer, the requirement of high concentrations to obtain complete autophagy inhibition and tumor regression is unsatisfactory for treatment regimens. In both cases, chloroquine functions as a lysomotropic agent and autophagy inhibitor, and development of more potent compounds is not only feasible, but necessary. In order to address both of these issues, we hypothesized that the development of novel, potent autophagy inhibitors using an analog of chloroquine was possible. Furthermore, potent inhibitors would not only better prevent autophagy-mediated cell survival in cancer cells, but would also function as effective antimalarial agents.

Quinacrine was commonly used in World War II until chloroquine was put on the market in 1953 (Wallace 1996; Lee, Silverman et al. 2011). This shift to chloroquine usage occurred because it was thought to be better tolerated than quinacrine (Jensen and Mehlhorn 2009). Although chloroquine was considered to have a safer toxicity profile, quinacrine has been used safely in humans for years and continues to be used in regions plagued by chloroquine resistance (Foley and Tilley 1998). Furthermore, epidemiologic studies support that use of quinacrine has reduced cancer risk rates (Ruiz-Irastorza, Ugarte et al. 2007; Sokal, Trujillo et al. 2010). Taken together, these facts support our choice to use quinacrine as a template for chemical synthesis.

Using quinacrine, a total of 34 novel compounds were tested in Chapter 2. Most compounds - assigned VATG names to reflect the partnership between V̲an A̲ndel Institute and

TGen - were found to more potently inhibit autophagy than quinacrine. Furthermore, these chemicals were characterized by a wide range of cytotoxicity profiles. We chose VATG014 and VATG032 for further interrogation as they represented a highly cytotoxic and less cytotoxic compound, respectively. Toxicity differences observed are expectedly due to the saturated 1,2,3,4-tetrahydroacridine backbone of VATG032 compared to the shared acridine backbone of QN with VATG014. We used several complimentary assays to confirm that these compounds function mechanistically as anticipated by increasing lysosomal pH and preventing lysosomal turnover, thereby impairing autophagy.

VATG Compounds in Oncogenic BRAF V600E

Given the crucial role of autophagy-mediated survival in cancer progression, we investigated the use of these autophagy inhibiting compounds on highly autophagic melanoma tumor cells containing oncogenic BRAF V600E, presented in Chapter 3 Section 1. We demonstrated that these novel compounds not only reduced colony formation as single agents, but were more than additive with the standard of care for V600E mutants, vemurafenib (PLX-4032). This result not only shows great promise for autophagy inhibitors as part of combinatorial treatment regimens to improve the efficacy of existing drugs, but also as single agents, potentially in cancers that lack effective options.

To begin exploring the use of these inhibitors *in vivo*, we chose to use a model of pancreatic cancer, which are particularly dependent on basal autophagy for survival and growth (Yang and Kimmelman 2011; Kang and Tang 2012). These cancers have higher basal autophagic levels compared to other epithelial cancers which correlate with poor patient outcome. Accordingly, chloroquine has shown promising in reducing pancreatic cancer growth

(Yang and Kimmelman 2011; Kang and Tang 2012). Pancreatic cancers respond poorly to most therapeutics, contributing to a 5-year survival rate of approximately 5% (Hezel, Kimmelman et al. 2006). The lack of therapeutic options and the apparent dependence on autophagy-mediated cell survival underscores the importance of evaluating potent autophagy inhibitors in pancreatic cancer. To this end, we evaluated the activity of VATG032 in the BxPC-3 pancreatic cell line, a well-studied pancreatic cancer cell line with tumorigenic potential *in vivo* (Merriman, Hertel et al. 1996).

Subcutaneous xenografts using BxPC-3 tumor cells were initiated in mice and the ability of VATG032 to reduce tumor growth was determined. Mice were treated with VATG032 as a single agent over the course of 12 days (orally) compared to the standard of care for pancreatic cancer, gemcitabine/abraxane. VATG032 showed no gross toxicity in mice. Important, VATG032 proved to be more effective in reducing tumor size than the standard of care, gemcitabine/abraxane (Figure 7.1). Strikingly, VATG032 reduced tumor volume by half when compared to vehicle control over the course of 3 weeks. The finding that our autophagy inhibitors can reduce *in vivo* tumor growth, independent of an additional chemotherapeutic, further underscores the need for effective autophagy inhibitors in autophagy-dependent cancers. The fact that autophagy inhibitors have been shown to be extremely effective in a highly autophagic cancer, even without an additional therapeutics, is an important lesson here. However, as the role of autophagy in cancer cells depends on tumor type, tumor stage, and genetic context, use of these autophagy inhibitors may not be appropriate for all contexts and needs to be investigated in more detail.

Identification of a Putative Revertant

Understanding the role that molecular underpinnings play in the development of therapeutic resistance is equally as important as identifying first-line therapeutics. The development of resistance to therapeutics is a real threat as new cases continue to be documented. Resistance is known to arise in many forms; including activation of compensatory pathways, an increase in target expression, and selection for molecular heterogeneity that has an inherent resistance (Holohan, Van Schaeybroeck et al. 2013). Identification of revertant mutants, which are mutations that return an organism to the original phenotype by a second mutation, is an extremely rare event and is not thought to occur frequently due to the inefficiency in returning to wild-type states (Telerman and Amson 2009). However, the fact that revertants are rare may discourage efforts to search for them. Here, a route of resistance by a putative revertant mutation is discussed in Chapter 3 Section 2 with the discovery of, to our knowledge, the first clinical case of a second-site mutation in BRAF conferring resistance.

Since the mother denied treatment until after the birth of her child, the initiating tumor was permitted to grow and metastasize and a process of clonal evolution could then occur allowing for higher tumor heterogeneity (Greaves and Maley 2012). Additionally, the lack of therapeutic selection would allow for the development of inefficient passenger mutations, such as a revertant (Vogelstein, Papadopoulos et al. 2013). The identification of this revertant will not only lead to a better understanding of the effect of vemurafenib in BRAF mutant melanoma, but should also expand the consideration that tumors that contain a high amount of heterogeneity, and are non-responsive to targeted therapies, may possibly contain more reversion and revertant mutations than previously thought. This is further supported by the fact that even cells with a

genetically uniform lineage may respond differently in response to a chemotherapeutic, as demonstrated in Kreso *et al*. in the journal *Science* earlier this year (Kreso, O'Brien et al. 2013).

VATG Compounds as Antimalarial Agents

Clonal evolution is not only an issue in cancer, but also in the development of antimalarial resistant *Plasmodium* species, as has been shown with spread of chloroquine-resistant *P.falciparum*. Even artemisinin-based combination therapies (ACTs), the standard of care approaches that are initially effective, require the long half-lives of quinolones to target residual parasites (Biamonte, Wanner et al. 2013). Ultimately, a more potent antimalarial that retains a longer half-life would be ideal since residual parasites can lead to prolonged disease. We believe that the development of novel antimalarial compounds, such as those described in Chapter 2, could be used to address this need. These compounds function by a similar mechanism of action as both chloroquine and quinacrine, albeit more potently, and it would stand to reason that they would also share their longer half-lives as well. VATG014 has already been shown to be potent in reducing parasitemia at 99% activity *in vivo* and its half-life will continue to be addressed using a murine model of malaria, as studies are still ongoing.

Given the autophagy inhibiting properties of chloroquine and its activity as an antimalarial, it could be hypothesized that the *Plasmodium* parasite is capable of undergoing autophagy. In 2010, a gene in the phosphoinositide 3-kinase (PI3K) family, which are lipid kinases critical for the control of autophagy and related pathways in yeast and mammals, was identified as a component of the *P.falciparum* food vacuole trafficking pathway (Vaid, Ranjan et al. 2010). This gene, PfPI3K, was inhibited by the well-characterized PI3K inhibitors, wortmannin and LY294002. Moreover, nine putative orthologues of autophagy genes were

195

identified: ATG1, ATG3-4, ATG7-9, ATG12, and ATG17-18 (Vaid, Ranjan et al. 2010; Duszenko, Ginger et al. 2011). ATG7 was shown to be vital for normal growth, while ATG8 was found to be necessary for apicoplast formation, a non-digestive chloroplast-like organelle essential to the parasite (Kitamura, Kishi-Itakura et al. 2012; Tomlins, Ben-Rached et al. 2013; Walker, Mahfooz et al. 2013). This is still a relatively young area of exploration, but may lead to new opportunities for antimalarial therapeutics. The use of chloroquine for cancer treatment demonstrates the utility of repurposing therapeutics. We have similarly demonstrated that our compounds are capable of being effective in both malaria and cancer models.

Novel Autophagy Assay: mEOS2

The use of these novel compounds relies on their potent ability to inhibit the lysosome and ultimately autophagy in cancer cells and is important for their effectiveness as anticancer agents, antimalarial agents, and tools to measure autophagic flux. Unfortunately, other cellular pathways that terminate in the lysosome, including endocytic trafficking and the lysosomal pathways itself, can be disrupted by the use of lysosomal inhibitors. This can cause problems when measuring autophagy, as both the endocytic and lysosomal pathways have been shown to play a role in the regulation of autophagy. Autophagy inhibition by mTOR on autolysosomes is needed for the reformation of lysosomes, while recycling endosomes are shown to be crucial in the reformation of autophagosomes (Liou, Geuze et al. 1997; Yu, McPhee et al. 2010; Longatti, Lamb et al. 2012). Finally, lysosomal-dependent activation of mTOR signaling is responsible for autophagy inhibition (Zoncu, Bar-Peled et al. 2011; Juhasz 2012; Hegedus, Takats et al. 2013). Disruption of these pathways by a lysosomal inhibitor creates the potential for

196

misleading results as inhibitors are required for interpretation of assays currently used to monitor autophagy.

With this in mind, we strived to create an autophagy assay that could better evaluate autophagic flux without the use of an inhibitor. This was achieved by fusing the autophagy protein, LC3, to a photoconvertible protein, mEOS2 (McKinney, Murphy et al. 2009). The photoconvertible mEOS2-LC3 labels autophagosomes which can then be selectively converted from green to red following stimulation with a 405 nm wavelength laser. Autophagosomes can then be monitored in both their green (unconverted) and red (converted) states within single cells. The advantage to this assay is the ability to track one or more autophagosomes within a larger population of autophagosomes in the cell. This is not feasible with most conventional fluorescent-based autophagy assays that universally label autophagosomes (i.e. GFP-LC3), or with photoactivation, which does not allow observation of the rest of the autophagic population (Hailey and Lippincott-Schwartz 2009; Klionsky, Abdalla et al. 2012). The ability to track a complete population of autophagosomes - from formation to delivery in the lysosome - is a significant advantage of this assay. This feature allows the determination of autophagic flux without the use of a lysosomal inhibitor, avoiding the potential for confounding issues that these inhibitors can create. Furthermore, the assay has the capacity to monitor the formation of new autophagic vesicles, which will appear green (unconverted) simultaneously, allowing for the additional observations of upstream autophagic regulation (autophagy induction and vesicle nucleation).

In addition to autophagic flux on the level of single cells, this assay is able to track individual autophagosomes over time. Monitoring single autophagosomes will enable characterization of subtle interactions that autophagosomes make with one another and other

197

vesicles. For instance, it is currently known that autophagosomes can fuse with lysosomes and endosomes (Hegedus, Takats et al. 2013). Yet, it is still less clear whether autophagosomes are able to fuse to one another through homotypic fusion. It is known that homotypic fusion of the autophagy protein ATG16L is required for autophagosome maturation; however, it has not been shown if this can occur after maturation (Moreau, Ravikumar et al. 2011). This assay allows for monitoring an entire population of autophagosomes in real time while simultaneously watching individual autophagosomes to determine whether they will eventually fuse with one another or exclusively fuse with endosomes and lysosomes. Finally, the approach of this assay could be extended to study other autophagy proteins by conjugating these to the mEOS2 reporter. A potential protein could include those more upstream in autophagic initiation, such as ULK1 which is required for nucleation of the phagophore to more closely monitor initiation events. Alternatively, autophagy proteins known to be involved in fusion, such as ATG16L mentioned earlier or STX17 which is involved in the fusion of autophagosomes to both lysosomes and endosomes, could be monitored to determine if these are also involved in fusion of autophagosomes with themselves.

There are some potential limitations with this assay. One issue is that this assay requires the use of a 405 nm laser, which is typically only found on confocal microscopes, creating a large investment in instrumentation. Further, photoconversion conditions needed for each independent assay requires large amounts of optimization and a monoclonal cell line to avoid differences in expression level variations. Finally, there are always concerns with the use of an overexpression construct in that increases of a specific protein could be biologically irrelevant. However, this issue can be mostly circumvented by titration of the expression down to more

physiological levels, especially as confocal microscopy is more sensitive than conventional microscopy.

Remarkably, this assay allowed for the unanticipated ability to detect the localization of cytosolic autophagic proteins as they traffic to their destined membranes. This unforeseen ability was due to the fact that there is not currently a microscopy technique specifically intended for this purpose. The new imaging technique <u>F</u>luorescent <u>L</u>ocalization <u>A</u>fter <u>C</u>onversion (FLAC), was created and optimized. FLAC involves the continual photoconversion of portions of the cytosol from green to red and monitoring as the cytoplasmic red proteins dissipate and become incorporated into membranes, in this case the incorporation of LC3-II onto autophagosomes. The determination of rate at which LC3 is incorporated into new autophagic vesicles, in addition to the rate of growth of these autophagic vesicles, can then be examined.

Summary

In conclusion, several gaps of knowledge were addressed throughout this work. First, the generation and characterization of novel, potent autophagy inhibitors that are effective as both anticancer and antimalarial agents was achieved. Several autophagy inhibitors are available; however, a majority target upstream pathways and can be non-specific (Yang, Hu et al. 2013). Some development into new autophagy inhibitors has been done, however these molecules relied on coupling two CQ molecules (McAfee, Zhang et al. 2012). Although these have shown better autophagy inhibition than CQ alone, our compounds demonstrate more overall potency at autophagy inhibition. These compounds not only address a need for more effective therapeutic options in cancer, but have shown efficacy in malaria models as well. Further, continued investigation of these compounds in xenografts and murine malaria models will give us better

pharmacodynamics and pharmacokinetics information to allow for potential future use in Phase I clinical trials. As CQ is also used in rheumatic diseases, future investigation into the use of these compounds as potential therapeutic options is interesting.

Secondly, the identification of a putative revertant mutation in oncogenic BRAF V600E, L567V, which allows for resistance to vemurafenib was identified. This is not only a rare case of transplacental metastasis, but the first clinical identification of a resistance mutation in BRAF, to our knowledge.

And finally, the development of a new autophagy assay that does not rely on the use of inhibitors was designed and also holds incredible potential for addressing critical questions in the realm of autophagy. To address the first outstanding question, "At what rate is a new autophagosome formed?", we were able to develop the new microscopy technique FLAC and will be able to continue to investigate the rate of autophagosome formation as well as autophagosome growth. Addressing the second question, "Can autophagosomes fuse with other autophagosomes through homotypic fusion?", we were able to show that we can monitor individual or multiple autophagosomes through time and Z-dimensions, allowing us to track different populations simultaneously and allow us to answer this question. Undertaking question 3, "At what rate do autolysosomes turnover?", we are able to photoconvert an entire autophagosome population which allows us to successfully track autophagosomes to completion without the need of an autophagy inhibitor. Finally, to address question *4, "*Can the progress and interaction of single autophagosomes with other vesicles or organelles be measured?", we can monitor two different populations of autophagosomes while simultaneously observing other organelles and vesicles, for example, using additional fluorescent markers, such as LysoSensor Blue for lysosomes.

Figure 7.1 Treatment of VATG-032 on BxPC-3 Human Pancreatic Xenograft Model.
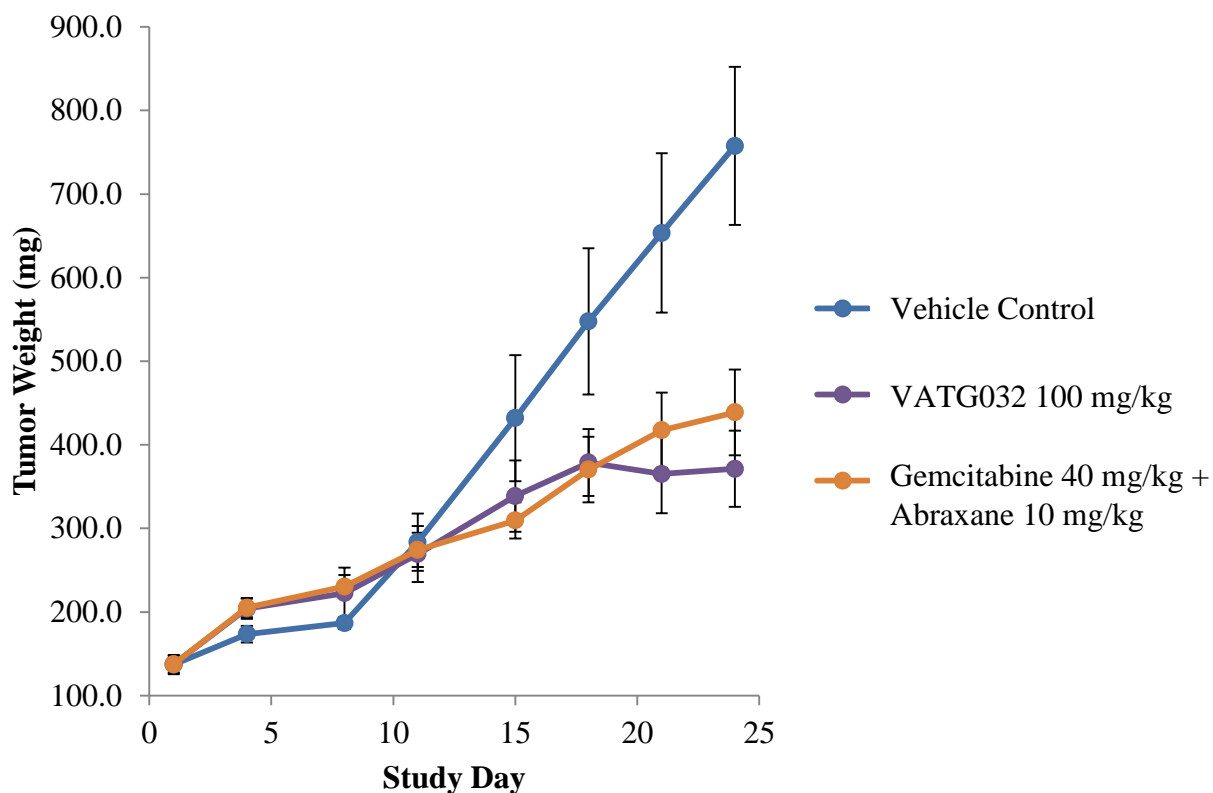
In vivo efficacy studies of VATG-032 in BxPC-3 human pancreatic cancer xenograft mouse models. Treatments were initiated when mean tumor volume reached approximately 140 mm^3. VATG-032 (100 mg/kg) was administered PO, QD for 12 total doses. Gemcitabine (40 mg/kg) was administered IP on Days 3, 6, 9 and 12. Abraxane (10 mg/kg) was administered IP on Days 1, 2, 4, 5, 7, 8, 10 and 11. Data is expressed as standard error of the mean (SEM).

REFERENCES

REFERENCES

(WHO), W. H. O. (March 2013). World Malaria Report 2012, WHO.

Alexander, A., W. E. Samlowski, et al. (2003). "Metastatic melanoma in pregnancy: risk of transplacental metastases in the infant." J Clin Oncol **21**(11): 2179-2186.

Alkaabi, K. M., A. Yafea, et al. (2005). "Effect of pH on thermal- and chemical-induced denaturation of GFP." Appl Biochem Biotechnol **126**(2): 149-156.

Biamonte, M. A., J. Wanner, et al. (2013). "Recent advances in malaria drug discovery." Bioorg Med Chem Lett **23**(10): 2829-2843.

Bollag, G., P. Hirth, et al. (2010). "Clinical efficacy of a RAF inhibitor needs broad target blockade in BRAF-mutant melanoma." Nature **467**(7315): 596-599.

Bollag, G., J. Tsai, et al. (2012). "Vemurafenib: the first drug approved for BRAF-mutant cancer." Nat Rev Drug Discov **11**(11): 873-886.

Chin, L. (2003). "The genetics of malignant melanoma: lessons from mouse and man." Nat Rev Cancer **3**(8): 559-570.

Davies, H., G. R. Bignell, et al. (2002). "Mutations of the BRAF gene in human cancer." Nature **417**(6892): 949-954.

Duszenko, M., M. L. Ginger, et al. (2011). "Autophagy in protists." Autophagy **7**(2): 127-158.

Flaherty, K. T., I. Puzanov, et al. (2010). "Inhibition of mutated, activated BRAF in metastatic melanoma." N Engl J Med **363**(9): 809-819.

Foley, M. and L. Tilley (1998). "Quinoline antimalarials: mechanisms of action and resistance and prospects for new agents." Pharmacol Ther **79**(1): 55-87.

Gilchrest, B. A., M. S. Eller, et al. (1999). "The pathogenesis of melanoma induced by ultraviolet radiation." N Engl J Med **340**(17): 1341-1348.

Gray-Schopfer, V., C. Wellbrock, et al. (2007). "Melanoma biology and new targeted therapy." Nature **445**(7130): 851-857.

Greaves, M. and C. C. Maley (2012). "Clonal evolution in cancer." Nature **481**(7381): 306-313.

Greaves, W. O., S. Verma, et al. (2013). "Frequency and spectrum of BRAF mutations in a retrospective, single-institution study of 1112 cases of melanoma." J Mol Diagn **15**(2): 220-226.

Hailey, D. W. and J. Lippincott-Schwartz (2009). "Using photoactivatable proteins to monitor autophagosome lifetime." Methods Enzymol **452**: 25-45.

Hegedus, K., S. Takats, et al. (2013). "Evolutionarily conserved role and physiological relevance of a STX17/Syx17 (syntaxin 17)-containing SNARE complex in autophagosome fusion with endosomes and lysosomes." Autophagy **9**(10).

Hezel, A. F., A. C. Kimmelman, et al. (2006). "Genetics and biology of pancreatic ductal adenocarcinoma." Genes Dev **20**(10): 1218-1249.

Holohan, C., S. Van Schaeybroeck, et al. (2013). "Cancer drug resistance: an evolving paradigm." Nat Rev Cancer **13**(10): 714-726.

Jabbour, E., H. Kantarjian, et al. (2006). "Frequency and clinical significance of BCR-ABL mutations in patients with chronic myeloid leukemia treated with imatinib mesylate." Leukemia **20**(10): 1767-1773.

Jensen, M. and H. Mehlhorn (2009). "Seventy-five years of Resochin in the fight against malaria." Parasitol Res **105**(3): 609-627.

Johannessen, C. M., J. S. Boehm, et al. (2010). "COT drives resistance to RAF inhibition through MAP kinase pathway reactivation." Nature **468**(7326): 968-972.

Juhasz, G. (2012). "Interpretation of bafilomycin, pH neutralizing or protease inhibitor treatments in autophagic flux experiments: novel considerations." Autophagy **8**(12): 1875-1876.

Kang, R. and D. Tang (2012). "Autophagy in pancreatic cancer pathogenesis and treatment." Am J Cancer Res **2**(4): 383-396.

Kitamura, K., C. Kishi-Itakura, et al. (2012). "Autophagy-related Atg8 localizes to the apicoplast of the human malaria parasite Plasmodium falciparum." PLoS One **7**(8): e42977.

Klionsky, D. J. (2007). "Autophagy: from phenomenology to molecular understanding in less than a decade." Nat Rev Mol Cell Biol **8**(11): 931-937.

Klionsky, D. J. (2012). "Guidelines to the use and interpretation of assays for monitoring autophagy." Autophagy **8**(4): 445-544.

Klionsky, D. J., F. C. Abdalla, et al. (2012). "Guidelines for the use and interpretation of assays for monitoring autophagy." Autophagy **8**(4): 445-544.

Kreso, A., C. A. O'Brien, et al. (2013). "Variable clonal repopulation dynamics influence chemotherapy response in colorectal cancer." Science **339**(6119): 543-548.

Lee, S. J., E. Silverman, et al. (2011). "The role of antimalarial agents in the treatment of SLE and lupus nephritis." Nat Rev Nephrol **7**(12): 718-729.

Liou, W., H. J. Geuze, et al. (1997). "The autophagic and endocytic pathways converge at the nascent autophagic vacuoles." J Cell Biol **136**(1): 61-70.

Lito, P., N. Rosen, et al. (2013). "Tumor adaptation and resistance to RAF inhibitors." <u>Nat Med</u> **19**(11): 1401-1409.

Longatti, A., C. A. Lamb, et al. (2012). "TBC1D14 regulates autophagosome formation via Rab11- and ULK1-positive recycling endosomes." <u>J Cell Biol</u> **197**(5): 659-675.

McAfee, Q., Z. Zhang, et al. (2012). "Autophagy inhibitor Lys05 has single-agent antitumor activity and reproduces the phenotype of a genetic autophagy deficiency." <u>Proc Natl Acad Sci U S A</u> **109**(21): 8253-8258.

McKinney, S. A., C. S. Murphy, et al. (2009). "A bright and photostable photoconvertible fluorescent protein." <u>Nat Methods</u> **6**(2): 131-133.

Merriman, R. L., L. W. Hertel, et al. (1996). "Comparison of the antitumor activity of gemcitabine and ara-C in a panel of human breast, colon, lung and pancreatic xenograft models." <u>Invest New Drugs</u> **14**(3): 243-247.

Moreau, K., B. Ravikumar, et al. (2011). "Autophagosome precursor maturation requires homotypic fusion." <u>Cell</u> **146**(2): 303-317.

Nazarian, R., H. Shi, et al. (2010). "Melanomas acquire resistance to B-RAF(V600E) inhibition by RTK or N-RAS upregulation." <u>Nature</u> **468**(7326): 973-977.

Poulikakos, P. I., Y. Persaud, et al. (2011). "RAF inhibitor resistance is mediated by dimerization of aberrantly spliced BRAF(V600E)." <u>Nature</u> **480**(7377): 387-390.

Prahallad, A., C. Sun, et al. (2012). "Unresponsiveness of colon cancer to BRAF(V600E) inhibition through feedback activation of EGFR." <u>Nature</u> **483**(7387): 100-103.

Ruiz-Irastorza, G., A. Ugarte, et al. (2007). "Antimalarials may influence the risk of malignancy in systemic lupus erythematosus." <u>Ann Rheum Dis</u> **66**(6): 815-817.

Sokal, D. C., V. Trujillo, et al. (2010). "Cancer risk after sterilization with transcervical quinacrine: updated findings from a Chilean cohort." <u>Contraception</u> **81**(1): 75-78.

Solit, D. and C. L. Sawyers (2010). "Drug discovery: How melanomas bypass new therapy." <u>Nature</u> **468**(7326): 902-903.

Solit, D. B. and N. Rosen (2011). "Resistance to BRAF inhibition in melanomas." <u>N Engl J Med</u> **364**(8): 772-774.

Sosman, J. A., K. B. Kim, et al. (2012). "Survival in BRAF V600-mutant advanced melanoma treated with vemurafenib." <u>N Engl J Med</u> **366**(8): 707-714.

Telerman, A. and R. Amson (2009). "The molecular programme of tumour reversion: the steps beyond malignant transformation." <u>Nat Rev Cancer</u> **9**(3): 206-216.

Tomlins, A. M., F. Ben-Rached, et al. (2013). "Plasmodium falciparum ATG8 implicated in both autophagy and apicoplast formation." <u>Autophagy</u> **9**(10).

Tsai, J., J. T. Lee, et al. (2008). "Discovery of a selective inhibitor of oncogenic B-Raf kinase with potent antimelanoma activity." <u>Proc Natl Acad Sci U S A</u> **105**(8): 3041-3046.

Vaid, A., R. Ranjan, et al. (2010). "PfPI3K, a phosphatidylinositol-3 kinase from Plasmodium falciparum, is exported to the host erythrocyte and is involved in hemoglobin trafficking." <u>Blood</u> **115**(12): 2500-2507.

Vogelstein, B., N. Papadopoulos, et al. (2013). "Cancer genome landscapes." <u>Science</u> **339**(6127): 1546-1558.

Wagle, N., C. Emery, et al. (2011). "Dissecting therapeutic resistance to RAF inhibition in melanoma by tumor genomic profiling." <u>J Clin Oncol</u> **29**(22): 3085-3096.

Walker, D. M., N. Mahfooz, et al. (2013). "Plasmodium falciparum erythrocytic stage parasites require the putative autophagy protein PfAtg7 for normal growth." <u>PLoS One</u> **8**(6): e67047.

Wallace, D. J. (1996). "The history of antimalarials." <u>Lupus</u> **5 Suppl 1**: S2-3.

Yang, S. and A. C. Kimmelman (2011). "A critical role for autophagy in pancreatic cancer." <u>Autophagy</u> **7**(8): 912-913.

Yang, Y. P., L. F. Hu, et al. (2013). "Application and interpretation of current autophagy inhibitors and activators." <u>Acta Pharmacol Sin</u> **34**(5): 625-635.

Yang, Z. and D. J. Klionsky (2010). "Eaten alive: a history of macroautophagy." <u>Nat Cell Biol</u> **12**(9): 814-822.

Yu, L., C. K. McPhee, et al. (2010). "Termination of autophagy and reformation of lysosomes regulated by mTOR." <u>Nature</u> **465**(7300): 942-946.

Zoncu, R., L. Bar-Peled, et al. (2011). "mTORC1 senses lysosomal amino acids through an inside-out mechanism that requires the vacuolar H(+)-ATPase." <u>Science</u> **334**(6056): 678-683.